Universidade de Aveiro Departamento de Química
2015

MARYAM NASIRPOUR

SYNTHESIS AND CHARACTERIZATION OF SILVER NANOPARTICLES: A TOXICITY AND METABOLIC PROFILING APPROACH IN SKIN CELLS

SÍNTESE E CARACTERIZAÇÃO DE NANOPARTÍCULAS DE PRATA: UMA ABORDAGEM DA TOXICIDADE E DO PERFIL METABÓLICO EM CÉLULAS DA PELE

Universidade de Aveiro Departamento de Química
2015

MARYAM NASIRPOUR

SYNTHESIS AND CHARACTERIZATION OF SILVER NANOPARTICLES: A TOXICITY AND METABOLOMICS APPROACH IN SKIN CELLS

SÍNTESE E CARACTERIZAÇÃO DE NANOPARTÍCULAS DE PRATA: UMA ABORDAGEM DA TOXICIDADE E DO PERFIL METABÓLICO EM CÉLULAS DA PELE

Dissertação apresentada à Universidade de Aveiro para cumprimento dos requisitos necessários à obtenção do grau de Mestre em Ciência e Engenharia de Materias, realizada sob a orientação científica da Doutora Helena Cristina Correia de Oliveira, Estagiária de Pós-doutoramento do Centro de Estudos do Ambiente e do Mar e Departamento de Biologia da Universidade de Aveiro e sob co-orientação científica da Doutora Iola Melissa Fernandes Duarte, Investigadora Principal do CICECO – Instituto de Materiais de Aveiro, Departamento de Química da Universidade de Aveiro e do Doutor Ricardo João Borges Pinto, Estagiário de Pós-doutoramento do CICECO – Instituto de Materiais de Aveiro, Departamento de Química da Universidade de Aveiro.

Funded by European Commission
under the Erasmus Mundus Program

...dedico este trabalho
ao meu corpo,
à proxima geração,
e a si...

o júri

presidente	Professora Doutora Ana Margarida Madeira Viegas de Barros Timmons Directora de curso do mestrado functionalized advanced materials and engineering (FAME), Professora auxiliar do Departamento de Química da Universidade de Aveiro
arguente principal	Professor. Doutor Tito da Silva Trindade Professor Associado com Agregação do Departamento de Química da Universidade de Aveiro
orientadora	Doutora Helena Cristina Correia de Oliveira Investigadora Pós-Doutoramento, CESAM - Centro de Estudos do Ambiente e do Mar da Universidade de Aveiro
	Doutora Iola Melissa Fernandes Duarte Investigadora Principal, CICECO – Instituto de Materiais de Aveiro, Departamento de Química da Universidade de Aveiro
	Doutor Ricardo João Borges Pinto Estagiário de Pós-doutoramento do, CICECO – Instituto de Materiais de Aveiro, Departamento de Química da Universidade de Aveiro

agradecimentos

First and foremost, I would like to thank my supervisor Dr. Helena Oliveira; she who accepted my initial proposal of collaboration in the middle of the year; who thought of a brilliant topic that made a compromise of my needs, my wishes, and the available time; she who has had confidence in my abilities, even when I had doubts. I would like to thank you for your guidance, your support, your positive attitude, and for giving me the opportunity, and the key, both figuratively and literally, to reach the next phase of my path. I would also like to thank my co-supervisors Dr. Iola Duarte and Dr. Ricardo Pinto. To Iola, thank you for making the metabolomics learning curve less steep, for dedicating the immense experimental time for this project, and for your help and guidance throughout the analysis and writing processes. To Ricardo, thank you for always having an open door and an open ear for a discussion, for the extracurricular hours of supervision in the chemistry building, and for your guidance and support through the experimental stages.

There were essential experiments that could not have been completed if not for the help of others. I would like to thank Ricardo for the STEM acquisition, Joana, Ivana and Iola, for the NMR, Ines for fluorescence microscopy, and Sara Fateixa for making Raman microscopy a last minute possibility. I would also like to thank Joana Carrola, Verónica Bastos, and Fernanda Rosário from our research group, whose work I was able to build on, and whose knowledge, help, and friendship have been invaluable throughout this thesis. My thanks also goes to Miguel, Rita, Márcia, Monica, and Isabel from biology, who made me feel welcome at the lab, and who have helped immensely as I tried to navigate the world of biology.

I would like to further thank the European people who, through the European Commission and Erasmus Mundus program, fund international students such as myself, giving us the opportunity and means to study, work, and travel throughout Europe. More specifically I would like to thank those involved with the Functionalized Advanced Materials Engineering Erasmus Mundus Master, especially my coordinator at the University of Aveiro, Ana Barros. Special mention also goes to all my FAME classmates and colleagues, especially Hannes, Geoffrey, and Louise for making school cool, and for all the memorable moments throughout the two years; adamantium.

Aveiro would not have felt like home without those that made me feel as if I was a part of theirs. My thanks goes to Filipe, my flatmate who went above and beyond to help me adjust to life in Portugal, whose constant support and friendship I will always cherish and remember. My other introduction to Portuguese life was my ESN buddy João, who I would also like to thank for inviting me to that first rugby match and the dinner that followed, and changing my life perhaps forever. Life would not have been the same if not for my involvement with rugby team and my amazing friends and teammates; special mention goes to Salsa Man, Zimmerman, Vilaça, Valentino, JT, Speedy, Nuno, and Capitão. I would also like to thank João, Luiz and Secundino for welcoming me into their home, for their friendship, and for all those nights of couchsurfing. Special mention should also be made of my friends, Hamed, Sara, and Pedram, in Canada, and Saghi in France, whose long distance support and technical help has saved me a number of times, and helped me stay sane.

Finally I would like to thank my parents, for their invaluable teaching in my early years, for the sacrifices they made to provide us with opportunities, and for their constant love and support; and my sisters Negin and Shirin, for making me smile and laugh, and for always believing in me.

Save the Best for Last. Save the Last for Love.

Thank you Adérito for making me live and keeping me alive.

palavras-chave

Nanopartículas de prata, AgNP, Síntese Verde, Metabolómica, Toxicidade, Linha celular HaCaT

resumo

As nanopartículas de prata (AgNPs) apresentam uma vasta gama de aplicações devido às suas inerentes propriedades físico-químicas e atividade biológica. Para além disso, a síntese verde de nanopartículas está a ser estudada como uma alternativa fiável e promissora para minimizar a utilização de substâncias prejudiciais utilizadas na síntese convencional. No presente trabalho, as AgNPs foram sintetizadas usando extratos de casca de *Eucalyptus globulus* e comparados com as sintetizadas por "Pulsed Laser Abalation in Liquids" (PLAL). Ambos os conjuntos de nanopartículas foram caracterizados por espectroscopia de UV-Visível, dispersão dinâmica de luz (DLS) e microscopia eletrónica de varrimento (SEM). A concentração de prata nas soluções aquosas de NPs foi avaliada por análise de Espectrometria de Emissão Ótica por Plasma Acoplado Indutivamente (ICP-OES). A toxicidade das partículas na linha celular de queratinócitos humanos, HaCaT, foi avaliada pelo ensaio convencional de MTT, para avaliação da viabilidade celular, e o ciclo celular foi analisado por citometria de fluxo. Finalmente, o perfil metabólico das células foi avaliado por espectroscopia de Ressonância Magnética Nuclear (NMR) e análise multivariada (metabolómica).

Os resultados da caracterização mostraram que as AgNPs foram de facto formadas e apresentaram uma ampla distribuição de diâmetros de aproximadamente 30 a 70 nm no caso das nanopartículas produzida por síntese verde (GS) e de 10 nm com distribuição estreita para as sintetizadas via PLAL. As partículas dispersas em meio de cultura celular apresentaram ligeira aglomeração, enquanto o armazenamento à temperatura ambiente não induziu nenhum efeito no tamanho final. Contudo, o “envelhecimento” resultou na formação de uma pequena quantidade de nanoestruturas com formato de agulha. O MTT indicou um IC_{50} para as células HaCaT de aproximadamente 15 μg/mL no caso das AgNPs preparadas por síntese verde e de 24 μg/mL no caso das NPs sintetizadas via PLAL. As partículas de GS também induziram redução da proliferação na dose mais baixa e extensa morte celular na dose mais elevada, com a análise do ciclo celular mostrando paragem na fase G2. Os revestimentos quer das nanopartículas de GS, quer de PLAL não induziram toxicidade nas concentrações testadas, e a interferência de AgNPs com o ensaio de MTT foi considerada insignificante. A análise metabolómica revelou que as AgNPs em concentrações sub-tóxicas causaram alterações a nível do metabolismo energético, proteção antioxidante e membranas celulares.

keywords

Silver Nanoparticles, AgNP, Green Synthesis, Metabolomics, Toxicity, HaCaT Cell line

abstract

Silver nanoparticles (AgNPs) present a wide range of applications due to their inherent physiochemical properties and biological activities. Moreover, green synthesis of metal nanoparticles is being studied as a reliable and promising alternative to minimize the use of harmful substances usually used in conventional synthesis. Here, AgNPs were synthesized using *Eucalyptus globulus* bark extract (GS) and compared against those synthesized externally via Pulsed Laser Abalation in Liquids (PLAL) technique. Both sets of particles were then characterized using UV-Visible spectroscopy, dynamic light scattering (DLS), and scanning transmission electron microscopy (SEM). The silver concentration of the aqueous solutions of NPs was also assessed by ICP-OES analysis. The toxicity of the particles on the human keratinocyte cell line, HaCaT, was evaluated using MTT, a conventional viability assay and cell cycle analysis was performed using flow cytometry. Finally, cellular metabolomics profiling was evaluated using NMR spectroscopy and multivariate analysis.

Characterization results showed that AgNPs were indeed formed; presenting diameters of approximately 30 to 70 nm, and a wide size distribution for the GS route and 10 nm with a narrow distribution for the PLAL synthesis. Dispersion of particles in cell culture media promoted a slight agglomeration, while aging of particles at room temperature did not have an effect on their final size. Nevertheless, this aging time resulted in the formation of a small amount of needle-like nanostructures. MTT results indicated an IC_{50} value of approximately 15 ug/mL of silver for the GS route and approximately 24 ug/mL for the PLAL AgNPs. The GS particles also induced slower proliferation at the low concentration and extensive cell death at the high concentration, with cell cycle analysis showing arrest at the G_2 phase. Neither the coating from the GS, nor the PLAL particles induced any toxicity at the concentrations tested, and the interference of AgNPs with the MTT assay was found to be negligible. Metabolomics using ^1H NMR revealed that sub-toxic concentrations also caused significant alterations in energy metabolism, membrane modifications, and antioxidant protection in a dose and particle dependent manner. More specifically, GSH levels saw an increase, whereas amino acids, creatine compounds, and choline compounds all saw decreases. The GS AgNPs induced a stronger response in HaCaT cells than that of the PLAL.

TABLE OF CONTENTS

List of Acronyms

A549	Cancerous human lung cell line
AC1 AgNPs	Autoclaved silver nanoparticles, Batch 1
AC2 AgNPs	Autoclaved silver nanoparticles, Batch 2
ADME	Absorption/Distribution/Metabolism/Excretion
ADP	Adenosine Diphosphate
AFM	Atomic Force Microscopy
Ag	Silver
AgNP(s)	Silver Nanoparticle(s)
ANOVA	Analysis of Variance
ANSES	Agence nationale de sécurité sanitaire de l'alimentation, de l'environnement et du travail
ATP	Adenosine Triphosphate
Au	Gold
AUC	Analytical Ultracentrifugation
BBB	Blood Brain Barrier
BEAS-2B	Normal human lung (bronchus) cell line
Chang	Normal/Cancerous human liver cell line
CNT	Carbon Nanotube
CoA	Coenzyme A
CoQ	Coenzyme Q
DAC AgNPs	Double Autoclaved silver nanoparticles
DAPI	4',6-diamidino-2-phenylindole
DMEM	Dulbecco's Modified Eagle Medium
DMSO	Dimethyl sulfoxide
DSC	Differential Scanning Calorimetry
EDTA	Ethylenediaminetetraacetic acid
EDX	Energy Dispersive X-Ray Spectroscopy
EGB	*Eucalyptus globulus* Bark
ER	Endoplasmic Reticulum
FBS	Fetal Bovine Serum
FEG SEM	Field Emission Gun Scanning Electron Microscope
FSC/SSC	Forward/Side Scatter
FT	Fourier Transform
FTIR	Fourier Transform Infra-Red Spectroscopy
GAg(NP)	Green Chemical Synthesis Silver nanoparticles
GPC	Gel Permeation Chromatography
GPC	Glycerophosphocholine
GS AgNPs	Green Chemical Synthesis silver nanoparticles
GSH	Reduced Glutathione
HaCaT	Normal human keratinocyte (skin) cell line
HEK	Human Epidermal Keratinocyte derived cell line
HeLa	Cancerous human cervix cell line
Hep-G2	Cancerous human liver cell line
HPLC	High Performance (Pressure) Liquid Chromatography
HRMAS NMR	High Resolution Magic Angle Spinning NMR
Huh7	Cancerous human liver cell line
IC_{50}	50% Inhibition Concentration
ICP AES	Inductive Coupled Plasmon Atomic Emission Spectroscopy
ICP OES	Inductive Coupled Plasmon Optical Emission Spectroscopy
IMR-90	Normal human lung cell line

ISO	International Standards Organization
L02	Normal human liver cell line
LC/GC MS	Liquid/Gas Chromatography Mass Spectroscopy
LDH	Lactate Dehydrogenase
LOAEL	Lowest Observable Adverse Effect Level
LV(s)	Latent Variable(s)
MIC	Minimum Inhibitory Concentration
MS	Mass Spectrometry
MSC	Mesenchymal Stem Cells
MTT	3-(4,5-dimethylthiazol-2-yl)-2,5-diphenyltetrazolium bromide
MVA	Multivariate Analysis
NAC	N-Acetyl Cysteine
NADH	Reduced Nicotinamide Adenine Dinucleotide
NMR	Neutron Magnetic Resonance
NOAEL	No Observable Adverse Effect Level
NP(s)	Nanoparticle(s)
NTA	Nanoparticle Tracking Analysis
OPS AgNPs	One Pot Synthesis silver nanoparticles
P53	A tumour suppressor protein
PAg(NP)	PLAL Synthesis silver nanoparticles
PBS	Phosphate Buffered Saline
PC	Phosphocholine
PC(s)	Partial Component(s)
PCA	Partial Components Analysis
PCr	Phosphocreatine
PDI	Polydispersity Index
PEG	Polyethylene Glycol
PI	Propidium Iodide
PLAL	Pulsed Laser Ablation in Liquids
PLS-DA	Partial Least Squares Discriminant Analysis
ppm	Parts Per Million
PTC	Phosphatidylcholine
PVA	Polyvinyl Alcohol
PVP	Polyvinyl Pyrrolidone
Q^2	Predictive ability of a model
QSPR/QSAR	Quantitative Structure Activity/Property Relationship
R^2	Coefficient of determination, fit of the model
RF	Radio Frequency
ROS	Reactive Oxygen Species
SD Rat	Sprague Drawley Rat
SEC	Size Exclusion Chromatography
SEM	Scanning Electron Microscopy
SOD	Superoxide Dismutase
SPR	Surface Plasmon Resonance
STEM	Scanning Electron Microscopy in Transmission Mode
TCA	Tricarboxylic Acid Cycle
TEM	Transmission Electron Microscopy
TiO_2	Titanium dioxide
TMS	Tetramethylsilane
TSP	Trimethylsilyl Propanoic Acid
TXI Probe	Triple Resonance Probe

U251 MG	Cancerous human brain cell line
UV Scaling	Unit Variance Scaling
UVB	Ultraviolet B Radiation
VIP	Variable Importance in the Projection
XPS	X-Ray Photoelectron Spectroscopy
XRD	X-Ray Diffraction

List of Figures

Chapter I: Introduction

I.1 THE NANO WORLD

As nanotechnology and nanomaterials become more commonplace, so does the probability of common people having contact with them; thus, government associations have recently begun to look deeper into their safety. The International Organization for Standards (ISO) defines nanomaterials as those with a length of 1 to 100 nanometres in any of their three dimensions, as well as those slightly outside that range displaying nano specific behaviour [1]. Nanomaterials are then divided into nano-objects and nano-structured materials with inner or surface structures at the nanoscale (e.g. nanoporous systems, nanofoams). Officially, a nanoparticle (NP) is a nano-object that has all three dimensions in the nanoscale, where typically, the ratio of the longest and shortest axes does not exceed three times. Where it does, the terms "nanofiber", a nano-object having two dimensions in the nanoscale, and “nanoplate”, a nano-object with one dimension in the nanoscale, can be applied [1].

Nanotechnology has been hailed as revolutionary, often being compared with the invention of the steam engine and automobile, or the growing use of computers and later the Internet at the end of the twentieth century. Nanoscience, or rather the “nano approach”, can be applied to almost any industry or process, making them more efficient, less costly, and more environmentally friendly. One of the first areas to benefit from the rise of nanotechnology was the electronics industry. This was closely followed by applications in composite materials; making objects stronger, lighter, harder, waterproof, rust proof, or with special optical or magnetic properties, using a fraction of the amount of bulk material needed. Nowadays one of the most thriving domains is the realm of biology and medicine; here nanomaterials have a wide range of applications including sensors, prosthetics, sanitation, imaging, detection, drug delivery, and omic techniques [2].

However, the downside of such exponential growth is a lack, or rather "lag", of regulation. Although nanomaterials are usually a new form of previously approved materials, their unique properties at this scale are reason enough that they be classified and treated as novel materials and thus subject to re-approval by governing bodies [3].

In 2007, the European Commission put into effect REACH, the European Regulation on Registration, Evaluation, Authorization and Restriction of Chemicals. The European Chemicals Agency, created in the same vein, works alongside national authorities in the implementation and administration of REACH [4]. A large part of this document, which has since been updated in 2012, concerns the regulation of nanomaterials, particularly with regards to their risk assessment. The regulation is indeed timely, considering an estimated market of 11 million tonnes of nanomaterials at a market value of EUR 200 billion; and a forecast of up to EUR 2 trillion in products by 2015 [4]. Nowadays, the three nanomaterials dominating the global production market are silver, zinc oxide, and titanium dioxide nanoparticles, at 452, 34 000, and 88 000 tonnes/year respectively [5].

In this light, the general aim of this thesis is to characterize the toxicity of "Green Synthesis" silver nanoparticles (AgNPs) by first applying a comprehensive physico-chemical characterization, followed by conventional toxicity studies, and finally an NMR metabolomics approach. This chapter will first provide a general background on the four topics involved: particle synthesis theory and applications in biosynthesis; characterization techniques for nanomaterials and their importance; toxicology workflow and the conventional assays utilized; and finally omic techniques, metabolomics, and cellular metabolism. An extensive state of the art on silver nanoparticles will then be provided, covering applications, properties, and a full review of the latest studies in toxicity and metabolomics. Lastly, the aims of this work and a plan of the thesis will be presented.

I.2 PARTICLE SYNTHESIS THEORY

Material synthesis can be divided into two general categories, namely that of top-down and bottom-up approaches. Top down methods involve starting from a bulk material and removing matter, and bottom-up methods involve the assembly of smaller pieces of matter such as atoms or molecules [6]. The latter is particularly applicable for the synthesis of nanoparticles as they are close in scale to the realm of molecules and clusters. For this specific case and in its simplest form, the synthesis of metal nanoparticles in solution starts with the formation of hydroxilated complexes, followed by the formation of clusters, then primary NPs, their growth and maturation (Figure 1) [7]. This process is governed by the standard nucleation and growth theory, which can also be applied to liquid condensation, crystallization of solids, phase changes in alloys and other colloidal phases [7].

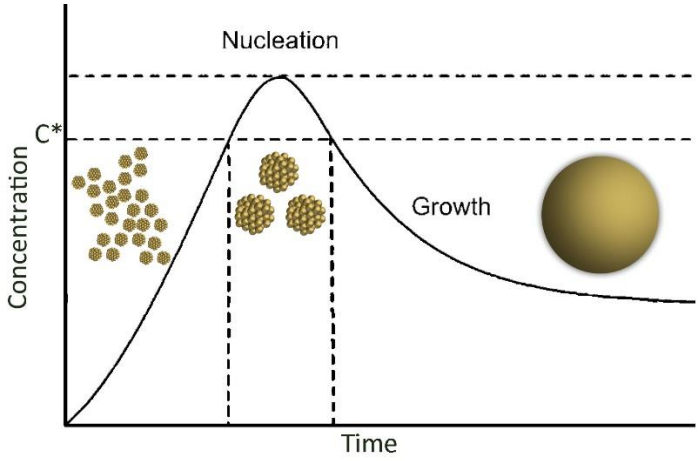

Figure 1: Particle nucleation kinetics profile of concentration over time, where C is the critical concentration.*

The hydroxilation of the metal ions occurs almost instantaneously after their dissolution in water; the exact complexes formed are related to the electro-negativity of the atom, its charge, and the pH of the solution. These complexes can then self-assemble to form polyions and metal clusters; in the latter case another species would be required to aid in the redox reaction. The concentration and size of such clusters would continue to grow until a critical radius, and a critical concentration of that radius, are reached [8]. The satisfaction of these criteria leads to the formation of nucleation sites, or nucleation; this event is based on the free energy given by the following equation:

$$\Delta G = -\frac{4}{3}\pi r^3 |\Delta G_v| + 4\pi r^2 \gamma$$

Where ΔG is the free energy of the system, ΔG_v the difference of free energy between the old phase (the ionic solution) and the new phase (the NPs), γ the interfacial energy at the crystal-medium boundary, and *r* the radius of the nucleus [8].The first term, having to do with the supersaturation of the solution and the volume of the clusters is always negative, while the second term, having to do with the surface energy of the particles is positive as it requires energy [9]. A graphical representation, showing the Gibbs free energy versus the radius is given in Figure 2.

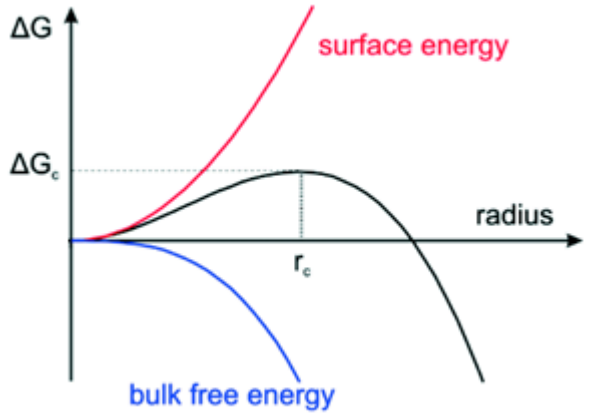

Figure 2: Gibb's free energy for particle nucleation given as the combination of surface energy and bulk free energy, where r_c is the critical radius [10].

The rate of nucleation is dependent on the supersaturation state *S*, the temperature *T*, and the surface energy of the particles γ, given by the equation:

$$J = A * \exp\left(\frac{-16\pi\gamma^3\Omega^2}{3k^3T^3ln^2S}\right)$$

Where Ω is the molecular volume, and *A* and *k* the Arrhenius and Boltzmann constants respectively. Homogenous nucleation occurs within the solution, whereas heterogeneous nucleation occurs at other surface boundaries; for example the vessel wall, impurities, or the interface with air [9].

For the formation of a uniform size distribution the nucleation and growth regimes need to be decoupled [11]. This means that the nucleation rate must be much faster than the cluster generation rate, so that all the available clusters are consumed and the system moves away from the critical concentration region. In this way, any further clusters generated are used for the growth of particles rather than the generation of new nuclei. This is often called the LaMer growth model [11]. After the formation of the nuclei, growth can also occur via Ostwald ripening, digestive ripening, or coalescence. Ostwald ripening is the gradual dissolution of smaller particles and their redeposition onto larger ones [12]. The physical reason behind this being that the higher surface area of smaller particles creates

greater surface energy and results in higher solubility. Digestive ripening is the opposite phenomenon, where larger particles dissolve to allow smaller particles to grow, usually due to the surface tension properties [13]. Coalescence is the flocculation or joining of two or more particles, first as agglomerates and then as aggregates. The rate of growth can in turn fall under two regimes; diffusion limited or surface reaction limited. The former is limited by the rate at which the clusters can reach the surface of the particles, whereas the latter is limited by the surface reaction for their incorporation [13]. Depending on the nuclei's size and the concentration of the precursor in solution, the growth may lead to a self-sharpening of the size distribution, or its broadening [9, 13]. Further discussion on the theory of nucleation and growth is outside the scope of this report.

I.3 NANOPARTICLES SYNTHESIS: GREEN SYNTHESIS

Parallel to the rise of these novel nanomaterials, the chemical industry has also evolved, becoming more concerned with chemical sustainable development. Innovations which strive to overcome challenges in reducing pollution levels and consumption of resources are greatly valued and a solid shift has been made towards minimizing their impact on the environment. It was Paul Anastas and John Warner that developed the Twelve Principles of Green Chemistry in 1998, in order to explain how to implement green chemistry concepts and other sustainable development ideas into practical terms. In general, the list targeted design of products and processes that minimize the waste of materials and energy; in fact, it advocated the prevention of waste as the best method of its disposal. With regards to materials, it advocated the use of those which have little or no toxicity or impact on human health and the environment, while maximizing the amount of raw material in the final product [14].

For the synthesis of metallic NPs, the most common method is chemical reduction in solution [15]; where hydrazine, sodium borohydrate or hydrogen are used as reducing agents [16, 17], and polymers such as chitosan [18], cellulose [19], and copolymer micelles can be used as stabilizing agents [20]. Aside from their intrinsic toxicity, some of these compounds require organic solvents such as ethanol, dimethyl formamide, ethylene glycol, tolulene, and chloroform [21]. Not only are these chemicals harmful to the environment, but also their residues on NPs can be a source of surface contamination, leading to adverse effects on consumers [22]. While physical approaches to synthesis pose a lower risk to human health and the environment, offering high purity and selective size control of NPs, they require complicated instruments and high power consumption [23]. These result in indirect environmental effects as well as high operating costs.

On the other hand, green synthesis is deemed attractive because it is sustainable, cheaper, quicker and environmentally friendly as compared to the mentioned conventional methods. While there are many approaches for making a synthesis process more "green", a particularly interesting one is biosynthesis. In these, life forms such as bacteria [24], yeast [25], fungi [26], algae [27], and plants are used in whole, or in part, to synthesize organic, inorganic or composite materials [23]. These routes have been recently applied to synthesize a variety of nanomaterials [28], particularly nanoparticles [29].

The underlying mechanism of biosynthesis is the exploitation of the natural defence of living organisms against heavy metals in their environment. Some of these mechanisms include: excretion

across membranes [30], enzymatic oxidation or reduction [31], accumulation of NPs outside plasma membrane [32]; chelating with peptides [33]; efflux pump systems [34]; metal precipitation as carbonates, phosphates, and sulphides; and volatilization through methylation and/or ethylation [35]. The rate of the above mentioned mechanisms is dependent on: metal salt uptake, metal inactivation, storage, and large biomass production; with the first being the critical step [33]. While these steps apply to synthesis within living organisms (intracellular), the same biomolecules involved can sometimes be used to induce the same reactions outside the organisms (extracellular).

In the case of bacteria, the most commonly used mechanism is the reduction of heavy metal ions in the environment to NPs. As mentioned earlier, the synthesis can be intracellular or extracellular; for bacteria this means allowing the bacteria to grow in media and removing the cell-free supernatant after centrifugation. The most commonly studied metal NPs are gold (Au) and silver (Ag), usually via bacteria isolated from mines and grown in metal-salt rich conditions [36, 37, 38]. Though advantageous compared to chemical and physical approaches, microbial synthesis has certain drawbacks as well. For example, NP characteristics are governed by parameters such as pH, temperature and reaction time. However, modifying pH or temperature might also effect the livelihood of the microbes, thus hindering the bioreduction process [23]. Moreover, special facilities and long incubation times are required, especially considering the risks that some of the organisms pose to human health; thus translating to high operating costs.

I.3.1 Plant Synthesis

While bacteria offer a low cost method of producing specific nanomaterials, plant biomass and plant extracts have been shown to offer even cheaper, easier and higher volumes in production [39]. Similar to bacterial biosynthesis, plant biosynthesis can occur using living or inactivated biomasses. Gold accumulation in plants has been documented for decades, especially for the indication of gold deposits in mining applications [40]. It was Gardea-Torresdey *et al.* who first demonstrated the synthesis of gold and silver nanoparticles inside a living plant; namely the *Medicago sativa* or "alfalfa" [41]. The same plant was later used for the biosynthesis of other NPs such as iron oxide [42], as well as titanium-nickel alloys [43]. Other plants used in a similar fashion include wheat [44], and *Avena sativa* (oat) [45], for the synthesis of various morphologies of Au. It is important to note that different parts of the plant accumulate metals of different size, size distribution and morphology, based on the available biomolecules in those parts [46]. A particularly interesting application of this process is the use of the *Sesbania drummondii* biomass with accumulated AuNPs to catalytically reduce hazardous and toxic pollutants such as 4-nitrophenol [47].

The main disadvantage of using plant biomass is the need of post-synthesis processing to extract or release the NPs. This can be performed by physicochemical methods such as freeze-thawing, heating, or osmotic shock, which may interfere with the morphology and aggregation state of the NPs; or alternatively, via enzymatic digestion, which is both expensive and difficult considering the rigidity of plant cell walls [48]. Although plant biomass offers advantages over microbial synthesis, it is best reserved for niche applications where the living plant itself is an essential component, as in the case for *S. drummondii*.

Therefore, it becomes easier to understand why the majority of recent research has focused on extracellular plant biosynthesis; more commonly named biosynthesis via plant extracts. The plant

biomass, which may include the root, stem, leaves, bark, flower or seed, is processed by creating a broth whereby the compounds responsible for the reduction and stabilization are extracted and added to the metal salt solution [49]. These compounds can generally be divided into five families of terpenoids, flavanoids, polysaccharides, proteins, and alkaloids. Flavanoids, are water soluble polyphenolic compounds, that together with carotenes, are responsible for the colouring of fruits, vegetables and herbs [50]. Whereas terpenoids are from a lipid family and responsible for the scent, flavour, and colour of certain plants. Both flavanoids and terpenoids have been shown to act as reducing agents, by donating electrons through the enol-to-keto conversion, as well as contributing to the capping of the NPs. In sugars, it is believed to be the free aldehyde groups that are the main reducing agents, while for proteins it is said to be the interactions with the amine groups of certain peptides [23]. As an example, Figure 3 shows the oxidation mechanism of Gallic acid and the simultaneous reduction of ionic silver to metallic silver.

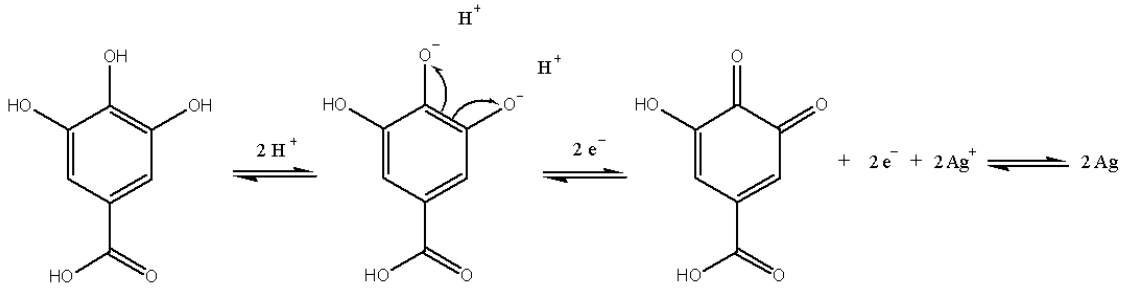

Figure 3: Oxidation mechanism of Gallic acid and the simultaneous reduction of ionic silver to metallic silver.

Although biosynthesis is attractive because of the advantages it offers, the limited capacity of plant and plant extracts for reducing metal ions results in the process being efficient only for metal ions with large electrochemical potential, such as Au and Ag [51]. Moreover, variations in regional soil, climate and plant strains cause minor differences between each batch in terms of the reducing compounds and capping agents, making it difficult to replicate work on a global scale.

I.4 PHYSICO-CHEMICAL CHARACTERIZATION OF NANOMATERIALS

As with the characterization of any novel object, a series of sequential steps must be followed. In this case, to assess the safety of nanomaterials and more specifically nanoparticles, the inherent properties must be evaluated. Working backwards, safety requires risk assessment; risk assessment requires various toxicity and exposure studies; and toxicity studies require knowledge regarding the material being tested, namely the physicochemical properties and characteristics that it holds.

However, in trying to evaluate the risk of nanomaterials, there are a number of challenges that present themselves; not only due to the change in scale and large variability within each material, but also because the adaptation of conventional instruments and discovery of new methods requires time. Some of the more prominent challenges, as outlined in ANSES's (Agence National de sécurité sanitaire de l'alimentation, de l'environnement, et du travail) report on the "Evaluation of the Risk of Nanomaterials" are: a lack of standardization (in terms of terminology, reference materials, test

methods, calibrations, etc.), realistic doses, and studies of error margins and confidence levels [52]. In order to better compare toxicology and clinical studies of nanomaterials, it has been often recommended that a comprehensive characterization of the material first take place.

ISO has proposed the following list of physico-chemical parameters pertinent to nano objects: particle size and size distribution, aggregation and/or agglomeration state, shape, specific surface area, composition, surface chemistry, surface charge, solubility, and dispersibility [53]. The high surface area to volume ratio of NPs is what sets them apart from their bulk counterparts; and it is these physicochemical parameters that set NPs apart from each other.

I.4.1 Techniques for Characterization

While there are many techniques that can be used for the characterization of NPs, the following is a list of the most commonly used instruments and tests available. In order to visualize the particles, in other words their morphology and approximate size, a number of microscopy techniques can be used; optical microscopy, light/florescence/Raman confocal microscopy, scanning or transmission electron microscopy (SEM, TEM), and atomic force microscopy (AFM). These can be coupled with image analysis software packages in order to determine size distribution. Diffraction techniques such as x-ray diffraction (XRD), x-ray photoelectric spectroscopy (XPS), and energy dispersive x-ray spectroscopy (EDX), can be used to determine elemental composition for a powder as a whole, on the surface, or at a particular point, respectively [54].

Fourier Transformed Infrared spectroscopy (FTIR) can be used to determine functional groups, as well as the mass of polymer particles or organic coatings. Differential scanning calorimetric (DSC) and thermogravimetric analysis (TGA) can be used to determine the melting point, glass transition temperature, and composition, respectively. While BET analyzers are generally used for the determination of porosity and specific surface area, zeta potential analyzers are used to determine surface charge. Particle size distribution can be determined using several light scattering techniques, with the most common being dynamic light scattering (DLS) [55], or by more novel methods such as nanoparticle tracking analysis (NTA) [56]. The nuclear magnetic resonance (NMR) of elements such as hydrogen, carbon, and nitrogen, can be utilized to determine the environment of those elements, the structure of the compounds, as well as to quantify their ratios [57].

As NPs are often coated, sometimes with small organic molecules such as peptides, or larger ones such as proteins, chromatography columns (for example HPLCs) can be used to separate the various molecules, while UV-Vis, mass spectrometers (MS) and NMR can be used to determine their concentration and or determine their composition respectively. Similarly, gel permeation chromatography (GPC) or size exclusion chromatography (SEC) can also be used to separate compounds, prior to characterizing their composition [58].

Characterizing the surface of NPs is particularly important for toxicity studies, for it is the first point of contact with the biological environment, and determinant of the particles' corona in that fluid. The change in surface chemistry in biologically relevant media often results in changes in the agglomeration state, hydrodynamic diameter, and surface potential; therefore, it is equally important to follow the physicochemical evolution of the NPs once they are in the targeted environment [58].

I.5 TOXICITY STUDIES

Risk assessment is generally divided into two main components: effect assessment (or more commonly toxicity), which covers hazard assessment and dose-response; and exposure assessment, which covers route, amount and frequency of release, bioavailability and bioaccumulation. The study of toxicity then divides into *in vitro*, *in vivo*, *ex vivo*, *in silico*, and environmental studies, though the five categories are not always mutually exclusive (Figure 4) [59]. *In vitro* methods are those performed with cultured bacteria or mammalian cell lines. While *in vivo* methods make use of live animal models, *ex vivo* methods study those animal models *post mortem*. *In silico* methods have emerged with the recent developments in computing power; they use informatics and or simulations to model cell behaviour. Furthermore, they can be used to study, sometimes quantitatively, the relationship between chemical compounds and biological activity; also known as Quantitative Structure-Activity Relationship (QSAR), or Quantitative Structure-Property Relationship (QSPR) [60]. Environmental toxicology, in turn, makes use of any of these methods to study the effects of potential toxins on the environment [59].

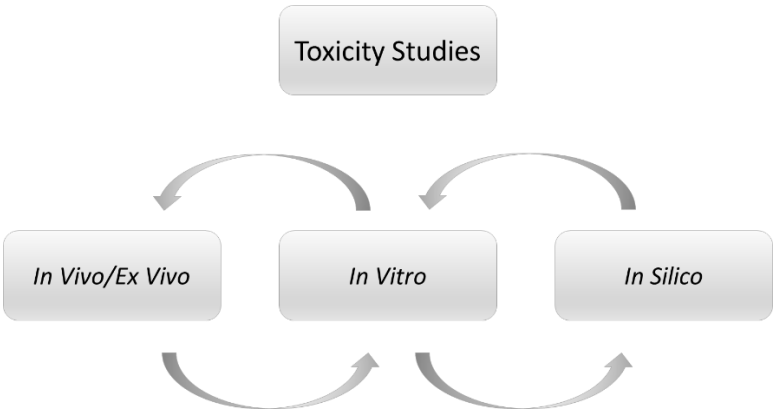

Figure 4: A schematic of the relationship between various forms of toxicity studies.

The workflow of such studies generally commences with *in vitro* studies in relevant models, and continues to a progression of *in vivo* models, depending on the nature of the agent being studied (Figure 4) [59]. For example in the case of a new pharmaceutical product, after thorough physico-chemical characterization, the compound is subject to *in vitro* testing, not only for its effectiveness as a drug, but also to test any toxicity it might induce. These are followed by studies in various established animal models, depending on the final end point of the product, and a progression from smaller animals to mammals that mimic human physiology best [61]. Through these, dose thresholds, such as the No Observable Adverse Effect Level (NOAEL), Lowest Observable Adverse Effect Level (LOAEL), as well as the therapeutic range and the safe dose for a "first-in-man" study, can be established. At this stage, if approved by a governing body, the product moves from pre-clinical, to clinical trials, whereby it is tested in three different phases, on humans [61]. Though consumer products and chemicals are not subject to as rigorous a process as pharmaceuticals, information regarding their toxicity on standard animal models and the environment is still required by regulating bodies such as REACH [4].

I.5.1 IN VITRO TOXICOLOGY

Toxicity studies can also be classified based on the route of entry, the most common of which include: inhalation, ingestion, injection, and transdermal delivery. It is sometimes suggested that a preliminary *in vivo* study based on the route of entry (or primary exposure organ) be conducted first, in order to determine the absorption, distribution, metabolism, and excretion (ADME) in the animal model, as well as the target organs (or secondary exposure organs). Then, based on those results, *in vitro* studies be conducted on a single, homogenous cell type, in order to ascertain more specific mechanisms and endpoints. In the ideal scenario, the preliminary *in vivo* would be followed by thorough *in vitro* work, and then performed in parallel as explained above. However, as is often the case, the cost, effort, time and special facilities required for animal experiments, make it difficult to perform the studies as explained. Added to this are various legislatures put into effect in recent decades [62], that aim to replace, reduce, and refine the use of animals for scientific purposes, as suggested by Russell and Burch's "3 Rs" in 1959 [63]. Thus, *in vitro* studies, though lacking complexity, are an attractive point of commencement.

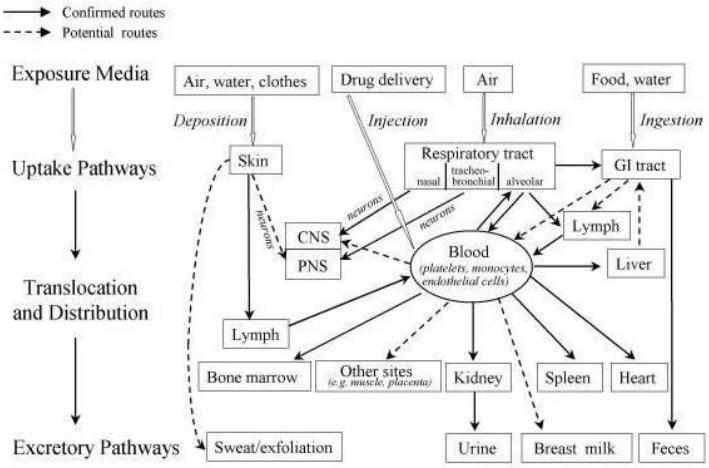

Figure 5: Biokinetics of Nano-sized Particles. Showing absorption, distribution, metabolism, and excretion of NPs [64].

There are a number of approaches to assessing the *in vitro* toxicity of a material, each with their own battery of available assays. The most common is tracking the viability or vitality of the cells, while others include, uptake, membrane integrity, genotoxicity and gene expression, immunogenicity and inflammatory effects, and oxidative stress [65, 66]. Viability testing itself can be subdivided into three types of assays; colonogenic assays, in which colonies of cells are counted by visual inspection [67], flow cytometry or image analysis [68, 69]; metabolic assays, in which the reduction of tetrazolium salts to formazan dyes [70], or total ATP content [71], is linked to the percentage of metabolically active cells; and cell cycle analysis, in which cell DNA is analyzed to determine if and at what point cell cycle arrest occurs [72]. A typical end point for these assays is the determination of the concentration that induces a 50% inhibition (IC_{50}).

Uptake deals with the amount that passes through the cell membrane, and the location in which they accumulate. It is typically studied visually using TEM or fluorescence microscopy; though quantitative

results can be obtained using Inductive Coupled Plasma Atomic Emission Spectroscopy (ICP-AES) or flow cytometry [73]. Other novel techniques include Raman confocal microscopy for Raman active materials [74], and susceptibility to a magnetic field for magnetic particles [75]. Membrane integrity assays exploit the ability of intact cell membranes in excluding various dye compounds such as Trypan blue [76], propidium iodide [77], and Neutral Red [78]; or the release of internal cell components such as the enzyme lactate dehydrogenase (LDH) into the extracellular medium upon cell death [79]. Genotoxicity assays use the frequency and extent of single or double DNA strand breaks to determine the amount of DNA damage; the most popular techniques include the cytokinesis-blocked micronucleus and Comet assays [80, 81]. Alterations in gene expression can be tracked using either real time PCR [82] or DNA microarrays [83] for specific genes, or other omic techniques when a broader approach is required.

Immunogenicity or inflammatory assays measure the amount of pro-inflammatory cytokines such as IL-6 or IL-8; this can be done directly using ELISA techniques [84], or indirectly by using PCR to measure mRNA expression of IL-18 or its receptor [85]. Similarly, oxidative stress can be measure directly, with dyes or compounds that bind to reactive oxygen species (ROS) [86]; or indirectly, by looking at the cell's response to ROS by measuring the amount of antioxidants such as superoxide dismutase (SOD) [87], or glutathione (GSH) [88].

I.5.2 Challenges Pertaining to the Study of Nanoparticles

As discussed in the previous section, the physicochemical characterization of NPs as compared to their bulk counterparts, requires more extensive testing to confirm the obtained values. Similarly, the toxicity testing of NPs also requires modifications of the conventional testing methods. In this case it is the NPs unique properties that cause them to interfere with the assays. Of these properties, first and foremost, is the high surface area-to-volume ratio that results in higher adsorption capacities, leading to numerous consequences [66]. A high adsorption capacity means that once immersed in biological fluids such as serum or cell culture medium, the particle's size, shape, surface charge and surface chemistry will change. The change will depend on the initial properties of the particle, as well as what is available in that medium. This may relay stealth to NPs *in vivo*, preventing their being marked as invading particles by the immune system, through a process called opsonization. Thus, either allowing them to remain longer in the bloodstream, or to facilitate their uptake into the cells themselves [89]. For *in vitro* cell culture, this process of adsorption results in the depletion of proteins and nutrients from the media, essential to cell survival [90]. Furthermore, higher adsorption capacities may also interfere with assays themselves. Carbon nanotubes (CNTs) and porous silica were able to adsorb the dyes of viability assays leading to false negatives [91, 92]; while in an assay measuring calcium ions, negatively charged chitosan NPs bound to those calcium ions [93]. In another study, AgNPs were able to adsorb LDH, one of the most common markers of membrane leakage, leading an underestimation of the LDH leakage [94]. Finally, adsorption allows contaminants to remain longer with the particles, as is the case with CNTs and heavy metal catalysts [95].

Similarly, the unique optical properties of NPs can interfere with spectroscopy techniques; whereby the particles' either scatter the incident rays causing false positives [96], or quench the intensity of the fluorescing dyes they are bound to causing false negatives [97]. Many NPs allow for the dissolution of metal ions; not only does this lead to direct interference with the assay dyes and substrates [98], but it also causes a change in pH, which then indirectly affects the assay [99, 100]. Finally, the high

catalytic or redox capacity of NPs may lead to the direct oxidation or reduction of assay dyes and substrates [101].

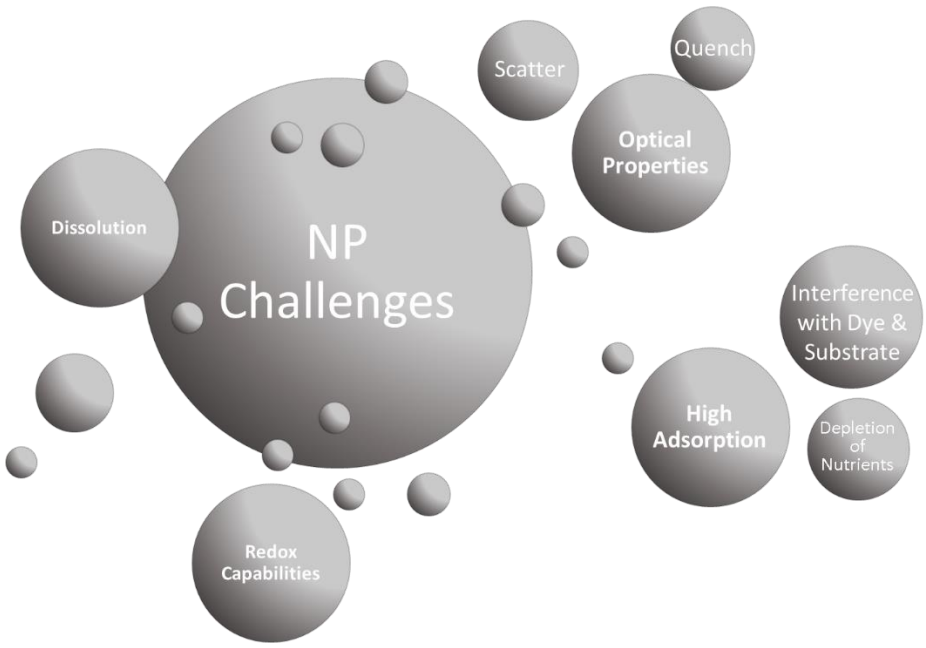

Figure 6: Graphic of NP properties and their interference with toxicology assays.

I.6 METABOLOMICS

Omic techniques are those dealing with fields of study in biology ending in "-omics"; they most commonly include, but are not limited to: genomics, transcriptomics, proteomics, and metabolomics. Their approach is the collective characterization and quantification of biological molecules: DNA, RNA, proteins, and metabolites, respectively (Figure 7) [102].

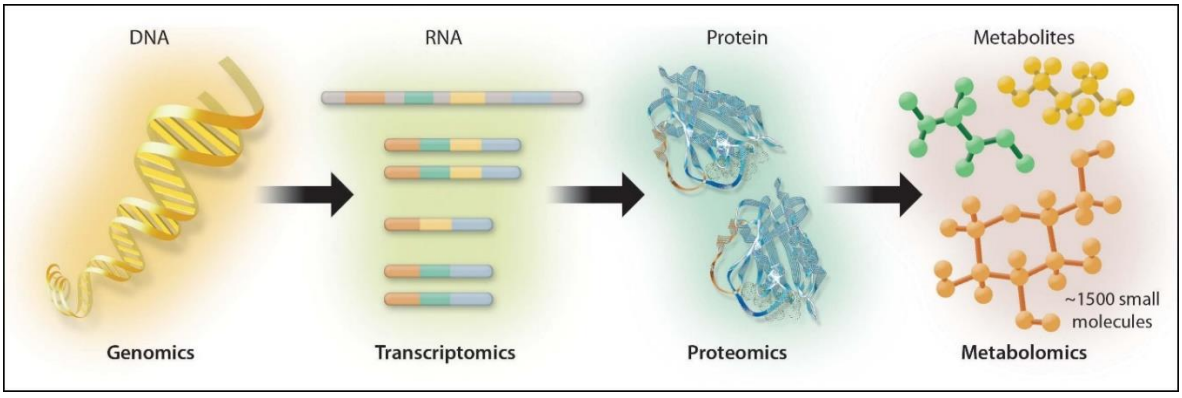

Figure 7: Schematic of the relationship between omic technologies as applied to biological systems [103].

The information offered by the four techniques is complementary, and offers a wider and deeper understanding of biological processes, in what is termed "systems biology". While genomics deals with the entire set of coding and non-coding DNA of a species, transcriptomics looks at the genes that are expressed and translated into RNA. As gene expression is influenced by events in the environment, it is a good preliminary indicator of cellular response. RNA in turn codes for proteins, which can be studied through proteomics; this is a broad field that ranges from post-translational modifications, to protein-protein interactions. Finally, metabolites, the subjects of metabolomics, are small molecules (less than 1kDa) that are the end products left behind by physiological processes. They reflect upstream changes in genes and proteins, though are equally capable of causing those changes as a response to alterations in the cell environment [104]. As metabolomics offers a snap shot of the physiology of the cell, it is a useful method in determining cell response to stimuli such as toxins.

In order to analyse and interpret alterations in the metabolome, an understanding of cellular processes and metabolic pathways is required. While an explanation of all cellular processes and metabolic pathways is outside the scope of this report, there are a number of important metabolic pathways in humans that will be discussed. Glucose is the substrate of two major metabolic pathways depending on oxygen availability. Under aerobic conditions glycolysis occurs, a process in which glucose is transformed into pyruvate, to be then used by the tricarboxylic acid (TCA) cycle, releasing energy for cell use. Under anaerobic conditions however, the pyruvate is transformed into lactate. Glucose itself can be obtained from three sources: directly from the bloodstream; through gluconeogenesis, by building it from smaller precursors; or through glycogen degradation, by breaking down previously stored polysaccharides ([105] for a review).

The TCA cycle is the process by which acetate in the form of acetyl-CoA, is oxidized to generate chemical energy, as adenosine triphosphate (ATP). The process can be divided into three stages; first the oxidation of fatty acids, glucose, or amino acids, to give acetyl-CoA; second, the oxidation of acetyl groups through the TCA, yielding four electrons; third, the electrons are transported to the mitochondria by NADH, to ultimately reduce O_2 to H_2O and generate ATP. The latter step, with NADH acting as a reducing agent, is also called oxidative phosphorylation or the electron transport chain . High concentrations of ROS have been shown to inhibit parts of the TCA cycle; to compensate, cells may use an alternative pathway of generating energy such as glutaminolysis. Glutamine, an essential amino acid, can be lysed to glutamate and ammonium, and further transformed to give oxaloacetate, pyruvate and lactate. Moreover, glutamate can also be combined with two other amino acids cysteine and glycine to give the antioxidant GSH, mentioned in the previous section.

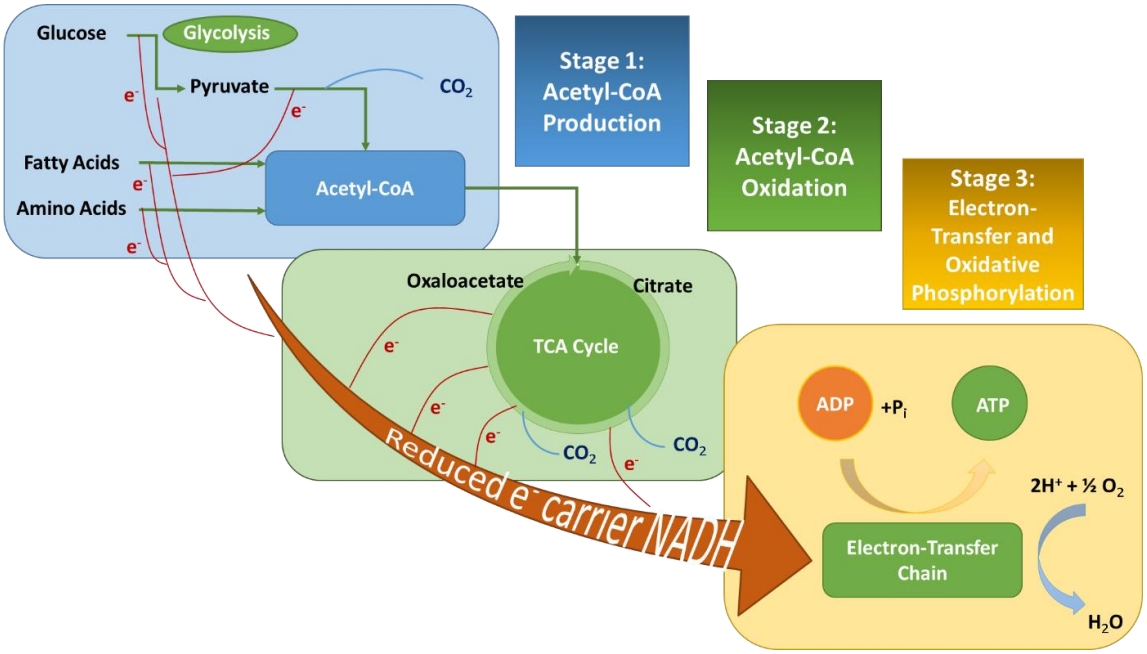

Figure 8: Tricarboxylic Acid Cycle based on various images in [106].

As these cellular processes are essential to most cells, they are typically the starting point for verifying metabolomic analysis. In studying toxicity through metabolomics, alterations in basic cell functions are followed by examining conventional pathways for cells under duress. Alterations that fall outside of stress-induced pathways are then explored further.

I.7 State of the Art on the Use, Synthesis and Toxicity of Silver Nanoparticles

I.7.1 Applications of AgNPs

Silver has been used for a large variety of applications throughout the millennia, including currency coins, ornaments, jewellery, tableware and utensils, and sometimes even as medicine [107]. Historically such uses include silver films for the preservation of water and wine by ancient Phoenicians, silver powders as anti-disease agents by the ancient Egyptians, and more recently silver nitrate for the prevention of gonococcal opthalmia neonatorum in 1884 [108]. Currently the main market for silver nanoparticles (AgNPs) is as an antimicrobial agent; however, they are also ideal candidates for molecular detection and cellular imaging due to their surface plasmon properties and signal enhancement [109], as well as applications in photothermal therapy for cancer treatment [110]. Outside of medical antimicrobial applications, these particles have also been used for air [111], water [112], and waste water disinfection [113], in paints [114], food packaging, clothing, linen, cosmetics, and even commodities such as toothpaste [115].

The discovery of antibiotics in the late nineteenth century led to a rampant expansion of the field and their widespread use. In turn, the overuse of antibiotics in the twentieth century led to the rise of antibiotic resistant bacteria [116]. This is especially true in hospital environments where the need for disinfection has created multi-drug resistant strains, all the while even minor infections can have dire

consequences for patients and staff. It is no wonder then that the most common use of AgNPs is for medical antimicrobial application. Silver has been routinely used to treat skin wounds for decades; with a move towards silver nitrate, followed now by silver nanoparticles [117]. Other medical applications have included coatings for heart valves [118], catheters [119], orthodontic adhesives [120], dental fillings [121], orthopaedic implants such as bone cements and grafts [122, 123], as well as the clothing of medical staff [124].

I.7.2 SYNTHESIS OF AgNPS

The synthesis of AgNPs can be divided into two general categories of chemical or physical synthesis. Chemical methods may be divided into chemical reduction, electrochemical techniques, irradiation assisted chemical methods, and pyrolysis; while physical methods encompass physical vapour deposition, direct method magnetron sputtering, thermal decomposition, and arc discharge [125]. The concepts of green chemistry can be applied to each of those categories. Biosynthesis, as explained in the previous section, is the use of living organisms or their extracts as reaction components, whereas examples of green physical synthesis are chemical free and typically involve lower energy consumption and less heat pollution. For example, laser ablation [126], or the application of electrical current between two wires [127], and more recently, the evaporation of silver granules and their condensation in helium, yielding particles with high purity, narrow size distribution and high surface area as compared to commercial products [128].

In chemical syntheses stronger reducing agents tend to create smaller and more uniform particles; however, as the electrochemical potential of silver is quite high, even weaker reducing agents, such as those found in plant extracts, are capable of making the reduction. Parameters such as temperature, reaction time, pH, concentration and ratio of reactants have a great influence on characteristics such as size, shape, and surface chemistry [23]. Typically higher temperatures increase the synthesis kinetic and lower the energy barrier for nucleation; this usually moves the reaction towards a LaMer model, resulting in a rather uniform particle size distribution [129]. Depending on the other parameters, longer reaction times may lead to continuous nucleation, and or the increase in particle size as more ions are deposited at the particles' surface [130]. This leads to size distribution broadening in the former case, and uniform particle growth in the latter. The pH typically influences the reactivity of the reducing agent; in biosynthesis higher pH environments are usually favoured for they shift the equilibrium towards the release of protons, thus making the reduction reaction more favourable [131, 132].

A comparison of conventional synthesis methods with biosynthesis for AgNPs was described by Faramarzi and Sadighi [133]; while morphologies resulting from various plants and extracts are discussed here [23, 134].

I.7.3 PROPERTIES OF AgNPS

Depending on the synthesis method and conditions, AgNPs can be made to have various shapes and sizes; these include nano spheres, rods, plates, and wires. Though silver itself has no charge, there is evidence that the outer layer of AgNPs is actually silver oxide, leading to dissolution [135]. The surface chemistry can also be modified with ligands or capping agents, with the most popular ones being citrate, poly(ethylene glycol) (PEG), poly(vinyl)alcohol (PVA), polyvinyl pyrrolidone (PVP), and peptides. There has been conflicting data on the agglomeration of these particles, mostly depending

on the surface coating and dispersant. The dissolution rate of AgNPs has been linked to temperature [136] and time [137], thus suggesting low long-term stability for these particles.

The most prominent biological property of AgNPs is their antimicrobial activity, including their well-known antibacterial properties, which will be discussed shortly, as well as antifungal abilities. A study of 44 strains of 6 fungal species found an 80% inhibition concentration (IC_{80}) of 1 to 7 µg/mL [138]. Moreover, antiviral activity has also been reported for AgNPs. Antiviral effects against Human Immunodeficiency Virus type 1(HIV-1) [126], Tacaribe Virus (TCRV) [127], Hepatitis B virus (HBV) [127], Respiratory Syncytial Virus (RSV) [128], Monkeypox virus (MPV) [129], Murine Norovirus type 1 (MNV-1) [130], Influenza A Virus subtype H1N1 (A-H1N1) [131], and Herpes Simplex Virus type 1 and 2 (HSV-1 and 2) [139] have been investigated with encouraging results. The anti-inflammatory properties of AgNPs were investigated on porcine skin with contact dermatitis as compared to $AgNO_3$ and saline solution; the results showed a return to near normal after 72 hours for those treated with AgNPs [140]. In the same light, this anti-inflammatory effect was also studied in a postoperative peritoneal adhesion model in mice, showing effective decrease in inflammation and no significant toxicity [141]. Furthermore, AgNPs have shown a potential for anti-cancer treatments against leukemia, breast and lung cancer, skin, oral and heptocellular carcinoma, and angiogenesis [142]. Finally, a recent paper reported the use of AgNPs at concentrations of 0.5 to 2.0 µg/mL as protection against UVB radiation on human keratinocyte (skin) cells [143].

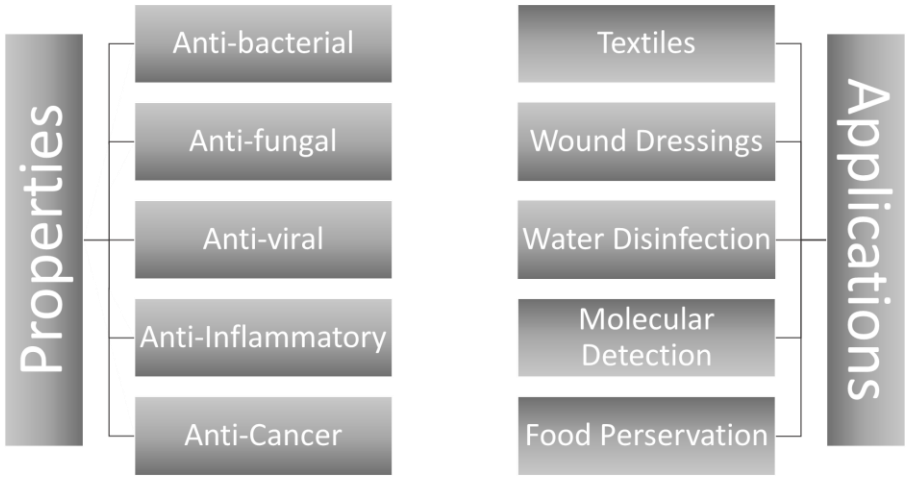

Figure 9: Graphical summary of AgNP properties and applications.

AgNPs are what is considered "broad spectrum" antibacterials as they inhibit both Gram positive bacteria such as *Staphylococcus aureus*, as well as Gram negative bacteria such as *Escherichia coli*, among many other highly pathogenic bacteria [144]. The minimum inhibition concentration has been found to be between 50 and 100 ng/mL, and IC_{50} values between 1 and 100 µg/mL [145]. The bactericidal effect is dependent on concentration [145], size [146], surface area, and shape [147]. Interestingly, it was found that truncated triangular AgNPs showed the highest antibacterial activity as compared to spherical and rod-shaped AgNPs [148]. This was proposed to be related to the crystallographic surface structure of the NPs, whereby nanotriangles have the {111}, a more reactive plane, exposed as oppose to the {100} plane of the spheres and rods [148].

Though the bactericidal effect of AgNPs is well documented, the mechanism of action is still not fully understood. Studies agree that at least part of the mechanism is related to the activity of the released silver ions; which can penetrate the membrane, and cause damage to cell components such as decreasing ATP levels and DNA synthesis [144]. However, the full extent of damage cannot be explained by the effect of silver ions alone [149]. AgNPs have a tendency to attach to the cell membrane, disrupting the permeability and respiration of the bacterial cell [150, 151]. Moreover, they are responsible for the creation of ROS, which in turn cause further damage to cell components and DNA [152]. The NPs themselves are also thought to interact directly with sulfur and phosphor compounds, once again, impairing cellular processes such as protein and DNA synthesis [153]. Finally, a recent study has shown that AgNPs induce an apoptosis-like response in certain bacteria [154]. The mentioned mechanisms are shown in Figure 10.

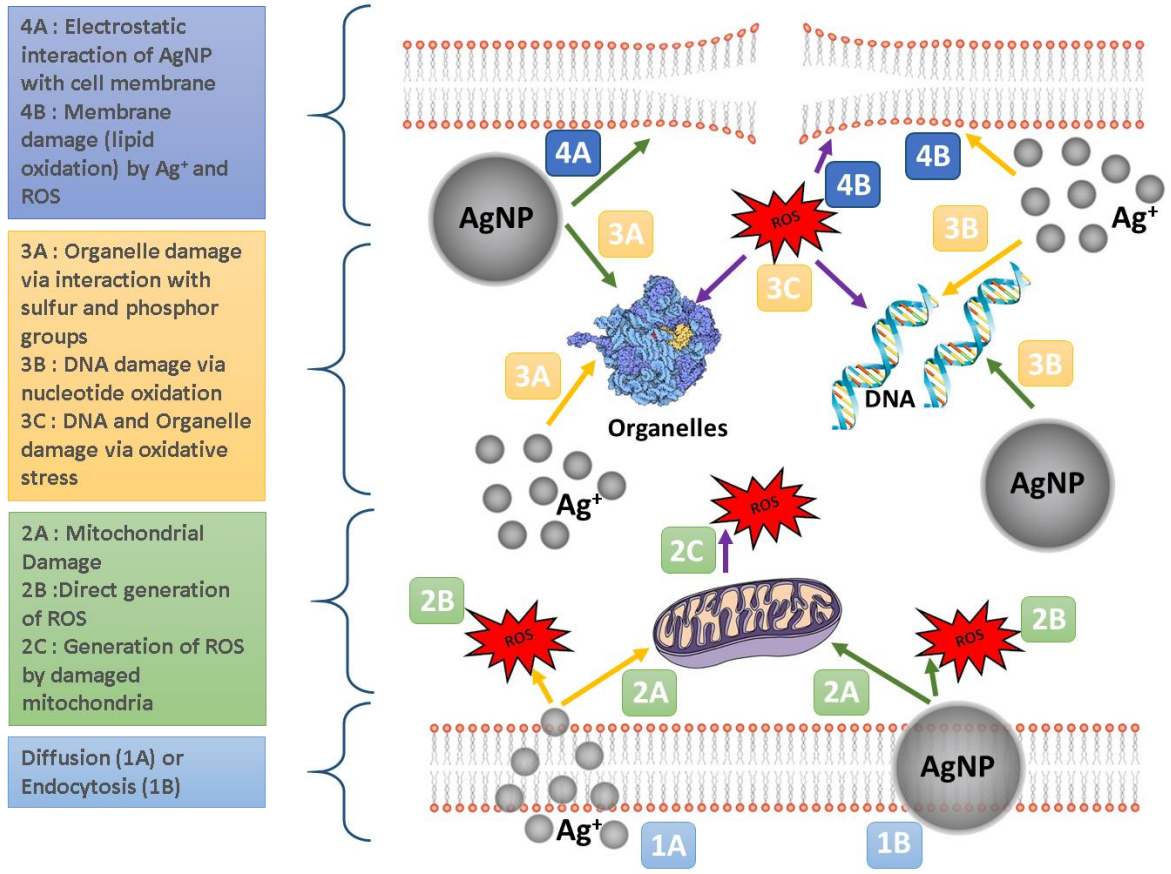

Figure 10: Bactericide mechanism of AgNPs.

Although rare, silver-resistant bacteria do indeed exist. Historically they could be isolated from silver-rich environments, such as mines, however, as early as the 1970s, they have also been isolated from human environments such as the burn units of hospitals [155]. This is thought to be due to the rise in use of silver nitrate and silver sulfadiazine to manage the infection of burns. While many fear that this will lead to an increase in resistant strains, it has been shown unlikely due to the multiple mechanisms with which silver effects bacteria [156]. Silver resistance is encoded into four genes; this means that bacteria would need to mutate all four genes simultaneously, from one generation to the next, in order to survive [157]. However, it has also been suggested that if the concentration of silver ions released is inadequate for killing all the bacteria, these mutations can occur sequentially at each

generation. In other words the concentration must be a number of times higher than the minimum inhibitory concentration (MIC) [157].

I.7.4 TOXICITY OF AgNPS TO HIGHER ORGANISMS

I.7.4.1 Human Studies

As expected, this toxicity towards bacteria is also seen in humans, although to a lesser extent. From the available literature on human toxicology, aside from wound healing studies [125], these are currently limited to a handful of case studies [158], one recent work on ingestion [159], and one relating to workers' health [160].

One of the case studies was conducted on a self-medicating arthritic man ingesting the equivalent of approximately 60.75 mg of homemade colloidal silver per day for ten months. Although the arthritis significantly improved, visual discolouration of skin and nail beds led him to a specialist where skin biopsies revealed extensive deposition in the dermis [161]. Another case study encountered a man similarly ingesting homemade colloidal silver as alternative medicine, with a variable frequency throughout a two year period. He too was diagnosed with argyria, due to the discolouration of his skin and nail beds, and silver granules in the biopsy of his skin [162]. This rare condition is associated with chronic exposure to silver-containing products [161]. Its occurrence suggests adsorption via the gastrointestinal tract into the blood stream and the systematic distribution of AgNPs or silver ions; those in areas exposed to sunlight are thought to be reduced back to metallic silver [161, 162].

On the other hand, a recent single-blind, placebo-controlled, crossover, intent-to-treat study on ingestion of commercial colloidal silver showed little effect on the subjects. Of the sixty healthy volunteers, between the ages of 20 and 76, 36 received a 10 ppm colloidal solution of 5 to 10 nm AgNPs, (equivalent to 100 µg per day) and 24 received a 32 ppm colloidal solution of 25 to 40 nm AgNPs (equivalent to 480 µg per day) for 14 days. No clinically important changes were identified with regard to metabolic, hematologic, urinalysis, and no morphological changes were found in lungs, heart or abdomen as measured by MRI [159]. Note that there is almost a 130 fold difference in per day dose between this clinical study and the case on argyria.

A health surveillance case study was conducted on silver nanomaterial manufacturing workers. Their exposure levels were extrapolated based on a one-time, one-day walk-through evaluation of the manufacturing process, and the health effects were assessed based on blood and urine samples. Two male workers who had worked in the silver nanomaterial industry for over seven years showed exposure levels of 0.35 and 1.35 ppt, blood silver concentrations of 0.34 and 0.135 ppb and urine silver concentrations of 0.43 ppb and undetectable [160]. Though the blood chemistry and haematology were within normal ranges and no adverse health effects were seen in the two men, this suggests silver accumulation in the body for long term chronic exposure scenarios.

The most extensive use of silver and silver products for medicinal purposes has been for dermal applications, namely for the healing of burn patients and chronic wounds. Silver nitrate and silver sulfadiazine were introduced in the 1960s in order to control infection in burn wounds. However, their rapid inactivation by the wound environment led to the design of new silver-impregnated dressings in

the 1990s, beginning with Acticoat™ [163]. Made of a rayon-polyester core sandwiched between two layers of silver-coated high-density polyethylene, this product has a steady dissolution rate of the metallic nanocrystalline silver which is thought to be responsible for its antimicrobial and anti-inflammatory effects [163]. Although such wound dressings have been extensively used to treat burns, high quality clinical trials are still lacking; most tend to be case studies, or low in the number of patients surveyed, with inadequate controls or insignificant results as compared to the conventional treatments [156].

Nevertheless, for those studies that went beyond healing rate and investigated toxicity, the results have been somewhat conflicting. A 28 day study on Acticoat™, with a 3- and 6-month follow up, was conducted on 30 patients with relatively small burns. Despite increased levels of silver in serum, there was no clinical, biochemical or haematological signs of toxicity [164]. Similarly, a random clinical trial of 166 wounds in 98 patients with Acticoat™ and silver sulfadiazine as control, revealed no local allergic or systematic symptoms [165]. On the other hand, a case study on a young male with 30% mixed depth burns resulted in argyria-like symptoms and the abortion of the Acticoat™ treatment, followed by a return to normal of silver levels in plasma and urine [166]. This is somewhat reflected in another study, where 191 second degree burn patients were divided into three treatment groups: group A receiving silver nanoparticle dressings, group B receiving silver sulfadiazine creams, and group C receiving Vaseline cream. Although group A showed a significantly shorter healing time for superficial burns as compared to the other two groups, there was no significant difference for deep burns as compared to group B. This suggests that while AgNPs may promote re-epithelialisation, they do not have an effect on deeper tissue generation such as angiogenesis or proliferation [167].

I.7.4.2 In Vivo Studies

A number of animal models have been used to study the toxicity of AgNPs, particularly in the last decade. These can be divided into those for environmental toxicity, and those meant to model human toxicity; only the latter will be covered in this section. These studies can be further divided based on the route of exposure; namely inhalation, intravenous and intraperitoneal, ingestion, implantation, and dermal application.

Of the inhalation studies available, most focus on either the respiratory or nervous systems. A 28 day study on Sprague-Dawley (SD) rats showed no significant changes in body weight, haematology or blood chemical values [168]. A similar study focusing on nasal respiratory mucosa showed that while AgNPs had an influence on neutral mucins, there was no toxicological significance [169]. Longer studies of 90 days and 13 weeks revealed decreased lung function and chronic alveolar inflammation, as well as citing lung and liver as target organs [170, 171]. A lack of genotoxicity of femur bone marrow, after a 90 day study, was revealed using a micronucleus assay [172]; while a similar lack in the lung tissue was shown by the Comet assay [173]. Because the above six studies were conducted by the same group, with the same NPs, durations, and similar doses, the experimental results are highly comparable to each other. A 10 day sub-acute study on mice showed minimal pulmonary inflammation or cytotoxicity [174].

The past five years have seen an increase in studies on the neurotoxicity of AgNPs. A genomics study in 2010 was conducted on the brains of mice exposed to AgNPs via inhalation, revealing alterations in genes related to motor neuron disorders, neurodegenerative disease, and immune cell function [175].

Two sequential inhalation studies performed by a different group investigated the neurotoxicity of AgNPs in neonatal SD rats over a 14 week period, discovering motor dysfunction, and its attenuation by Vitamin E, respectively [176, 177].

A 24 week study on Wister rats through subcutaneous injection showed that AgNPs, as compared to micro silver particles, were able to cross the blood brain barrier (BBB), accumulate in the brain, and cause neural degeneration [178]. Similarly, an intraperitoneal study on the brain of male mice, showed alterations in gene expression related to oxidative stress and disturbances in the immune systems [179]. On the other hand, male mice that were given intraperitoneal injections for a seven day period showed no impairment of cognitive outcome or hippocampal neurogenesis [180].

Intravenous injections are usually used to determine distribution and accumulation in target organs. A kinetics-based study on Wister rats, using three different AgNP sizes, revealed accumulation in liver, followed by kidneys, and spleen for the 20 nm particles, and spleen, followed by liver and lungs for the 80 and 110 nm particles [181]. Another study on Wister rats found significant changes in haematology and liver enzymes for doses above 20 mg/kg, as well as DNA damage [182]. Mice were used for an acute biokinetics and tissue distribution study; after two weeks, no obvious acute toxicity was apparent, though there were inflammatory reactions in liver and lung cells for the highest dose of 120 mg/kg, and accumulation in spleen and liver. An interesting find was the gender-related difference in the biokinetic profile, namely that male mice had higher clearance rates [183]. Wister rats were also used in a study of systemic and immunotoxicity where various doses of AgNPs were intravenously administered daily for 28 days. Although the treatments were well tolerated by the subjects, growth retardation, immuno-suppression, an increase in spleen size, and AgNP accumulation in spleen, liver and lymph nodes were detected [184]. The immuno-suppression was confirmed by a follow-up study focusing on T-cell antibody response by the same group [185]. Two other interesting studies include a dissertation on the tissue distribution and embryonic development following intravenous exposure of pregnant mice to AgNPs [186]; and the improvement of stealth properties of AgNPs using dextran coating in a rabbit model [187].

There are few available *in vivo* ingestion works on the toxicity of AgNPs. A 28 day oral-exposure study of tissue distribution and bone marrow genotoxicity in SD rats showed a similar trend as the intravenous study cited above [183]; namely that the AgNPs accumulated in female kidneys twice as much as male ones. Moreover, although dose dependent accumulation was apparent in tissue, no significant toxicity or genotoxicity were seen, and only slight liver damage was indicated for the medium dose of 300 mg/kg [188]. The same group later investigated sub-chronic oral toxicity on Fisher 344 rats over a 90 day period; there was a significant decrease in the weight of male rats. Additionally, similar outcomes such as gender-related differences in kidneys, slight liver damage for the medium dose of 125 mg/kg, and dose-dependent tissue accumulation were also discovered in this model [189]. The neurotoxicity of the ingestion of AgNPs and ionic silver on rats was recently examined over a 14 day period; the results showed ultrastructural changes in synapses for both forms of silver, though AgNPs caused a more severe synaptic degeneration [190].

The dermal toxicity of a commercial nanocrystalline wound dressing was investigated in a porcine burn model. Analysis of internal liver, heart, kidney and brains showed a significant increase of silver deposition even when the total body surface area burn ratio was 2%; however, the study did not

mention any clinical end points [191]. Healthy porcine skin doused with four different types of AgNPs showed no macroscopic irritation; however, microscopic and ultrastructural analysis revealed areas of focal inflammation and AgNP localization at the upper stratum corneum layers of the skin [192]. A rather rare study was conducted on the acute dermal and ocular toxicity of colloidal AgNPs using guinea pigs, with observations of up to 14 days. No deaths or abnormalities were reported for either scenario; and only a transient ocular irritation during the first 24 hours [193]. In another study using SD rats with deep partial-thickness wounds, the combination of AgNPs on a chitosan film was able to reduce the concentration of silver in blood by a factor of four, as compared to silver sulfadiazine [194]. A recent publication investigated the activity and toxicity of biogenic AgNPs complexed with enoxaparin in improving wound healing on a burn model using Wister rats. Although there was a significant acceleration as compared to the control after the 28 days of treatment, there was little difference between enoxaparin alone, AgNPs alone, and AgNP-Enoxaprin complex. No toxicity was found in the biochemistry or haematological parameters; however an increase in urea levels was attributed to inflammation and proteolysis [195].

I.7.4.3 In Vitro Studies

In vitro studies allow for the creation of controlled environments in which specific responses can be elicited, leading to the derivation of cellular pathway. Cell models can originate from the primary organ of exposure, or from the secondary, or so called target, organs or systems. Primary organs of exposure typically include the lung, gastro-intestinal tract, and skin, while secondary sites include the circulatory, nervous, lymphatic, immune and reproductive systems, and organs such as the liver, spleen, and kidneys. The following section summarizes and compares various *in vitro* studies on AgNPs, with a more in-depth discussion of studies using human cell lines from the lung, liver or skin.

The results from various studies agree on changes in morphology, reduced viability, decrease in GSH, and an increase in ROS, DNA damage, and changes in gene expression relating to oxidative stress and heat shock proteins [71, 196, 197]. However, the particle characteristics and the administered dose are not always comparable. A trend of increased cytotoxicity with decreasing size has also been noted, though whether this can be attributed to a higher surface area, a greater release of ions, a facilitation for uptake, or something entirely different is still a topic of debate [158]. Similarly, various coatings that have been investigated by different groups include citrate, PVP, PEG, starch, peptides, and carbon. Due to different experimental parameters, the results from these studies are sometimes conflicting and difficult to compare directly.

The lung is an important organ to study for it is one of the main routes of entry for NPs. The most common cell line used for AgNP toxicity studies on the lung is the A549, derived from human lung adenocarcinoma epithelial cells. A multi-cell line study in 2010 showed IC_{50} concentrations of 1.02, 9.96, and 14.31 µg/mL for 5, 20, and 50 nm AgNPs, respectively, through the MTT viability assay. Of the four cell lines studied, the A549 were the most sensitive to the 20 nm and 50 nm particles, and the least sensitive to the 5 nm [198]. On the other hand, a study using silver uncoated AgNPs in a range of 1 to 100 nm on the same cell line, with the same assay, had an IC_{50} of over 100 µg/mL [199]. Foldbjerg *et al* showed an increase in ROS and DNA damage, G_2 cell cycle arrest, and gene expression for oxidative stress [197, 200]. A frequently cited paper comparing IMR-90 cells (lung) with U251 cells (brain) also reported cell cycle arrest at the G_2 phase, as well as a decrease in metabolic activity and an increase in DNA damage [71].

While mentioned studies have reported a size effect, with smaller particles inducing higher toxicity, some contradictory evidence exists. One study showed that by converting the dose unit from μg/cm^2 to cm^2/cm^2 it was in fact particles with the largest diameter of 200 nm that had the highest toxicity [201]. On the other hand, a study of size and surface coating on BEAS-2B lung cells found the smallest tested diameter of 10 nm to be the most toxic, regardless of the surface treatment; namely citric acid, PVP and uncoated [196]. Another study on surface coating found the common citric acid capping agent to produce more cytotoxicity as compared to L-lactose and an oligonucleotide [202].

The liver has been identified as one of the main target organs in NP toxicity. The most commonly studied is the HepG2 cell line, originating from human hepatoma; though others include the L02, Chang, and Huh7. Viability assays with liver cells have yielded IC_{50} values between 4 μg/mL in Chang cells (30 nm) [203], to 25 μg/mL in L02 cells (38 nm) [204], and 0.59, 25.35, and 33.57 μg/mL in HepG2 cells depending on the size (5, 20, 50 nm) [198]. The latter also showed an increase in ROS levels, a higher uptake of smaller particles, as well as cell cycle arrest in the S phase [198]. Cell cycle arrest at the G_2 phase was also reported for 21 nm AgNPs, in dispersion of deionized water, phosphor buffered saline, and cell culture media [205]. Interestingly, nontoxic concentrations, below 0.05 μg/mL, have been shown to increase proliferation of the cells [206]. A comparison of 10 and 75 nm, citric and PVP coated AgNPs showed 10 nm citric acid coated to be the most potent in terms of stress-response [207]; similarly between 4.7 and 42 nm AgNPs the smaller were more cytotoxic, and induced higher ROS levels, GSH depletion and SOD inhibition [208]. Genotoxicity has also been shown on HepG2 cells, with an increase in DNA damage and alterations in gene expression related to metabolism, development, differentiation, and death [209, 210]. The role of ROS in inciting damages has been confirmed with an inhibition assay, where the addition of antioxidants was successful in alleviating the induced stress [208, 211].

Skin can be considered a primary route of exposure, for in many cases it the first organ that comes into contact with a new object or material; it can also be considered a secondary or target organ, for it has been shown that in medical cases of argyria, ingested silver accumulates in skin layers. At the same time, the increasing use of AgNPs in commercial and medical products makes the validation of its safety essential. Although one of the main functions of the skin is to act as a barrier layer, AgNPs and silver ions have been shown the ability to penetrate and permeate the skin under certain conditions; these include mechanical stress, abrasions and wounds, dissolution in sweat, and through hair follicles [212, 213, 214]. To complicate matters further, the studies on wound dressings, which are the most common use of AgNPs, often present conflicting results, especially *in vitro*. A study of Acticoat™, with human keratinocyte cells grown on a cultured Laserskin, resulted in a 90% loss of cell viability [215]; similarly cells exposed to extracts from a number of wound dressings showed that those containing silver were the most toxic [216]. However, though a more recent study also shows a reduction in dermal fibroblast cell metabolic activity, the nuclear integrity was maintained and no signs of death were visible [217].

The standard battery of assays, however, have yielded similar results as those of other cell lines. A study on two cancerous cell lines, A431 and HT-1080, showed IC_{50} values of 10.6 and 11.6 μg/mL for 7 and 20 nm particles, respectively, obtained using the XTT assay [218]. Normal human keratinocytes (HEK) were used in another study of 24 and 48 hour exposure periods to 15 nm PVP coated AgNPs. The decrease in viability was dose and time dependent, with longer exposures also showing an increase in caspase 3 and 7 activation and DNA damage [219]. Tamankova *et al* investigated five types

of commercially purchased NPs, three of which were silver, and two titanium dioxide (TiO_2). AgNPs showed higher cytotoxicities while TiO_2 particles had higher genotoxicity; the uptake of particles was measured using Raman confocal microscopy [220].

The effect of size (20, 50, and 80 nm) and surface coating (washed, unwashed, and carbon coated) were also investigated with HEK cells, via three viability assay and four immuno-markers over a concentration range of 0.000544 to 1.7 µg/mL. Only the unwashed showed a dose-dependent decrease in viability, and a significant increase in pro-inflammatory mediators [192]. HaCaT cell recovery from exposure to AgNPs was investigated by Zanette *et al*; the results showed that an acute exposure of 24 hours to the particles resulted in reduced proliferation and viability, though not necessarily death, with IC_{50} values of 6.8 and 15.3 µg/mL after 24 hours and 6 days, respectively. The effect was found to be independent of cell penetration or ROS levels [221]. While an investigation on the performance of an AgNP embedded hydrogel confirmed its superiority over current commercial ones, it also showed that the HEK and HaCaT cell lines do not always respond in the same way. The HEK were found to be more sensitive at longer exposure times [222]. The HaCaT were also more resilient as compared to the HeLa cell line, attributed to its higher natural antioxidant levels [223]. A summary of these studies is presented in Table 1.

Table 1: Summary of In Vitro studies on AgNPs performed using skin cells.

Cell Type	NP Properties	Findings	Ref
HEK Fibroblast	15nm, PVP-coated	Longer exposures lead to death via caspase 3 and 7 DNA damage, reduced viability, reduced proliferation	[219]
HEK Fibroblast	20,50,80/20,50,80/25,35 nm Unwashed, washed and Carbon-coated	MTT, Alamar Blue, 96AQ & Inflammation Only unwashed showed toxicity in dose dependent manner. AB the most sensitive technique.	[192]
HEK/HaCaT	Hydrogel AgNP vs commercial dressings	Cell viability tested; hydrogel out performed others HEK & HaCaT don't have the same response	
HaCaT	28 nm	HeLa cells are more sensitive MTT is most sensitive assay tested Increased ROS, and depleted GSH levels ATP/ADP ratio shows apoptosis	[223]
HaCaT	25 nm, PVP-coated	Short exposure has long effect on proliferation; independent of penetration or ROS	[221]
HaCaT	24 nm, citrate-coated	Protection against UVB, 0.5 to 80 µg/mL has no toxicity and higher viability, lower ROS, G_1/S arrest, protein pathway also studied	[143]
HaCaT	70 nm, PVP-coated	Air vs argon or storage; Air leads to more dissolution, ROS, and toxicity	[224]

Keratinocyte (Foreskin)	Cells+Dressing+ H2O, PBS, Media; 30mins	Solvent study on subconfluent cells; viability reduced to : 0, 0, 9.3%	[215]
SVK14	Commercial TiO2 and AgNPs	Raman/AAS uptake, increased ROS and genotoxicity; Genotoxicity doesn't correspond to ROS for TiO2; Ag has higher cytotoxicity	[220]
BJ (Foreskin)			
Dermal Fibroblast	Acticoat™ dressing, 3D culture model	Ag release investigated; Reduced mitochondrial activity, but nuclear integrity maintained and no visible cell death reported.	[217]
Dermal Fibroblast	50 nm Citrate, lactose, and oligonuclide-coated	Performed MTT, Comet, Annexin, P53 RNA; Reported that citrate coated induced more toxicity than others,	[202]
A431 Carcinoma	7 – 20 nm	Reported increase in GSH, and lipid oxidation, SOD inhibition, apoptosis threshold <1µg/mL	[218]
HT-1080 Fibrosarcoma			
Keratinocyte	Extracts from various wound dressings	Silver containing were most toxic, but all inhibited proliferation (MTT)	[216]

I.7.4.4 Cellular Toxicity Mechanism

A number of studies have focused on uncovering the mechanism through which AgNPs induce toxicity to mammalian cells. Silver, whether in its ionic or nanoparticle form, can enter the cell via endocytosis, diffusion, or protein channels in the membrane. There is evidence that there is a preferential uptake of AgNPs via endocytosis, leading to what is called a "Trojan Horse Effect" [196]. Once inside, the silver becomes activated and more bioavailable as it degrades into ions at the lower pH environment of the lysosome [225]. These then generate reactive oxygen species (ROS) that interact with cellular components and cause oxidative stress. There is a general consensus that oxidative stress is the leading cause of cell death, implied by an increase in measured ROS levels, depletion of GSH, and loss of mitochondrial function, reported in the previous section. However, whether this is generated directly by the particles or by the ions, or even the result of dysfunctional mitochondria, is still unknown.

The ROS, in turn, inflict damage in a number of ways; to the cell membrane by lipid peroxidation, to DNA by modification of base pairs and strand breakage, and to the cell itself by the induction of apoptosis [226]. Evidence for this mechanism has been cited by showing a decrease in ROS levels accompanied by increased viability upon the addition of an external antioxidant species such as *N*-acetylcysteine (NAC) [208, 211]. On the other hand, a loss of viability accompanied by a lack of ROS species or GSH depletion has also been reported, with the suggestion that another mechanism is responsible for the toxicity [227, 228]. Elsewhere, AgNPs were reported to induce perturbations in the function of the endoplasmic reticulum (ER), thereby causing ER stress, leading to unfolded protein response, and eventually apoptosis [229].

The extent of the contribution of silver ions has been a subject of debate. An investigation of storage conditions revealed that AgNPs were subject to dissolution as a function of time, temperature and surface coating; with some particles losing up to 90% of their weight over a 125 day period. This

release of ions subsequently lead to a considerably higher toxicity towards human mesenchymal cells (MSC) [137]. Similarly, a comparison of AgNPs stored under oxygen and argon revealed those in oxygen of having a higher concentration of silver ions and subsequently higher toxicities towards HaCaT cells [224]. On the other hand, a study that investigated the effect of ionic silver found that when the percentage of ions was below 5.5%, a contribution of toxicity from the AgNPs was evident [136]. Similarly, others that had investigated AgNPs with low silver ion percentages, could not explain the full extent of toxicity by the amounts of silver ions [206, 211].

I.7.4.5 Toxicity Studies on Biosynthesized AgNPs

In recent years a small number of toxicity studies on biosynthesized AgNPs have also been executed. In one case, AgNPs synthesized using *Nigella sativa* were compared in terms of their physico chemical characteristics and toxicity to bone-building stem cells of mice (MSC) and six strains of plants. The particles were approximately 15 and 30 nm respectively. These showed IC_{50} of over 0.4, 0.2, 0.2 µg/mL and 0.1, 0.1, 0.1 µg/mL for 24, 72, and 96 hour exposures, respectively [230]. While another group having synthesized 4 to 35 nm AgNPs from *Albizia adianthifolia* leaf saw no toxicity on normal peripheral lymphocytes, and only a decrease of 21% viability on the A549 cell line, as measured by the MTT [231]. Similarly another study on A549 cells using AgNPs of 12 nm synthesized using garlic clove extract, only showed a 10% increase at the highest tested concentration of 50 µg/mL [232]. Moulton *et al* showed an increase in HaCaT cell viability after their exposure to various diameters of AgNPs, ranging 10 to 90 nm, synthesized from various ratios of either epicatechin or tea extract at concentrations of 100 µg/mL. Viability, as measured by mitochondrial function, increased for all samples, ranging 10 to 40%; this was attributed to the antioxidants present on the surface of the NPs [233].

Elsewhere, AgNPs were synthesized using the extract of *Sabucus nigra* (European black elderberry), a mixture that is said to be rich in antioxidants compounds such as polyphenols, and anthocyanins. AgNPs of diameters ranging from 20 to 80 nm were exposed to HaCaT cells and viability testing using the MTT assay was conducted concentrations of AgNPs and the extract. The results showed an IC_{50} of approximately 300 µg/mL for the AgNPs (concentration not tested), and 79.4 µg/mL for the extract. Inflammation studies, using UVB, showed that although the initial addition of AgNPs increased cytokine levels, AgNP pre-treated particles had lower levels than controls, while pre-treatment with the extract had no effect. *In vivo* studies conducted on male Wister rats with induced paw edema; and human psoriasis lesions also reduced inflammation [234].

I.7.4.6 Metabolomic Studies with AgNPs

The application of metabolomics to toxicology allows for the simultaneous measurement of multiple endpoints, and the discovery of unexpected ones. However, as it is an emerging field, the studies using this approach are far and few in between, particularly for nanotoxicology. Moreover, most tend to focus on biological fluids, such as blood plasma and urine, rather than cell extracts. Studies on other inorganic nanoparticles such as gold, silica, iron oxide, and titanium oxide have received more attention as compared to silver. The trends show alterations in substrate and end-products of metabolic pathways such as glycolysis and the TCA cycle, suggesting changes in energy metabolism; alterations in lipid and choline compounds, suggesting disturbance of the cell membrane; and alterations in antioxidant compounds, reflecting oxidative stress.

For silver in particular, one group investigated metabolic changes in male and female Wister rat urine after exposure to PVP-coated 14 nm AgNPs administered orally for 28 days; this was performed using high performance liquid chromatography-quadruple time-of-flight mass spectrometry (HPLC-QTOF-MS). The results confirmed earlier research that had shown gender-related differences in kidney toxicity, for the urine from male rats did not show any metabolic alterations. Urine from female rats showed an increase in uric acid and its degradation product allantoin, indicating alterations in purine metabolism resulting from oxidative stress [235].

Another study made use of high resolution magic angle spinning (HR-MAS) NMR spectroscopy to investigate the metabolic profile of intact human Chang liver cells exposed to AgNPs. Changes in pyruvate and lactate levels indicated changes in energy metabolism; while an increase in choline, phosphocholine (PC) and glycerol-phosphocholine (GPC) suggested disruption of the cell membrane. Glutamine, glutamate and glycine showed a decrease, matching that of low GSH levels and indicating oxidative stress; while an increase in branched chain amino acids such as leucine, valine, isoleucine, and alanine match that of pyruvate. Similar levels of metabolites as compared to the controls were recovered when the cells were pre-treated with the antioxidant NAC [236]. These alterations were in agreement with their previous work that showed a decrease in GSH levels upon exposure to AgNPs and its subsequent attenuation with NAC [203].

A recent publication by our workgroup highlights alterations in the metabolome upon exposure of HaCaT cells to 30 nm citrate coated AgNPs using NMR metabolomics. The cells were exposed to a sub-toxic and toxic concentration, 10 µg/mL and 40 µg/mL respectively, as determined by MTT viability assay, and the intracellular aqueous and organic extracts, as well as the extracellular culture medium was analyzed. The results, given by multivariate analysis showed increase glutaminolysis, energy depletion and cell membrane modification. Furthermore, alterations in the TCA cycle were noted, suggesting a downregulation of the cycle's activity. Glutathione (GSH) levels showed an increase at both concentrations, indicating an upregulation in antioxidant protection [237].

I.8 AIMS

The general aim of this work is the comprehensive physico-chemical characterization and toxicity assessment of silver nanoparticles synthesized via green synthesis, namely by one chemical and one physical method using conventional toxicity assays and the metabolomics approach.

The specific aims of this work are:

Synthesis of silver nanoparticles via biosynthesis using the *Eucalyptus globulus* bark extract as reducing agent

Characterization of silver nanoparticles synthesized via Green Chemistry Synthesis (GS) and Pulsed Laser Ablation in Liquids (PLAL) in terms of their physico-chemical properties.

Evaluating the cytotoxicity of said particles in a skin keratinocyte cell line (HaCaT) using conventional cytotoxicity assays.

Characterizing the metabolic response of the HaCaT cell line to silver nanoparticles synthesized via GS and PLAL routes using ^{1}H NMR.

To this end, this thesis will be organized in the following manner. Chapter 2 will introduce the analytical techniques utilized throughout this thesis, providing general information about the techniques, as well as presenting their benefits and limitations. Chapter 3 will then detail the procedures followed for each experiment. Chapter 4 will present and discuss the results from the physico-chemical characterization of the AgNPs, in fulfillment of the first and second goals. Similarly, Chapter 5 and 6 will present and discuss the results from the cytotoxicity assessment, third goal, and metabolomics response, fourth goal, respectively. Chapter 7 will summarize the results and conclusions of the three studies, and present future perspectives for the continuation of this work.

Chapter II: Principles of the Analytical Methods Employed

II.1 Characterization of NPs

In order to properly characterize the AgNPs in terms of their physicochemical properties according to ISO recommendations, a number of techniques were employed. UV-Visible Spectroscopy was used to confirm the formation of nanoparticles, as well as to give a qualitative indication of their size distribution. Dynamic Light Scattering was used to determine the hydrodynamic diameter, as well as the respective agglomeration, in various media; zeta potential was measured with the same instrument. The particles' shape and morphology were visualized using Scanning Electron Microscopy in Transmission mode; the average size and size distributions were measured and calculated using image analysis, namely the ImageJ program. The composition was assumed to be pure, based on the reagents used and the closed environment. The surface chemistry for the Green Synthesis AgNPs was assumed to be similar to that of previous work, namely that of sugar compounds [238]; for the PLAL it was assumed to be citric acid, based on the producers' specifications, and ubiquitin coated, after incubation with ubiquitin [239].

II.1.1 UV-Visible Spectroscopy

The surface plasmon resonance (SPR) properties of silver nanoparticles have been firmly established in the recent years [240]. The exact resonance frequency, or alternatively wavelength, is highly dependent on size and shape. For AgNPs, this resonance band falls within the visible spectrum, is tunable between 393 to 738 nm, and can be detected with a UV-Vis Spectrometer [241]. Such spectrometers typically consist of a light source, filter, monochrometer, sample holder and detector. The filter and monochrometer allow only a specific wavelength of light to shine at the sample at each time, whereby the detector then determines the amount of transmitted or reflected light as a percentage of a reference. For this particular application, a range of wavelengths are tested in order to determine the SPR absorbance band for the sample [242]. The advantages of this technique lie in its simplicity, speed, ease of sample preparation and execution. However, the results are sometimes difficult to interpret, and can only contribute qualitative information unless calibrated with the help of another technique.

II.1.2 Dynamic Light Scattering

Cited as one of the most user-friendly, rapid, and consistent methods, Dynamic Light Scattering (DLS) has become the preferred technique to routinely determine the size distribution of NPs [56]. The instrument itself is made of a monochromatic light source, a red or green laser, two polarizers, before and after the sample chamber, the photodetector, and the computer [243]. The technique is based on three principles; Firstly, Rayleigh scattering asserts that particles smaller than 250 nm scatter light in all direction. Given a colloidal solution, the scattering from these particles would create patterns of constructive and destructive interference, called a Speckle Pattern. Secondly, Brownian Motion Theory asserts that particles in a fluid are in constant motion due to collisions with the fluid's molecules. Therefore, the Speckle Pattern of a colloidal solution would change over time, in other words the intensity at a particular point would be seen to fluctuate. Thirdly, the Brownian motion of

a particle can be related to its diffusion coefficient and hence its radius, based on the Stokes-Einstein equation [243].

$$D = \frac{k_B T}{6\pi\eta r}$$

DLS works by measuring the fluctuations in scattering intensity, and using correlation algorithms and polynomial series, to relate those fluctuations to an exponential decay that is directly proportional to the diffusion coefficient. The diffusion coefficient is then put into the Stokes-Einstein equation to calculate particle size; with large particles diffusing slower and small particles diffusing faster. The software then generates an intensity-based size distribution for the colloidal solution. The intensity distribution can be converted to a volume distribution based on Mie Theory, or even a number distribution. However, these models are less reliable as small errors in data collection can have a great effect on the correlation function [243].

$$I = I_0 \frac{1 + cos^2\theta}{2R^2} \left(\frac{2\pi}{\lambda}\right)^4 \left(\frac{n^2 - 1}{n^2 + 2}\right)^2 \left(\frac{d}{2}\right)^6$$

Nevertheless, it is important to realize the difference between the three types of distribution. A solution made of an equal number of 5 nm particles and 50 nm particles would have a number size distribution of two equal peaks. The 50 nm peak on a volume distribution graph for the same sample would have 1000 times the area of the 5 nm peak; this is because the radii differ by a factor of 10, thus the volumes are related by 10^3 (Volume=$(4\pi r^3/3)$). Similarly as the intensity is related to the radius by the Rayleigh Scattering Equation, i.e. a factor of r^6, the area of the 50 nm peak would be 1,000,000 times the area of the 5 nm peak. Thus it becomes obvious why even small amounts of large particles would have a high impact on the intensity size distribution calculated by the DLS [243].

DLS has a number of disadvantages that must be taken into consideration when working with the obtained analyses. According to the manufacturer, the Z-Average particle size, obtained from the intensity distribution, though a useful value for quality control purposes, is only suitable for comparing with other techniques if the sample is monomodal, spherical and monodispersed. Otherwise, meaning for samples that have a polydispersity index (PDI) above 0.5, the z-average value is misleading [243]. In addition more weight is attributed to larger particles, as discussed above. Thus, while able to provide a general perspective of how particle size distributions compare to each other, the average values and distribution curves calculated by this technique may greatly differ from the actual ones. Nevertheless, it was chosen for this study for it allowed for a quick and easy way to qualitatively compare similar samples under various conditions.

II.1.3 Scanning Electron Microscopy in Transmission Mode

Scanning electron microscopy (SEM) detectors are typically set to capture back scattered electrons and secondary electrons from the sample. The former gives information about the composition of the sample, while the latter yields images of surface morphology. However, if a detector is placed beneath the sample, and if the appropriate sample holder is used, the microscope can be used in transmission mode. This is particularly useful when analyzing small particles as the images obtained show the outer shape, while the contrast indicates elemental composition and thickness [54]. The downfall of using SEM or STEM for morphology and size distribution is misrepresentation as only a minute fraction of the sample can be captured in the images. Furthermore, the image analysis may be influenced by the subconscious bias of the analyzer in how they choose and measure the particles being assessed.

Nevertheless, in the case of AgNPs, STEM remains one of the most routine methods for measuring average size and size distribution.

II.1.4 Electrophoresis and Zeta Potential

Charged particles placed in a solution have a tendency to attract counter ions to their surface; those on the inner region are strongly bound, while those on the outer region are less firmly attached. These counter ions continue to stay with the particle, even when an external force is applied. The boundary at which counter ions no longer move with the particle is called the hydrodynamic shear or slipping plane. The electrostatic potential at this boundary is known as the zeta potential. The magnitude of this value indicates the colloidal stability of a solution; those with high zeta potential, typically greater than |±30|, repel each other such that there is little or no tendency to agglomerate [244].

Electrophoresis is the phenomenon where charged particles in a fluid move towards the electrode of the opposite charge when an external electric field is applied. The viscosity of the solvent will work to counteract this movement; an equilibrium is eventually reached where the particles move with constant velocity. This velocity can be related to the zeta potential, based on the Henry equation [244].

$$\mu_e = \frac{2\varepsilon\zeta}{3\eta} f(ka)$$

The same instrument that measures DLS can also measure zeta potential, using the concept of Laser Droppler Velocimetry. Here the velocity of the particles, as they move towards each electrode, is determined by measuring intensity fluctuations between the reference beam and light scattered at 17^o [242]. The advantage of this technique is that it is rapid, user-friendly, and can be directly combined with DLS measurements. However, as the Henry equation is strongly dependent on solvent viscosity and ion concentrations, it may not be a suitable for media other than ultra-pure water.

II.2 Toxicity Studies *In vitro*

The HaCaT cell line was chosen for assessing the potential cytotoxicity of AgNPs. Two qualitative and two quantitative methods were chosen to fulfill this purpose. Changes in morphology and proliferation were checked qualitatively using a light microscope; while preliminary uptake experiments were conducted with a Raman confocal microscope. The viability of the cells was determined via metabolic activity using the colourimetric 3-(4,5- dimethyl-2-thiazolyl)-2,5-diphenyl tetrazolium bromide (MTT) assay; while cell cycle alterations were explored using flow cytometry. As the uptake experiments were preliminary in nature, an in depth analysis of the nature of the techniques is not included in this section.

II.2.1 Model Cell Line

Given that the majority of commercial AgNP applications place the particles in contact with the skin, skin cell lines constitute appropriate *in vitro* models to study potential toxic effects of AgNPs. The skin consists of two parts: the dermis and the epidermis, for the inner and outer parts respectively (Figure 11) [245]. Each is composed of a number of layers, with the outermost layer of the epidermis made entirely of dead cells. The innermost layer of the epidermis, called the *stratum basal*, mainly consists of keratinocyte cells. These can continuously proliferate or begin differentiation; secreting keratin proteins which contribute to the skin's functional and mechanical properties, as they move further towards the outermost layer. In the final stages, they lose their nucleus and fuse into sheets that are eventually shed [245]. The HaCaT cell line is a nontumorigenic immortalized human keratinocyte cell

line that may be kept in continuous proliferation for over 140 passages [246]. Although it is a well-established cell line for the *in vitro* modeling of skin, the end application must be kept in perspective. As proliferating keratinocytes are found at the inner layers of the epidermis, in a realistic situation the AgNPs must have somehow breached or diffused through the outer layers. Though there is evidence for penetration and permeation of AgNPs across intact and damaged skin, the amounts were found to be negligible [212]. Therefore this model is best suited for wound healing applications of AgNPs, and would only apply to AgNPs in textiles in cases where there has been a skin damage.

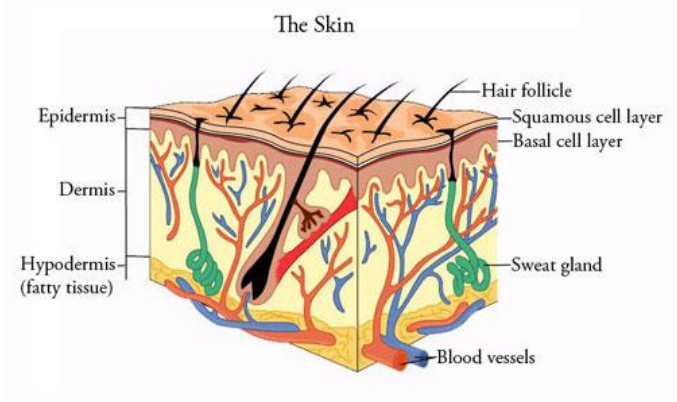

Figure 11: Simplified anatomy of the skin [247].

II.2.2 Cell Viability

Of the viability assays mentioned in section 1.3, the reduction of tetrazolium salts to formazan is by far the most common method. While there exist a number of variations of tetrazolium compounds, MTT is the most widely used version. The MTT dye is a soluble yellow compound that the mitochondrial enzyme succinate dehydrogenase is able to reduce to the insoluble purple formazan (Figure 12). Formazan can then be released from the cells using a detergent and detected with a spectrophotometer as it has a strong absorbance at 570 nm.

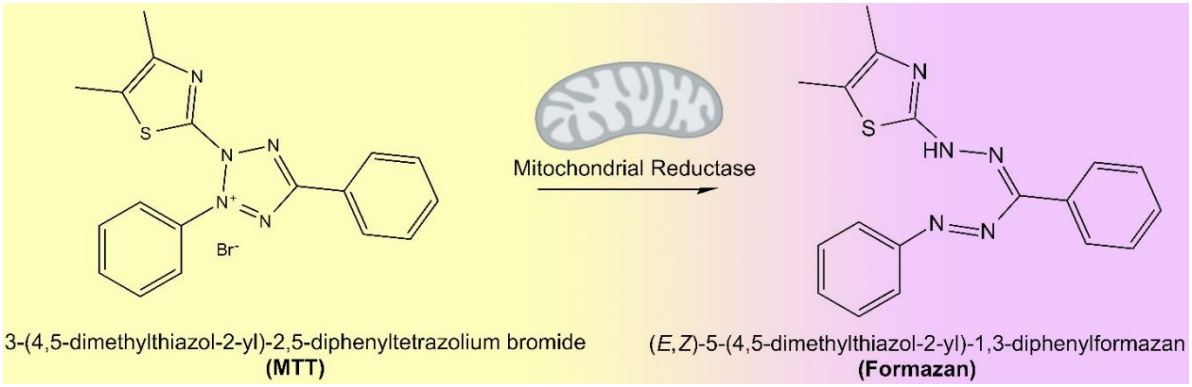

Figure 12: Reduction reaction of MTT to Formazan by mitochondrial reductase.

The cell viability can be calculated by comparing the absorbance of exposed cells to controls using the equation below. Furthermore, by testing a range of concentrations, the half maximal inhibitory concentration (IC_{50}) can be calculated using the appropriate data regression fit [248].

$$\%\ Cell\ Viability = ((Sample\ Abs)/(Control\ Abs)) * 100\%$$

The main advantages of MTT are its simplicity, easy of execution, low cost, and reproducibility. However, the MTT dye is sensitive to pH and has previously been shown to offer false positives with certain NPs [96, 97]. At the same time, it must be noted that a change in metabolic activity is not necessarily a sign of cell death [249]. A comparison of MTT, Alamar Blue, Neutral Red, with the same concentrations of AgNPs showed Alamar Blue to be the most sensitive and therefore the recommended assay of use [192]. Nevertheless, since the interference reported in this study was minimal, and otherwise not reported elsewhere for AgNPs with the MTT, as well as its availability and ease of execution, it was chosen as the principal method for assessing viability.

II.2.3 Cell Cycle Analysis

II.2.3.1 Cell Cycle

Alterations in cell cycle can be used as an early indication of DNA damage and even cell death by determining the percentage of cells in each phase of the cell cycle [226]. Non-proliferating cells are said to be in a quiescent state, called Gap 0 or G_0. Proliferating cells go through interphase, where they grow, and mitosis where they divide. Interphase is divided into three stages; Gap 1 or G_1, where the cells increase in size; Synthesis or S, where the DNA is replicated; and Gap 2 or G_2, where the cells continue to grow, having twice as much DNA. The cycle is completed with mitosis, or M phase, where the cell divides into two identical daughter cells, each having the entire genome of the original cell (Figure 13). Therefore, the cells in each phase can be distinguished based on the amount of DNA present; G_0 and G_1 having one set of DNA, G_2 and M having two sets of DNA, and S having a number in between [226].

In order to regulate and monitor the progress of cell division, each of these stages has a check point, allowing for the verification of cell processes and the repairing of damaged DNA. The main checkpoints occur at G_1/S, G_2/M, and M; with the G_1/S transition being the rate-limiting step (Figure 13). Typically, the cells cannot continue onto the next stage if the requirements for the checkpoint have not been met; if the cell is not able to repair itself, it goes through programmed cell death, called apoptosis. This is to prevent damaged DNA from being passed on to the daughter cells [226].

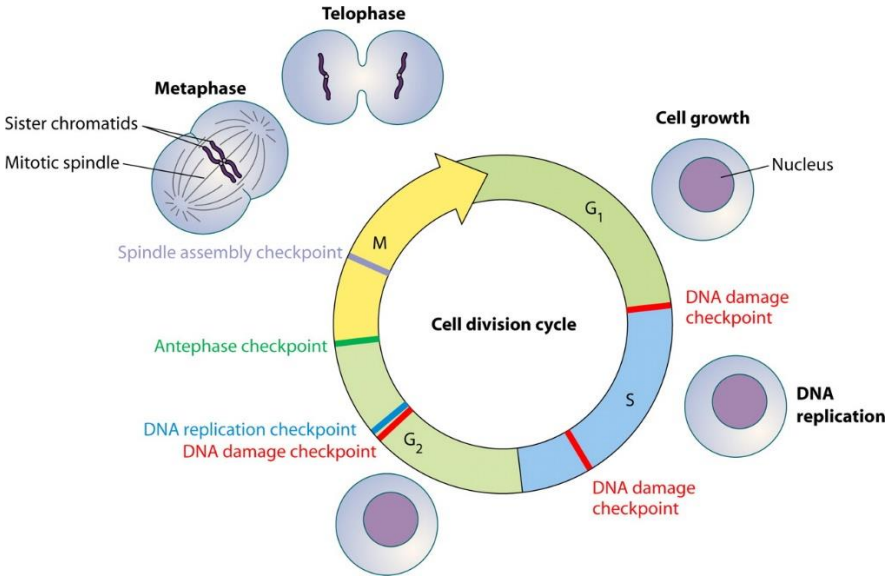

Figure 13: Cell cycle checkpoint pathways impinging upon the cell division cycle [250].

II.2.3.2 Flow Cytometry

DNA quantification is performed using a flow cytometer; an instrument that is also used for cell counting, cell sorting, biomarker detection, and protein quantification [251]. It consists of five main components: the flow cell, where cells suspended in a continuous stream of liquid (sheath fluid) are carried and aligned to pass in a single file through the light beam; the measurement system, typically a laser; the detectors, measuring forward scattered (FSC) light, as well as side scattered (SSC) light and fluorescence; the amplification system, where the detected signals are amplified and converted from analogue to digital; and finally the computer (Figure 14). While FSC and SSC give information about the size and shape of the cell, the fluorescence detectors are capable of simultaneously measuring signals from multiple markers. For example, the different antigens on a cell surface can be labelled with various fluorescent markers, and detected at the same time as measuring the intrinsic fluorescence of an internal component of the cell. These multiplexing capabilities are enhanced even further as more lasers and detection channels are added. Recently optics that allow the direct visualization of the cells have also been adopted for flow cytometers [251].

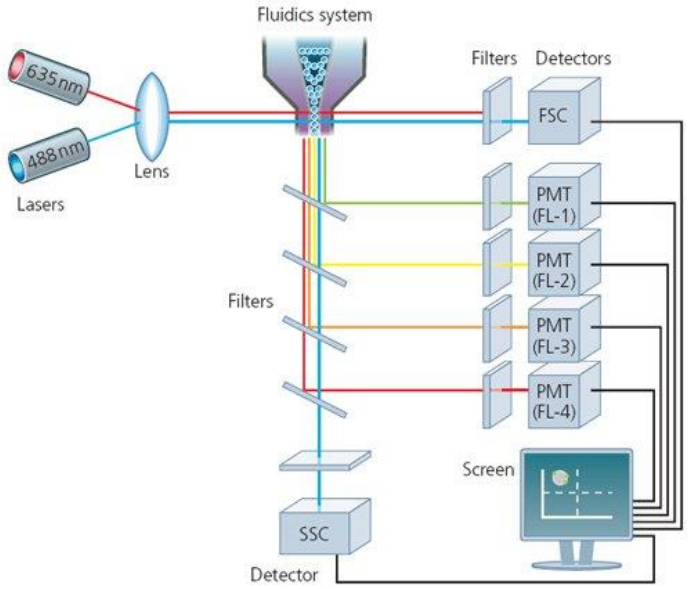

Figure 14: Schematic of a flow cytometer [252]

In order to assess DNA content, a fluorescent dye that binds to specifically and proportionally to DNA, such as propidium iodide or 4',6-diamidino-2-phenylindole (DAPI) can be used. As such, the frequency of cells can be graphed as fluorescence intensity, or DNA content, with G_0/G_1 having approximately half as much fluorescence as G_2, and the S phase falling between the two. False negatives can arise from the binding of the fluorescent dye, not only to the DNA molecules, but also to double strand RNA (dsRNA); therefore, special precaution must be taken to remove all RNA and to avoid any further contamination. False negatives can also occur for the G_2 phase if two nuclei in the G_1 phase pass through the beam at the same time. However, as the signal-intensity versus peak-area is different for these instances, they can be discriminated by changing the DNA peak-to-area threshold [251]. Despite these disadvantages, flow cytometry remains the standard for cell cycle analysis, offering rapid and easy measurements, relatively low cost, and higher accuracy as compared to visual inspection with a microscope.

II.3 METABOLOMICS

The two analytical techniques generally used for metabolomic studies are Nuclear Magnetic Resonance (NMR) spectroscopy and Liquid or Gas Chromatography coupled with Mass Spectrometry (LC-MS or GC-MS). NMR allows for the direct and non-destructive analysis of complex biological fluids, tissues, cells or their extracts; while LC/GC-MS techniques usually require more extensive sample preparation and separation prior to analysis. On the other hand, NMR has low inherent sensitivity, with detection limits typically in the micromolar to millimolar range, while LC/GC-MS allows for the detection of molecules at lower concentrations [253]. The main advantage of NMR is its ability to perform untargeted analysis, allowing for the discovery of unexpected results. This can in fact work to complement LC/GC-MS techniques; broad analyses can be performed with NMR and followed through with LC/GC-MS for a more efficient and sensitive analysis of a targeted family of compounds [253]. The NMR technique has been chosen here for its broader perspective offers a more appropriate first-analysis of alterations in the cell metabolome.

As metabolomics requires the processing and comparison of complex data sets with hundreds of variables, the aid of statistical tools such as multivariate analysis (MVA) are drawn upon [254]. The work flow of metabolomics, given in Figure 15 generally follows a route where sample collection and preparation are followed by data acquisition, by either NMR or LC/GC-MS techniques; the data is then pre-processed and compared to existing databases for compound identification; the change in concentration of these compounds are compared to each other or the controls using MVA methods such as Principal Component Analysis (PCA) and Partial Least Squares Discriminate Analysis (PLS-DA); the PLS-DA data is converted to a set of loadings, showing the importance of each compound in separating the data; univariate analysis is then applied to those peaks, in order to calculate compound-specific changes, and eventually elicit the overall changes in cellular processes [254].

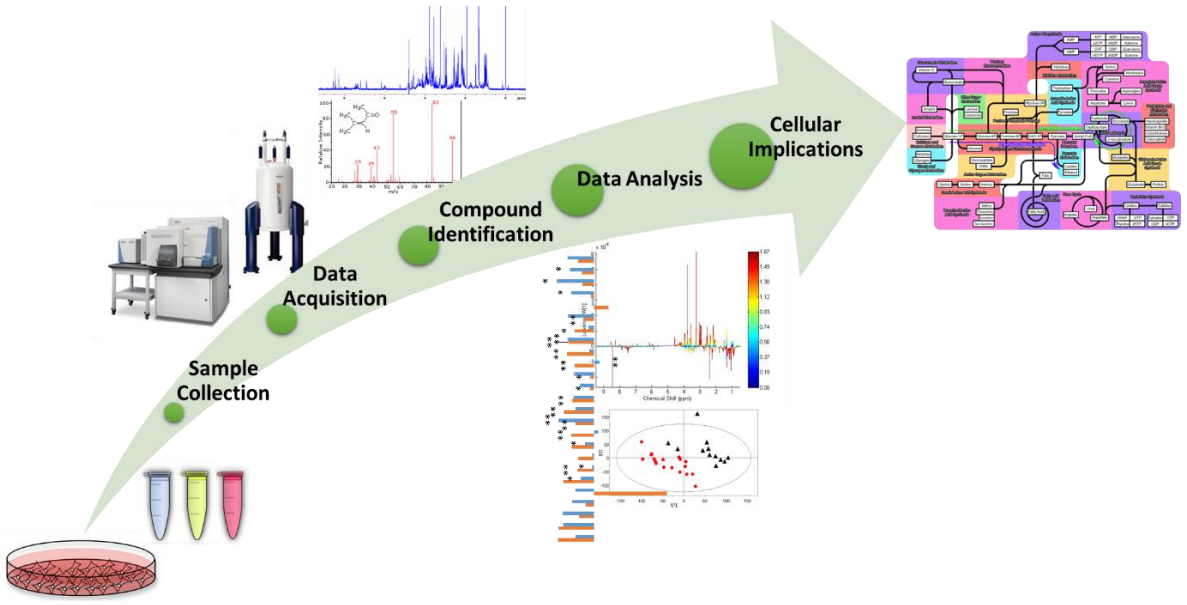

Figure 15: Workflow process of metabolomics.

II.3.1 NMR PRINCIPLES

Nuclear Magnetic Resonance (NMR) is a phenomenon that occurs when nuclei are placed in a magnetic field, as they absorb and reemit electromagnetic waves. In its simplest form it is present in nuclei with an odd number of protons and/or neutrons. This is due to the resulting non-zero magnetic

moment of the nucleus. As such, only certain isotopes of certain elements are available for use. While the most commonly used isotopes are ^{1}H and ^{13}C, isotopes of boron, nitrogen, fluorine and chlorine are also utilized for more specific applications. The classical set up employs a constant magnetic field and a perpendicular radio frequency (RF) pulse over a range of frequencies, to perturb the alignment of the nuclear spins. The frequency at which a particular nucleus emits a signal is called its "resonance frequency" [57].

There are two factors that affect the resonance frequencies of a nucleus: the type of nucleus and the local atomic environment. The type of nucleus dictates the basic resonance frequency with which an isotope needs to be excited. While a number of nuclei may be excited by the "carrier frequency", it should closely match the basic resonance frequency of the "observed nucleus". For example, ^{1}H nuclei would require a carrier frequency of approximately 500 MHz if an 11.7 T is used, whereas ^{13}C would require one of 126 MHz. It should also be noted that the obtained frequencies from a sample also depend on the abundance and sensitivity of a particular isotope [57].

The local atomic environment of the nucleus changes based on the atoms it is bonded to and surrounded by. Electrons, similar to the nucleus, have a rotation and charge, creating a magnetic field opposite to that of the nucleus. This field reduces the magnetic field the nucleus experiences, which in turn determines its NMR frequency, and hence the term "shielding". For practical purposes this means that the NMR frequency of a particular nucleus will be different, not only based on its number of protons and neutrons, but also by the number of electrons in its environment [57].

The most common method, proton NMR, uses the carrier frequency of ^{1}H and detects the minor shifts in its local environment. Proton NMR owes its popularity to the abundance of the ^{1}H isotope, its high sensitivity, and the large number of materials into which it is incorporated. The raw data gathered is the free induction decay, to which a Fourier Transform is applied, in order to obtain a frequency domain spectrum. Furthermore, the spectra are typically given in terms of relative frequency instead of absolute frequencies. This is done using a chemical reference, tetramethylsilane (TMS), which is made to be the "zero" point. Finally, the x-axis of the spectra are usually in parts per million (ppm) as opposed to Hertz (Hz). As the strength of the magnet affects the absolute resonance frequency, by dividing the frequencies by this value, variations between spectrometers (and different magnets) can be taken into account [57].

Proton NMR is commonly applied in determining and validating the structure of organic and biological compounds. There are three main pieces of information that can be derived from each spectrum; the position of a peak indicates the chemical shift (reflecting the electronic environment), the area under a peak is proportional to the number of nuclei in that environment (reflecting concentration), and the peak splitting indicates the coupling with neighbouring NMR-active protons. Protons that are in the same chemical environment are said to be "chemically equivalent" and will resonate at the exact same frequency without coupling; benzene, for example has six chemically equivalent hydrogen, resulting in a single peak with a shift of 7.5 ppm and 6 fold intensity (Figure 16). Ethanol on the other hand, has hydrogen in three different chemical environments, resulting in 3 different peaks at approximately 1.3, 3.5 and 6 ppm, with area ratios of 3:2:1 respectively (Figure 16) [57].

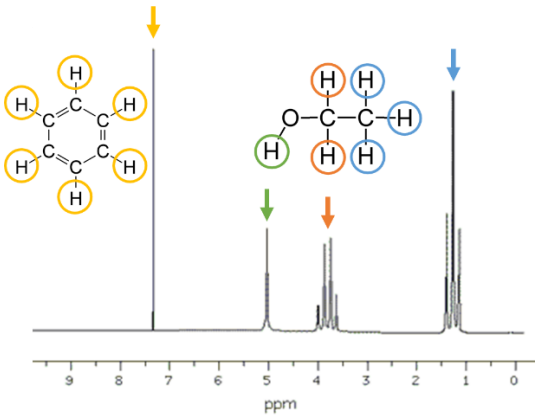

Figure 16: 1H NMR spectra of Benzene and Ethanol. Arrows indicate the peak relating to the hydrogen of the same colour.

Spin-spin coupling occurs between protons, or groups of chemically equivalent protons, that are magnetically inequivalent but connected via bonding electrons. For example, consider an ethyl group, with carbon A having three hydrogen, H_A (shown as blue in Figure 16), and carbon B having two hydrogen, H_B (shown as red in Figure 16). As there exists n+1 spin states for chemically equivalent protons, the three H_A would combine in four possible magnetic states, and split the peak of the H_B into a quartet. Similarly, the two H_B would combine in three possible magnetic states and split the peak of H_A into a triplet. While quite complex for larger compounds, this phenomenon allows for the distinction of a variety of molecules [57]. In complex mixtures, like that of biological samples typically analysed through metabolomics, the proton spectrum comprises a large multitude of signals, requiring the use of bidimensional (2D) experiments to assign those signals to specific metabolites.

Before applying MVA to the ^{1}H NMR spectra, a few pre-processing steps are usually required: peak alignment, to correct for shifts due to differences in pH or ionic strength; normalization, to account for differences in sample dilution and cell numbers, usually be dividing each point of the spectra by its total integrated intensity (total area); and scaling, to balance the weight given to larger and smaller signals in the MVA [255]. The most common scaling method is Unit Variance (UV), where the mean value is subtracted and each variable is divided by the standard deviation; similarly, Pareto scaling also subtracts the mean value from the variables, but divides each by the square root of the standard deviation. While UV scaling gives equal weight to all metabolites, because of the difference in this division factor, Pareto gives more weight to metabolites of lower concentration without inflating baseline noise [256]. The processed NMR spectra are then placed into a matrix of *n* samples and *m* variables. These variables are the peak intensity values and are inputted into the matrix as “buckets”; a bucket can be an individual ppm point or a range of values.

II.3.2 Multivariate Analysis (MVA)

Multivariate statistical analysis is applied to datasets in order to detect consistent variation patterns. If each variable (metabolite signal in metabolomics) is considered a dimension, this statistical approach allows for the reduction of highly complex multi-dimension spaces, to simpler ones from which meaningful information can be extracted [257]. The data can be treated in two different ways: unsupervised methods, such as Principal Component Analysis, where no *a priori* information about sample class is provided in order to reveal inherent clustering and outliers; or supervised methods, such as the Partial Least Squares – Discriminant Analysis (PLS-DA), where information about the sample class is provided to maximize class separation (for example placebo and drug) [257].

PCA is a projection-based method; in simple terms, the plane that provides the most information, in this case the grouping of data in clusters, is chosen, and the coordinates of the original data are converted to the new coordinate system of this plane (for a visual explanation of projection-based methods see Appendix A). Thus the data transforms from a complex multi-variable set, into one of two, or more, principal components (PCs), where PC1 shows the largest variation in the data set, followed by PC2 and so on, with each component being orthogonal to all others [258]. More rigorously, linear algebraic algorithms are used to decompose the original matrix *X* into a scores matrix *T*, a loadings matrix *W*, and a residual matrix *E*.

$$X = T \cdot W + E$$

Where *W* is the matrix of eigenvectors given by $X^T X$, and *E* is the part of matrix *X* that cannot be explained by the model [258]. A scores plot is given by plotting the scores of any two PCs against each other; information can be extract by means of comparing how the samples have grouped together or separated along the axes. The loadings in turn, provide information about the variables responsible for such clusters or separations [257].

The PLS is a regression model that works in a similar way; however, the plane of projection is chosen such that it provides the greatest differentiation between the pre-defined classes provided by the user, given by a second matrix *Y* [259]. In cases where *Y* provides qualitative information, for example control versus treated, discriminant analysis can be applied for more enhanced results. The data is thus converted into a series of Latent Variables (LVs) that show the variance in matrix *X* considering its correlation with *Y* according to the following equations:

$$X = T \cdot W + E$$

$$Y = U \cdot Q + F$$

Where similar to PCA, the *T* and *U* are the scores matrices, *W* and *Q* the loadings, and *E* and *F* the residual errors for *X* and *Y* respectively [259].

As PCA is an unsupervised method, it enables the identification of outliers, trends, and groups, and allows for the clustering of data based on unexpected variables. PLS-DA on the other hand, provides more quantitative results, with the ultimate aim of plotting the variables against the loadings, and colouring the spectra as a function of variable importance in the projection (VIP). However, PLS-DA can also fall prey to overfitting of the algorithm, and is best used in combination with PCA and other validation techniques.

II.3.3 Univariate Analysis

Univariate analysis is the statistical analysis of data when only one variable is involved; it explains the sample with tools such as the mean, median, mode, standard deviation, and variance. Moreover, inferential methods may also be used in order to determine the statistical significance or fit of the data. The *t*-test, Wilcoxon test, effect-size estimation, and analysis of variance (ANOVA) are typically used for assessing the robustness of scientific data, and are here applied to validate and complement the MVA results [260].

The significant difference between two groups of data, for example the mean value of the control samples and the mean value of the exposed samples, can be evaluated by setting a significance threshold, and performing one of the abovementioned tests; for normally distributed results the *t*-test can be applied [260]. The test calculates the probability of the null hypothesis being true, and provides a *p*-value. If this value is below the set criteria, the null hypothesis is rejected, meaning that

the observed results do indeed show a relationship between the two groups compared. The threshold is usually set at <0.05 or <0.001. The Wilcoxon test is a similar method for data that is not normally distributed, and ANOVA for comparing three or more groups of data [260].

However, the use of the *p-value* has fallen to a great amount of criticism in recent years [261]. While greatly influenced by the sample size, the *p-value* does not provide any information about the magnitude of variation between the two groups or their practical (for example medical) significance. Hence in the last decades, another parameter called "effect size" was proposed, and has been increasingly gaining momentum [261, 262]. The effect size estimate allows for the comparison of two groups based on the magnitude and direction of their variation. This parameter is particularly useful in the fields of medicine, toxicology, and metabolomics for two reasons. Firstly, its lower sensitivity to the sample size allows for the extraction of significance even when enough cases do not exist; an example would be orphan diseases. Additionally, it also allows for the meta-analysis of large quantities of data by calculating comparable values; something that is becoming more prominent as more databases are established [262]. Effect size, and its corresponding 95% confidence interval can be calculated according to the equations below (Table 2). The factor *J* is applied to correct for the upward bias when sample sizes are small [262].

$$J = 1 - \frac{3}{4(n_1 + n_2 - 2) - 1}$$

$$s = \frac{\sqrt{(n_1 - 1)\sigma_1^2 + (n_2 - 1)\sigma_2^2}}{n_1 + n_2 - 2}$$

Table 2: Summary of equation for calculating Effect Size and its Standard Error.

Effect Size based on Standardized Mean Difference	**Effect Size based on Standardized Mean Difference for Small Sample Sizes**
$ES = \frac{\overline{x_1} + \overline{x_2}}{s}$	$ES_g = J * ES = J * \frac{\overline{x_1} + \overline{x_2}}{s}$
$SE = \sqrt{\frac{n_1 + n_2}{n_1 n_2} + \frac{ES^2}{2(n_1 + n_2)}}$	$SE_g = J * SE = J * \sqrt{\frac{n_1 + n_2}{n_1 n_2} + \frac{ES^2}{2(n_1 + n_2)}}$
$ES \pm 1.96 * SE$	$ES_g \pm 1.96 * SE_g$

Chapter III: Experimental Procedures

III.1 Synthesis of Silver Nanoparticles (AgNPs)

III.1.1 Green Synthesis

Silver nanoparticles were synthesized according to the method outlined by Santos *et al.*, with minor modifications [238]. Ground *E. globulus* bark samples, having a granulometry lower than 2 mm (RAIZ, Forest and Paper Research Institute, Aveiro, Portugal), were subject to a 1:50 mass-to-volume water extraction at 100 °C for two minutes under constant stirring. The water and bark suspension was filtered using a Buckner funnel and 87 g/m^2 filter paper. This extract was then autoclaved using standard parameters; 20 minutes at 121 °C and 2 atmospheres. A 1 mM solution of silver nitrate (99.9%, Sigma-Aldrich), was prepared in distilled or ultra-pure water. The autoclaved extract was added to the $AgNO_3$ solution at a 1:3 volume ratio, sealed, and allowed to react for 72 hours. The NP suspension was centrifuged at 6000 rpm for 15 minutes, and the supernatant was removed. This was repeated three more times, with the addition of distilled or ultra-pure water, and removal of supernatant at each time for a complete "washing" of the sample.

A small volume of the pre-wash solution was kept for analysis. Similarly, a small volume was taken for reanalysis after approximately five and nine weeks; with these being considered "aged" nanoparticles. Part of the AgNP sample was autoclaved under the same conditions after approximately five weeks, and these too underwent characterization. The final synthesis was made by autoclaving the extract at and the silver nitrate the same ratio as cited above, under standard autoclaving conditions based on the method by Kora *et al* [263].

III.1.2 Pulsed Laser Ablation in Liquid (PLAL) Synthesis

Silver nanoparticles, synthesized via PLAL, and already concentrated 6-fold using centricons in 2 mM citrate buffer, were kindly provided by Dr Prof. Fabio Arnesano, Department of Chemistry, University of Bari "Aldo Moro". Briefly the synthesis procedure by PLAL described by Mangini *et al.* [239] is the following: A silver target (Goodfellow Cambridge Limited, 99.95% purity, 6 mm thickness), was placed inside a cuvette of ultra-pure Milli-Q water, and subjected to focused laser pulses from a 532 nm ND-YAG laser (Quanta System PILS-GIANT, 10 Hz repetition, 8 ns duration) for an ablation time of 3 minutes at an irradiance of 131 GW/cm^2. The AgNPs were then diluted at a ratio of 1:2.5 with ultra-pure water and left to stabilize for 24 hours.

Upon being received, the AgNP were characterized and from these, a portion was aliquoted for functionalization with 25 μM ubiquitin (Giotto Biotech); both types of particles, with and without ubiquitin, were used for toxicity and metabolomic testing.

III.2 PHYSICO-CHEMICAL CHARACTERIZATION OF AgNPS

III.2.1 UV-VIS SPECTROSCOPY

A UV-Visible spectrophotometer (Evolution 220, Thermo Scientific) was used to record the optical spectra of the nanoparticles. The AgNPs were diluted in both ultra-pure, and phosphate buffered saline (PBS) or cell culture media and the spectra recorded. Diluted samples were placed into quartz cuvettes and the spectrum was taken over an interval of 250 to 750 nm, with a bandwidth of 1 nm, and integration time of 0.25 seconds, using the instrument's Insight software.

III.2.2 DYNAMIC LIGHT SCATTERING (DLS)

Dynamic Light Scattering (DLS) was used for the determination of the size distribution and zeta potential of the AgNPs (Zetasizer Nano Series Analyzer, Malvern Instruments). Particles were first diluted in the dispersant of interest (distilled water, PBS, cell culture media), and placed into the instrument using the disposable folded capillary cell. Particle size distribution, as well as zeta potential measurements, are each an average of three separate measurements, each consisting of 12 to 18 runs. For the study on the effect of concentration and time, the samples were each vortexed prior to the measurement; incubated at 37 °C and measured again after 24 and 48 hours.

III.2.3 SCANNING ELECTRON MICROSCOPY IN TRANSMISSION MODE (STEM)

The particles were visualized using a field emission gun scanning electron microscope (FEG SEM, Hitachi SU70), operated at 15 kV. The samples were prepared by dipping a carbon-coated copper grid into the AgNP solution, and allowing the water to evaporate. Samples were mounted on a TEM stage, allowing the auxiliary electron detector below to capture the images in STEM mode. Image processing was conducted with ImageJ software. Average particle size and size distribution were determined by taking measurements of the particles' diameters (at least 50 particles were measured for each sample).

III.2.4 ICP-OES

The concentration of silver in solution was determined using Induction Coupled Plasma Optical Emission Spectroscopy (ICP-OES, Jobin Yvon 70 Plus) at Laboratório Central de Análises (LCA) - Universidade de Aveiro. The AgNP solutions were delivered as previously diluted in distilled water. They were then digested using concentrated nitric acid at an elevated temperature of 160 °C, and further diluted as required. Potentiometric studies were performed using a silver ion-selective electrode (ISE: silver/sulphide) coupled to a Consort C933.

III.3 CYTOTOXICITY OF AgNPS

III.3.1 CELL LINES AND CELL CULTURE METHODS

HaCaT cells (Cell Line Services, Eppelheim, Germany) were previously sub-cultured and frozen according to cell bank creation protocols. Upon thawing the cells were maintained in Dulbecco's Modified Eagle Medium (DMEM) (Life Technologies, Carlsbad, CA, USA) containing glucose, and further supplemented with 10% fetal bovine serum (FBS, Gibco, USA), 2 mM L-glutamine (Life

Technologies, Carlsbad, CA, USA), 100 U/mL Penicillin Streptomycin (Life Technologies, Carlsbad, CA, USA), and 250 μg/mL Fungizone (Life Technologies, Carlsbad, CA, USA) in a 37 °C incubator with a humidified atmosphere and 5% CO_2 saturation. The cells were sub-cultured every three to four days, once they had reached 60 to 80% confluence. A flow hood, Level II, was used to carry out all cell culture related work; standard aseptic techniques were followed.

For the sub-culturing of the cells, the old media was first removed. The cells were then washed for approximately one minute with phosphate buffered saline (PBS, Gibco, USA) in order to remove traces of serum, calcium, magnesium and any dead organic matter that would prevent the dissociation reagent from lifting the cells. The PBS was removed, and the cells were incubated for ten minutes with a solution of 0.05% ethylenediaminetetraacetic acid (EDTA, Sigma Aldrich) in PBS to further wash any metal ions. Once this was removed, the cells were incubated for 5 minutes with 0.25% Trypsin-EDTA (Gibco, USA), a digestive enzyme whose role is the hydrolysis of proteins, to detach the cells from the adhered surface. Once the cells had fully detached, they were diluted using fresh media and passed through a syringe (21G), using gravity only, to create a uniform cell suspension. A portion, usually 10%, was then put into a new flask. The cells for this project began at passage 53 and continued onto passage 84.

III.3.2 Morphology and Growth

Cells were observed under a phase contrast microscope (Nikon Eclipse 80i, Mexico) at each sub-culture step, as well as before and after exposure to the AgNPs for signs of contamination, growth rate, and changes in morphology. Digital images were obtained using a Nikon Digital Sight Series camera (Nikon, Japan), and the images were processed using the NIS-Elements F software.

III.3.3 MTT Assay

The same procedure as above was followed in order to create a uniform cell suspension. Here, the cells were counted using a haemocytometer (Neubauer Improved), always taking two samples out of the suspension and counting the four corner squares. The cell suspension was then diluted such that each well of the 96-well plate would be seeded with 6 000 or 5 000 cells in a volume of 100 μL, for the 24 hour and the 48 hour assays respectively. The assay wells were surrounded by a row of media on each of the four sides, in order to compensate for evaporation in the incubator.The seeded plates were placed in the incubator, and the cells were given a 24 hour period to adhere and grow.

For the exposure step, various concentrations of AgNPs were freshly prepared by diluting the nanoparticles in cell culture media. For the Green Synthesis AgNPs the concentrations included: 0, 5, 7.5, 10, 12.5, 15, 17.5, 20, 25, 50, 100 μg/mL; while the PLAL AgNPs included: 0, 2.5, 5, 7.5, 10 μg/mL with and without the ubiquitin coating. The old media in each of the assay wells was removed and replaced with 100 μL of the vortexed AgNP dilution. Preliminary assays consisted of three or five technical replicates, while standard assays consisted of four technical replicates and three independent assays. Exposed plates were once again placed in the incubator for their respective assay times of 24 or 48 hours.

The MTT Assay protocol, as described by Twentyman and Luscombe, was followed with minor modifications [70]. A 1 mg/mL solution of MTT (Sigma-Aldrich, USA) in sterile PBS was freshly prepared

and 50 μL was allocated to each assay well. The plates were then placed in the incubator for four hours, upon which the media and MTT solutions were removed from each well, to be replaced with 150 μL of dimethyl sulfoxide (DMSO, Sigma Aldrich, USA) for the solubilisation of formazan crystals. Three additional wells, designated as blank, were also filled with 150 μL of DMSO. This was followed by two hours on a rotational shaker and medium speed.

Finally, the optical density of reduced MTT (formazan) in each well was measured at 570 nm using an automatic plate reader (Synergy HT Multi-Mode, BioTek Instruments Inc, USA); the data being collected by the BioTek Gen5.1.1 software. The absorbance values of the blank wells, considered as background from the plastic and the DMSO, were averaged and subtracted from the assay wells. The following formula was then used to compare the results.

$$\%\ Cell\ Viability = \left(\frac{(Sample\ Abs - DMSO\ Abs)}{(Control\ Abs - DMSO\ Abs)}\right) * 100\%$$

These results were then fit with a sigmoidal curve of three parameters (*a*, *b*, and x_0) using the SigmaPlot 12.5 software (Systat Software Inc.) and the equation below. The equation was then used to calculate the IC_{10}, IC_{20} and IC_{50} for each AgNP type.

$$y = \frac{\mathrm{a}}{1 + \left(\frac{\mathrm{x}}{\mathrm{x_o}}\right)^{\mathrm{b}}}$$

Based on these results the doses of 5 μg/mL, 10 μg/mL and 15 μg/mL were selected for the Green Synthesis AgNPs for the IC_{10}, IC_{20} and IC_{50} respectively; while 1.09 μg/mL and 3.42 μg/mL were selected for the PLAL AgNPs for the IC_{10} and IC_{20}.

III.3.4 Cell Cycle Analysis

Cell cycle was analyzed by flow cytometry according to the method previously described by Oliveira *et al.* [72]. Briefly, cells were seeded into six-well cluster plates, with each well receiving 100 000 cells in a volume of 2 mL. They were allowed 24 hours to adhere and grow in the incubator before being exposed to the IC_{10}, IC_{20} and IC_{50} concentrations (5, 10 and 15 μg/mL) of the Green Synthesis AgNPs; in short the old media was removed and the AgNPs, diluted in media and vortexed, were added to each well. Each assay concentration consisted of three technical replicates. This was followed by an incubation time of 24 or 48 hours.

Afterwards, the media and AgNPs were removed, the cells were washed with PBS, trypsinized, and resuspended in media. The suspensions were placed in microtubes and centrifuged at 300g for 5 minutes. The supernatant was removed and the pellet was washed with PBS. Finally the pellet was resuspended in cold 85% ethanol and samples were subsequently kept at -20 °C until the day of the analysis.

To prepare the samples for analysis, the fixed cells were centrifuged at 300g for 5 minutes, and washed with PBS to remove the ethanol. The suspensions were vortexed, followed by filtration using a 55 μm nylon mesh in order to remove large clusters of cells. Propidium iodide (PI, Fluke, USA) was added for the staining of nuclear DNA, while RNAse (Sigma Aldrich, USA) was added to enzymatically dissolve any RNA in the samples. This was followed by 20 minutes of incubation in the dark.

A flow cytometer (Beckman Coulter XL) having an argon laser (15 mW, 488 nm) was used to measure the relative fluorescence intensity of approximately 5 000 stained nuclei, per sample. The data were processed using FlowJo software (Tree Star Inc, Ashland, Oregon, USA), with the ratio of peak intensities and peak areas used to determine the percentage of nuclei in each cell cycle phase: G_0/G_1, S and G_2 phases.

III.3.5 Cell Uptake

Cells were seeded onto round microscope glass covers (18 mm), inside 12-well cluster plates; each well receiving 300 000 cells in a volume of 1 mL. The same exposure protocols as above were followed for the exposure of the cells to 2.5, 5, 7.5, 10, and 15 μg/mL of AgNPs. After 24 or 48 hours of exposure, the glass covers were washed three times in PBS, and fixed using 1.5 mL of 4% paraformaldehyde for 20 minutes. The covers were then washed, three more times, in PBS. 50 μg/mL PI was used to stain the cells for visualization of nuclei, for a five minute duration, followed by washing in PBS. The glass covers were kept in PBS at 4 ^{o}C until the day of imaging.

Steps were taken to create a protocol for the visualization of particles with a fluorescence microscope, as well as a Raman confocal microscope. The preliminary acquisition parameters for the Raman microscope (Alpha300AR; WITec, Ulm, Germany) were as follows: two lasers with wavelengths of 633 and 532 nm were used to excite the samples, at 22 and 35 mW respectively. Images were acquired at 150 points per line and 150 lines per image, with an integration time of 0.05 seconds, and an area of approximate 70 to 40 um. The 50X magnification objective was used for all measurements.

Image processing was performed with WITec's Project Four software. Heat maps were created through an iterative process based on the few peaks available in the spectra.

III.4 Cell Metabolomics

III.4.1 Sample Preparation

Cell culture plates with a diameter of 10 cm were seeded with 800 000 cells; the cells were given 24 hours to adhere and were then exposed to the pre-selected concentrations of AgNPs (IC_{10} and IC_{50} for the Green Synthesis AgNPs, and IC_{10} and IC_{20} with and without ubiquitin for the PLAL AgNPs), using the same protocol as described above. Cells were exposed to the AgNPs for 24 hours, followed by their extraction as described below. A plate with media only was included as a further control.

The extraction of cells for metabolomics followed the protocol described by Teng et al. with minor modifications [263]. The media from each plate was discarded and the cells were washed four times

with cold PBS. The cells were removed using a scraper after the addition of cold 80% methanol, and put into Eppendorf tubes already having glass beads. After being vortexed for two minutes, chloroform and MilliQ water were added to each sample, followed by further vortexing. A waiting period of 10 minutes was followed by centrifugation at 4 °C at 2000g for 15 minutes, at which point the solutions separated into two phases. The top aqueous phase was removed and dried under vacuum using a rotary evaporator for approximately 7 hours. The bottom lipid phase was removed and dried using mild nitrogen flow for approximately ten minutes. The beads, protein layer and pellet were also stored for possible analysis. Furthermore, a sample of media, before washing with PBS, was removed from each plate, centrifuged for 5 minutes at 1000 rpm, and had the supernatant taken for analysis. All parts of the extraction, aqueous, lipid, media, and pellet, were frozen and kept at -80 °C until the day of the analysis.

In order to prepare the aqueous samples for ^{1}H NMR analysis, the dried extract was dissolved in 1 mM phosphate buffered saline of pH 7.4, prepared fresh using only deuterium oxide. The solution also contained 0.1 mM tetramethylsilyl propionate (TSP, Sigma Aldrich, USA) for the calibration of the NMR spectrum. The solution was then poured inside a glass 5 mm NMR tube. Similarly, the dried lipid extracts were dissolved in deuterated chloroform containing 0.1 mM tetramethylsilane (TMS, Eurisotop, France), and poured into glass NMR tubes. Finally, the medium samples were thawed at room temperature, vortexed, and mixed in a 9:1 ratio with deuterium oxide containing 0.25% TSP, before being poured into glass NMR tubes.

III.4.2 NMR Acquisition and Processing

NMR spectra were acquired on the Bruker Avance DRX-500 spectrometer operating at 500 MHz for ^{1}H observation using a Triple Resonance Probe (TXI) at 298 K. Both acquisition and the pre-processing of the spectra were performed with the Bruker TopSpin 3.2 software (Bruker BioSpin, Germany). Acquisition parameters, based on previous studies using the same cell line and similar nanoparticles, were used as a starting point and modified so as to improve quality of the spectra. For each sample, a standard 1D spectrum with water presaturation was recorded (pulse program 'noesypr1d' in Bruker library), consisting of 512 scans collected into 32 000 data points with a spectral width of 7002.8 Hz. The relaxation delay was 4 s and the acquisition time was 2 s (D1). For some samples, with lower cell numbers, 2048 scans were used instead. All spectra were Fourier Transformed (FT) with a squared cosine window function (SSB2) and a zero filling factor of 2, equivalent to approximately 64 000 points. They were then subject to manual phase and baseline correction, as well as calibration using the TSP or TMS peaks at 0 ppm. The parameters are summarized in Table 3.

Spectral assignment for HaCaT cell extracts was previously performed by our work group and used throughout this work [264]. Briefly, based on the chemical shift and multiplicity information gathered from 1D and 2D experiments, peaks of various metabolites and lipidic species were identified through cross referencing with data available in already established databases (e.g. Bruker Biorefcode database and HMDB – Human metabolome database [265]).

Table 3: Summary of ^{1}H NMR Acquisition and Processing Parameters.

1D ^{1}H NMR (500 MHz) 298 K	
Acquisition Parameters	
Experiment	Standard 1D
Pulse Programme	*noesypr1d/zg*
Number of Scans	512/2048
FID data points	32k
Spectral Width	7002.80 Hz
Acquisition Time (AQ)	2.34
Relaxation Delay (D1)	2 s
Mixing Time	100 ms
Processing Parameters	
Window Function	Squared cosine
SSB	2
Spectrum Data Points	64k

III.5 STATISTICAL ANALYSIS

III.5.1 UNIVARIATE ANALYSIS

Univariate analysis was performed for the MTT and cell cycle data; the results are reported as the mean average ± the standard deviation of four technical replicates in each of the three independent experiments, and the three replicates, respectively. The one-way ANOVA test was used to determine the statistical significance between control and exposed cells for the MTT assay, followed by Dunnet or Dunn's method (as parametric and non-parametric tests, respectively), using Sigma Plot 12.5 software (Systat Software Inc.). The Holm-Sidak test was used in place of Dunnet or Dunn's method where applicable.

Univariate analysis was also performed on the integrated peaks of NMR spectra. The integrals for each peak were normalized using the total area. The average value, standard deviation, variation from control and standard error were subsequently calculated. The student's *t*-test was applied to compare the mean value of the samples and the controls. Finally, effect size was calculated based on the method discussed in Chapter 2, with the *J* factor included for all parameters [262].

III.5.2 MULTIVARIATE ANALYSIS (MVA) OF NMR DATA

Multivariate Analysis (MVA) was performed on all data sets of the same type, i.e. aqueous, lipid, medium, using the SIMCA -P 11.5 software (Umetrics, Sweden). Prior to MVA, interfering solvent signals (e.g. methanol, chloroform, water) were removed and normalized by total spectral area and scaled. Different scaling types were tested and Pareto scaling was selected based on the resulting MVA quality parameters. PCA was first applied, followed by PLS-DA. The default seven-fold internal cross validation was utilized in order to derive predictive ability (Q^2), and explained variance (R^2). The PLS-DA models were used to create loadings plots in R (R Foundation for Statistical Computing, Austria);

showing the obtained weight loadings as a function of the spectrum, and coloured using the Variable Importance in Projection (VIP).

While the scores scatter plots show the dispersion of sample scores in the multivariate space, thus giving information on grouping trends, the loading plots give information regarding the magnitude and importance of the variation in metabolites between the data sets. Peaks of metabolites showing high VIP, as well as those previously found to play an important role in cell function, were subject to signal integration using the AMIX-Viewer software 3.9 (Bruker, Germany) in order to quantify those variations.

Chapter IV: Physico-Chemical Characterization of Ag NPs

Although only one batch of AgNPs from the Green Synthesis was used throughout the cytotoxicity and metabolomics testing, a number of modifications were made to the process in order to optimize the safety, and the resulting particles were characterized. Furthermore, as the cytotoxicity and metabolomics each required a number of weeks to complete, the same batch of particles was also evaluated in terms of stability and uniformity over an extended period of time.

Table 4 summarizes the various batches of Green Synthesis (GS) AgNPs synthesized, as well as the characterization studies that were carried out for each one. Throughout the text, AC refers to AgNPs that were synthesized using an "Autoclaved" plant extract; of these, two identical batches AC1 and AC2, differ only in the type of water used, distilled and MilliQ water respectively. The "Double Autoclaved" or DAC sample is an aliquot of AC1 that was subject to standard autoclave conditions approximately one month after the initial synthesis. The One Pot Synthesis (OPS) refers to a batch of AgNP where a mixture of as-filtered extract and $AgNO_3$ were autoclaved under standard conditions.

Table 4: Summary of syntheses and respective parameters studied.

	Synthesis	Washing	Aging	Solvent	Incubation
Autoclaved 1 (AC1)	✓	✓	✓		
AC1 at One Month			✓	✓	
AC1 at Two Months			✓		✓
Autoclaved 2 (AC2)	✓	✓			
Double Autoclaved (DAC)	✓				
One Pot Synthesis (OPS)	✓	✓			
PLAL	✓				

Five different studies were conducted on these particles employing one or more characterization techniques. The "Synthesis" study looked at minor modifications, such as the type of water used, and the step at which the particles were autoclaved, using UV-Vis, DLS, and STEM. The "Washing" study made a comparison of the AgNP immediately after the synthesis, and after the centrifugation and washing; termed "Pre Wash" and "Post Wash" respectively, using UV-Vis and DLS. For "Aging" the Post Wash of the AC1 batch was compared against the same Post Wash particles after one and two months, using UV-Vis, DLS and STEM. Immediately before the start of the cytotoxicity testing, the AC1 batch had aged one month, and was thus used to compare the effect of solvent (water, PBS, DMEM), using UV-Vis and DLS. Similarly before starting the metabolomics, two months after the initial synthesis, the particles were once again characterized using UV-Vis and DLS in the most relevant solvents, water and DMEM. Finally, the effect of 24 and 48 hour incubation at 37 °C in water and DMEM was studied for the same concentrations as those of the MTT test, using DLS.

The AgNPs synthesized via PLAL were also characterized in order to confirming that they indeed had the properties suggested by the partnering laboratory and thus, were not subject to an extensive study

[239]. Moreover, it is important to note that the small volume available created a large hurdle for thorough characterization.

Outside of the mentioned studies, the results from the ICP-AES for the AC1 batch showed a concentration of 2.36 mg/mL and the results for the PLAL AgNPs showed a concentration of 0.170 mg/mL.

The following sections describe and discuss the results for the various studies, using processed data from the UV-Vis, DLS, and STEM instruments.

IV.1 Characterization of Green Synthesis AgNPs

IV.1.1 Study of Modifications in Synthesis Parameters

Since the surface plasmonic resonance (SPR) properties of silver are detectable at the nano scale, namely an absorption band in the visible region (approximately at 400 nm) [240], UV-Vis spectroscopy was firstly used to confirm the formation of the NPs. The resonance band, the wavelength at which the particles show the highest SPR, is related to the size of the particles; with smaller ones resonating at shorter wavelengths and creating a blue shift. Consequently, the narrower the size distribution, the narrower the peak [240]. Figure 17 shows the UV-Vis spectra of the four batches of Green Synthesis.

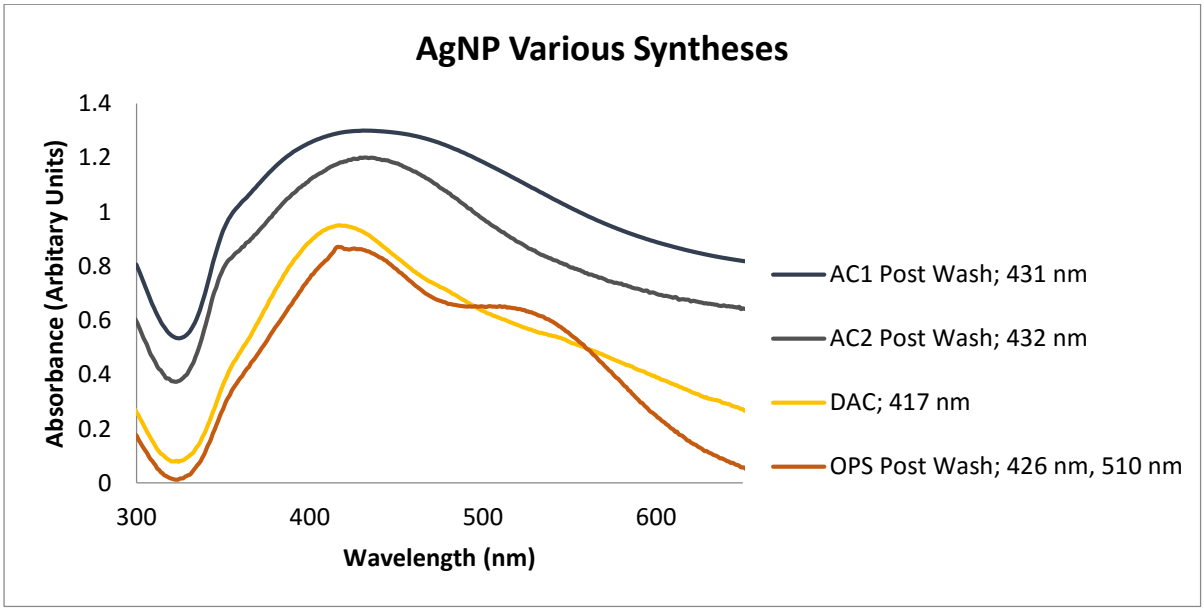

Figure 17: UV-Vis Spectra of AgNPs of Various Syntheses and respective maximum absorbance.

As expected, the change in the water source does not translate to a change in the UV-Vis spectra for AC1 and AC2 have almost identical curves. The peak values are also very similar, however AC1 appears to be slightly broader than AC2, suggesting a wider size distribution. Autoclaving the particles a second time (DAC) seems to create a narrower band, perhaps as a result of the silver ions in solution being reduced to AgNPs by the remaining trace amount of extract at the surface of particles and in between. It may also be attributed to the dissolution of smaller particles and their deposition at the surface of the larger ones at the higher temperature, resulting in a more uniform distribution [12]. The OPS synthesis, on the other hand, shows a double peak at 426 nm and 510 nm respectively, suggesting a

bimodal distribution of particles; this is probably due to an increase in reaction kinetics resulting from the initial increase in temperature [7].

Keeping in mind the discussion on the limitations of size distribution analysis by DLS in Chapter 2, the results are discussed in terms of the qualitative information they provide. Similar trends, as those of UV-Vis, are observed in the data acquired by the DLS for the hydrodynamic diameter based on intensity (Figure 18). Once again, the AC1 and AC2 have similar curves, though vary slightly in their mean size. The OPS shows a higher hydrodynamic diameter than the others, while the DAC has a diminished left shoulder, suggesting an increase in the percentage of larger particles. As this is the distribution by intensity, there may be a distortion due to larger particles or contaminants, as they have a greater weight in the scattering equation [243]. Size distribution by number was also generated in order to extract more information (Figure 19).

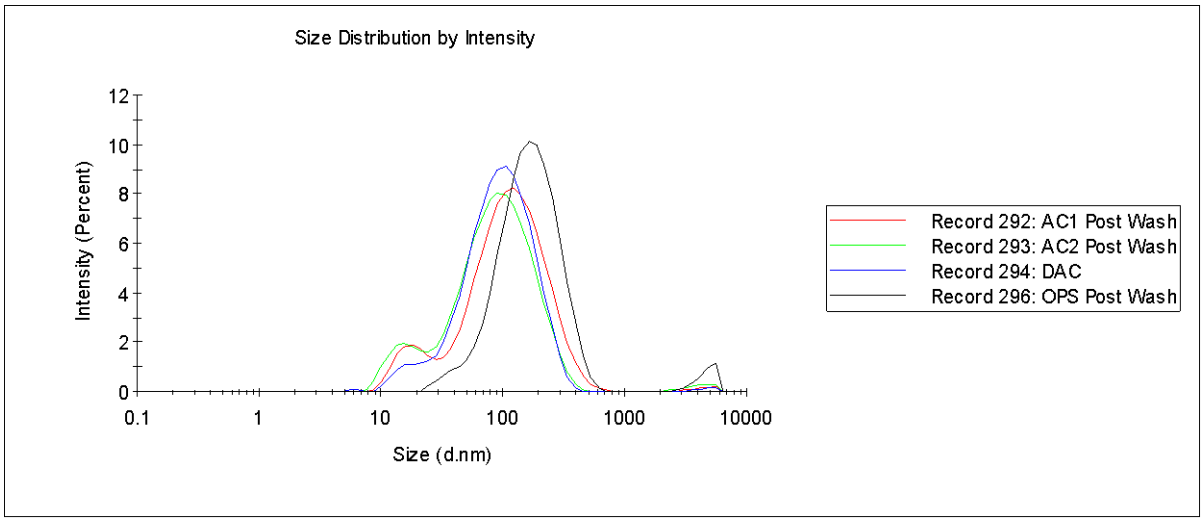

Figure 18: Hydrodynamic size distribution by intensity for various AgNP syntheses (Zetasizer Software).

In studying the size distribution by number, the profile of AC1 and AC2 remains identical as compared to each other, though they both lose the shoulder on the left (Figure 19). The profile of DAC changes drastically when compared with the intensity distribution showing a bimodal distribution with approximately half the particles at the lower range and half at the higher. The micro-sized particles for OPS disappear from the curve, though they are most likely what causes the peak to shift further right as compared to the other samples. As the size distribution by number allows for a better separation of the syntheses batches, and keeping in mind that the average values are not reliable as discussed in Chapter 2, it was the analysis type used for all following studies.

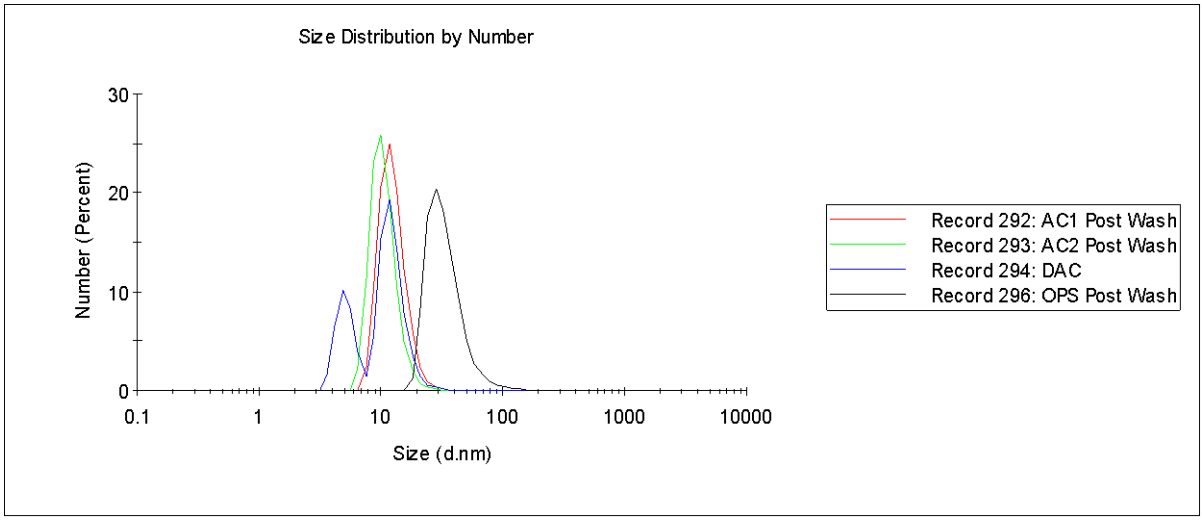

Figure 19: Hydrodynamic Size Distribution by Number for Various AgNP Syntheses (Zetasizer Software).

In order to obtain a more accurate value for the average size and size distribution, particle diameters were measured from the STEM images. Here, the analysis revealed new information about the characteristics of the particles; namely the striking difference between AC1 and AC2. Comparing the STEM images (Figure 20 and Figure 21), the AC1 batch seem to be blurry and highly agglomerated; however, as the inset reveals, this is due to a host of much smaller particles surrounding the larger ones. This is subsequently reflected in the size distribution graph, with the 10 to 20 nm group clearly outside the Gaussian distribution curve. AC2 on the other hand has a more uniform size distribution, both visually and as measured, shown by the smaller standard deviation. As the only difference between their syntheses is the purity of the water used, it would suggest that perhaps there are certain components in the distilled water that interfered with the reduction of silver ions; whether through side reactions with the reducing agents or direct interaction with the silver.

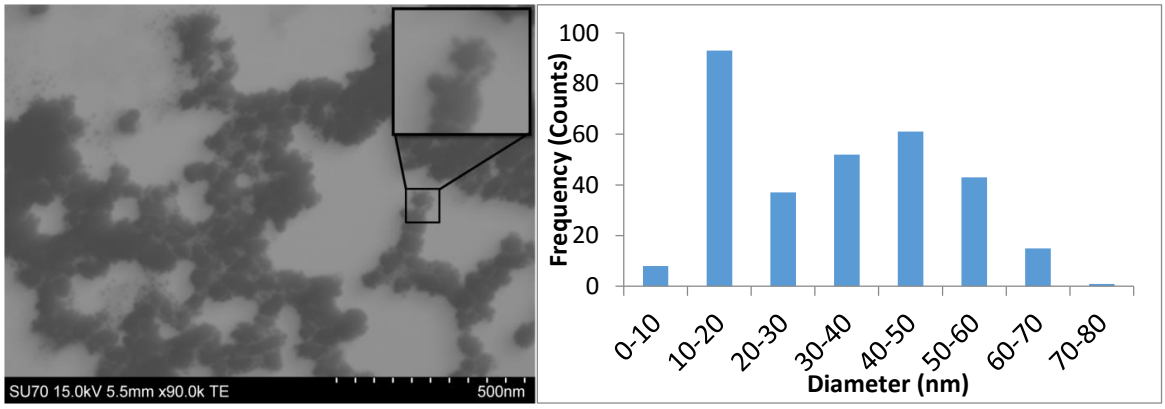

Figure 20: STEM Image of AC1 Post Wash at 90X Magnification and respective size distribution: 3 Images, 310 Measurements.

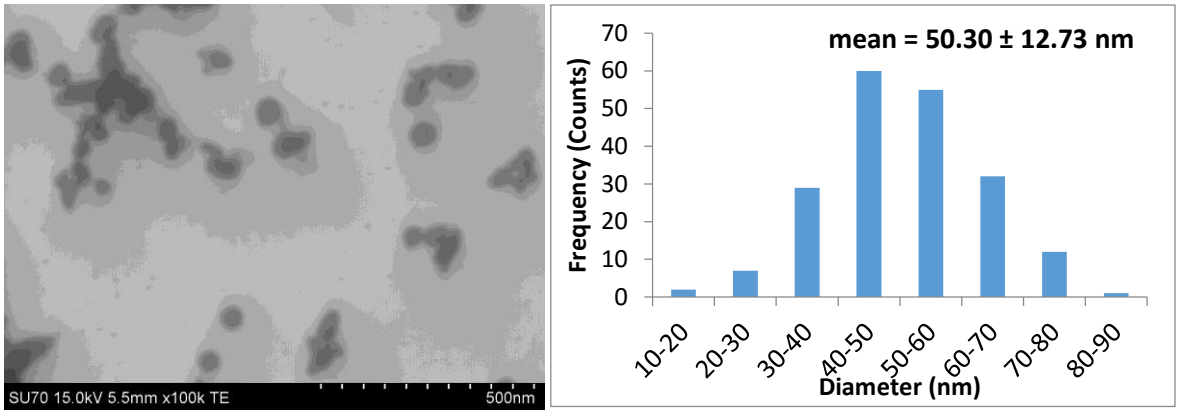

Figure 21: STEM Image of AC2 Post Wash at 100X Magnification and respective size distribution: 2 Images, 198 Measurements.

The particles that were autoclaved one month after their synthesis (DAC) also showed a more uniform distribution, with the STEM images confirming the lack of the smaller particles. As it stands, the uniformity can be equally attributed to aging or the second round of autoclaving. Although the STEM results indicate a relatively normal distribution, neither the UV-Vis nor the DLS show that. This can be attributed to the way the human eye can distinguish between particles in an agglomerate, whereas neither the UV-Vis nor DLS algorithms are able to do so. Upon inspection of images with a lower magnification, it becomes apparent that aside from the spherical nanoparticles measured, there are many elongated particles, as well as a number of high aspect-ratio nano wires (Figure 23). This would in turn explain the discrepancy between the diameter values suggested by the three techniques.

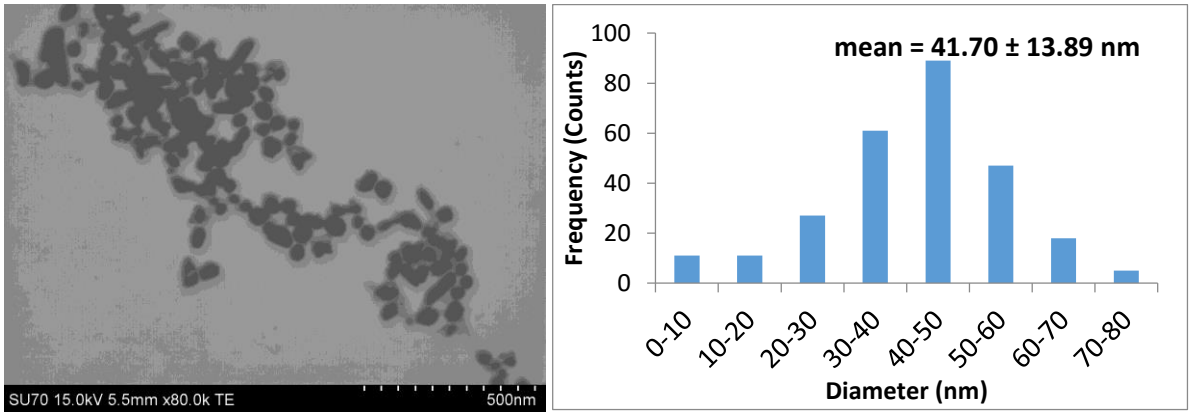

Figure 22: STEM Image of DAC at 80X Magnification and respective size distribution: 2 Images, 269 Measurements.

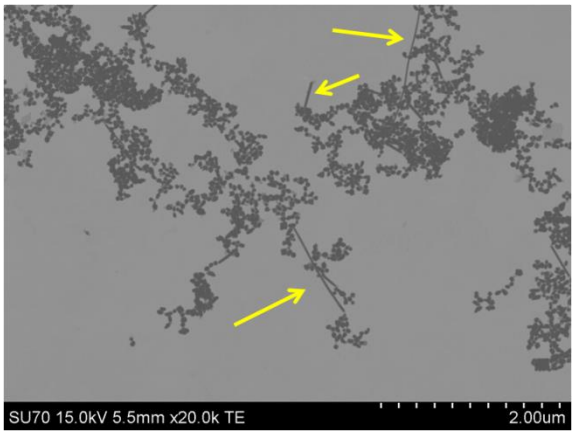

Figure 23: STEM Image of DAC at 20X Magnification showing Nano Wires.

IV.1.2 Effect of Washing

Centrifugation and washing were used to separate and remove the excess extract remaining in the solution. However, as shown in the following sections, this process caused a significant change in the properties of the particles.

Looking at the UV-Vis data (Figure 24), once again, AC1 and AC2 present similar absorption curves; in both cases the Pre Wash shows a double peak, and the Post Wash is a broader single peak, with a slight red shift. The double peak in this case would suggest a bimodal size distribution. The disappearance of the first peak after the washing would confirm this; the smaller set of particles would not be subject to an equivalent amount of centrifugal force, thus remaining in and being removed with the supernatant. Furthermore, the main peak of the Post Wash is at the same wavelength as the second peak of the Pre Wash, showing that it is in fact the larger particles that remain [266].

It is rather interesting that the OPS displays the inverse trend, with the Pre Wash having a single, rather narrow peak, and the Post Wash as a double. The narrow single peak of the Pre Wash is most likely due to the high temperature and pressure conditions of the synthesis, in which a large number of nucleation sites are created at the same time and grow into particles at the same rate, perhaps following the LaMer model [11]. The double peak of the Post Wash can probably be attributed to agglomeration during the centrifugation step. That the second peak is at a higher wavelength would further suggest that it is the combination of the smaller particles rather than the creation of smaller ones. As for the reason that this type of agglomeration does not occur for the other syntheses, it is possible that the capping agents of the extract were modified during the autoclaving such as to have a preference for this state [267, 268].

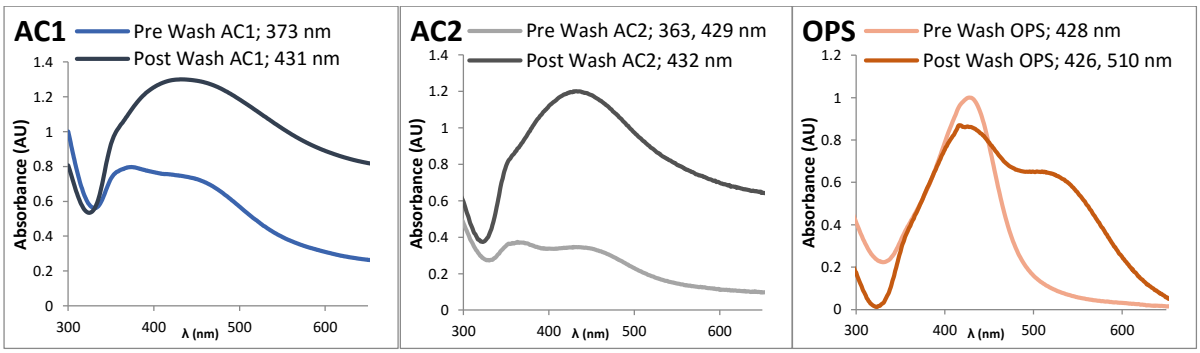

Figure 24: UV-Vis Spectra of Pre versus Post Wash for the Various Syntheses.

As Figure 25 shows, there is very little difference between the Pre and Post Wash hydrodynamic diameters as detected by DLS. This is especially true for the AC1 and AC2 batches. Both of the OPS batches show a larger diameter than the AC batches, with the Post Wash even larger than the Pre Wash.

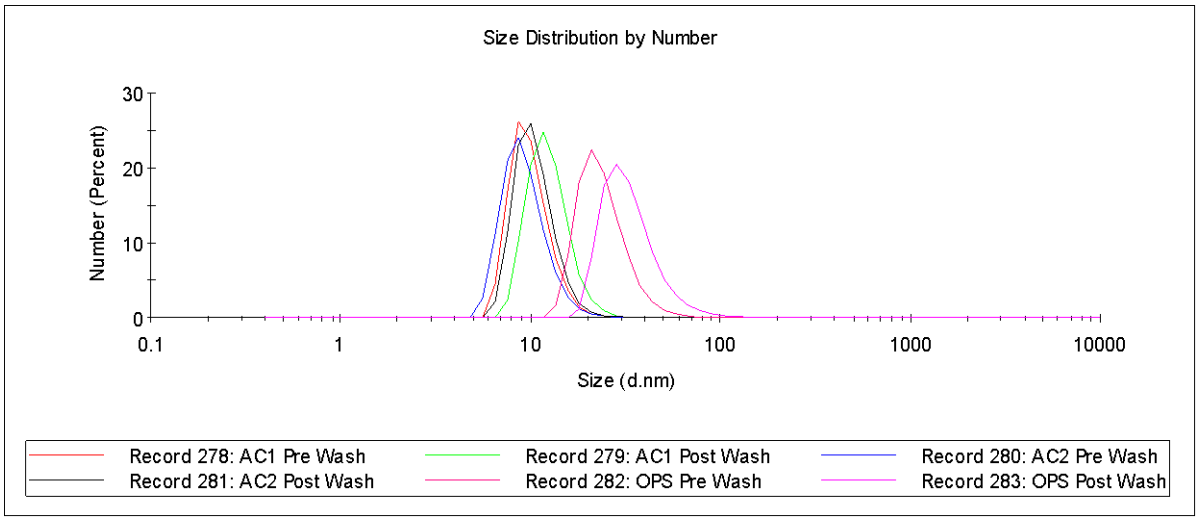

Figure 25: Hydrodynamic Diameter Size Distribution of Pre versus Post Wash of Various Syntheses (Zetasizer Instruments).

IV.1.3 Effect of Aging time

Due to the experiments progressing through a number of months, a study on "Aging" or rather, the evolution of the particles' characteristics over time, was conducted. Here the initial AC1 batch is compared to two other time points of one and two months.

The UV-Vis spectra showed little to no change with the passage of time (Figure 26). The peak seems to have become narrower for the AgNPs aged two months and a definite blue shift, indicating a narrower size distribution and smaller particle sizes.

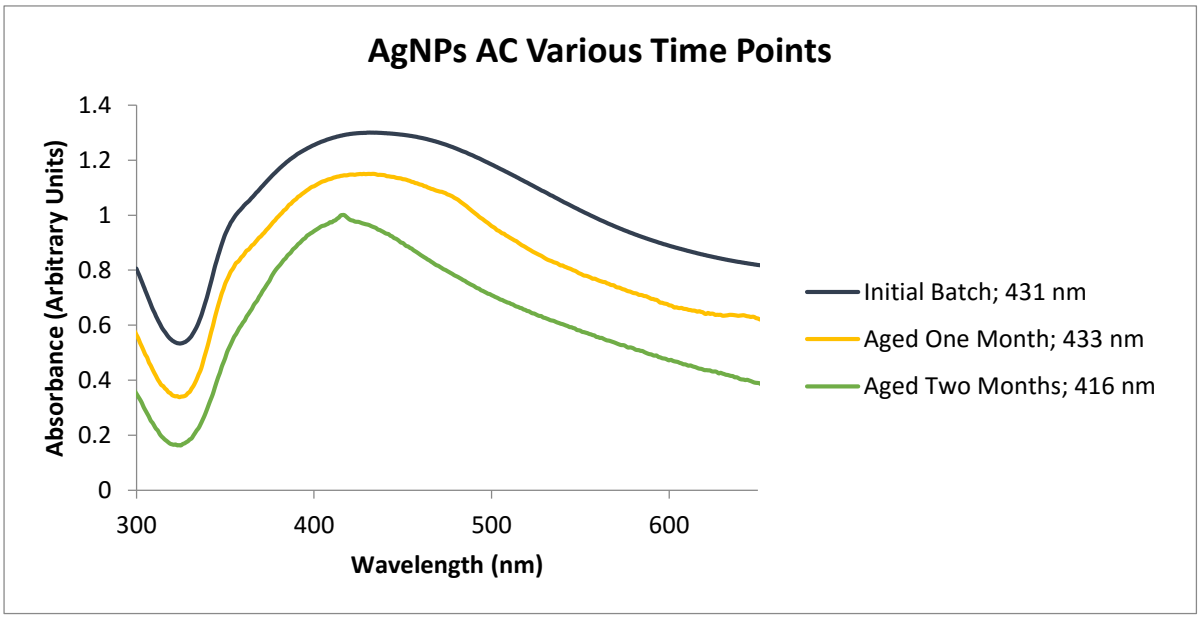

Figure 26: UV-Vis Spectra of AC1 Particles at Various Time Points with respective maximum absorbance.

The size distributions shown for the hydrodynamic diameter by the DLS in Figure 27 is somewhat surprising when compared to the STEM images and their respective diameter size distribution (Figure 20 and Figure 28). The DLS seems to suggest that after one month of aging, the particles fall into two size categories, whereas the initial AgNPs and the ones aged for two months fall into one. The suggested bimodal discrepancy can be attributed again to the limitations of the DLS. When compared, the STEM images and corresponding size distributions, offer a different but more logical explanation. The particles in the aged sample look more distinct and uniform (Figure 28), compared to the haze of smaller particles that surrounded the larger ones in the AC1 sample (Figure 20). The measured distribution confirms this; while the 10 to 20 nm category is still outside of the Gaussian curve, its magnitude has greatly decreased. This change can be attributed to the aging that other colloids, and often alloys as well, are subject to [13]. It is interesting to note that, while the value of the standard deviation has decreased, it is still relatively high as compared to the mean value.

At the onset of the reaction, a number of nucleation sites are created; under certain conditions, namely that the concentration of the precursors drops below the critical concentration for nucleation, these nucleation sites all grow at the same rate to become particles of the same size (LaMer model) [11]. Otherwise if the precursor concentration is above the critical point, nucleation sites are continuously created and so the particles grow to be of various sizes [13]. In the latter case, once the initial source of reactants has been depleted, the smaller particles are gradually dissolved, leading to re-deposition onto the larger particles; this phenomenon is the so-called Ostwald Ripening effect discussed in Chapter 1 [12].

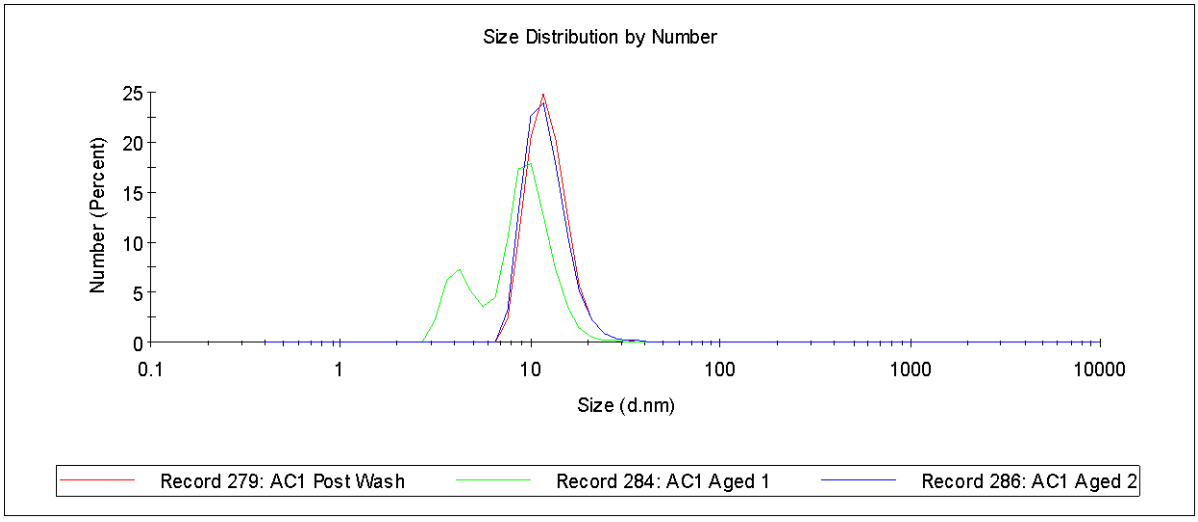

Figure 27: Size Distribution of Hydrodynamic Diameter for AC1 sample at various reaction times (Zetasizer Software).

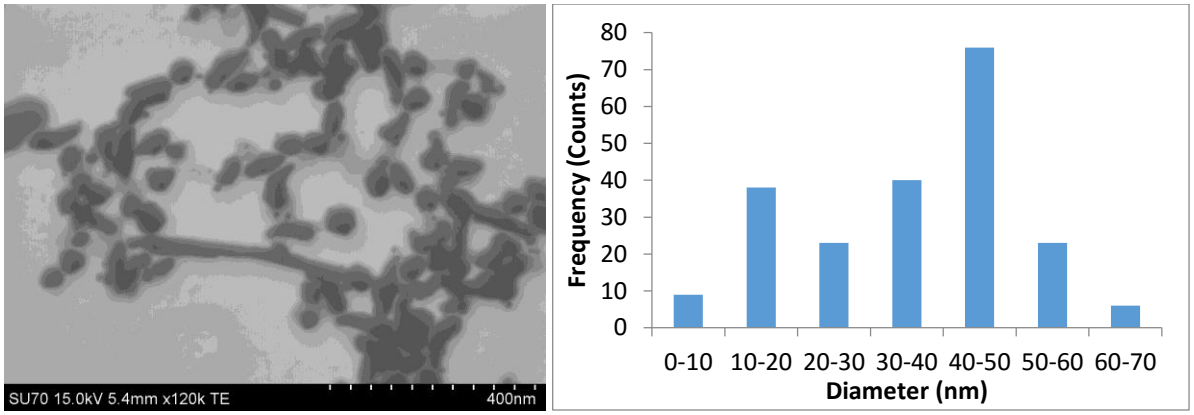

Figure 28: A) STEM Image of AC1 Aged One Month at 120X Magnification B) AC1 Aged One Month Size Distribution: 2 Images, 215 Measurements.

IV.1.4 Effect of the Solvent

It has been confirmed that the dispersing solvent has a great influence on the physico-chemical properties of NPs [269, 270]. The characteristics most affected are surface charge, hydrodynamic diameter, and agglomeration state. Here, the AgNPs were dispersed in two additional solvents, PBS and DMEM, in order to determine these changes. While DMEM is the solvent in which the particles are dispersed for *in vitro* testing, PBS is a good model for the use of AgNPs for signal enhancement in immunohistochemistry or similar applications [109]. While PBS consists of water with sodium phosphate and sodium chloride ions, DMEM also contains various amino acids and proteins, as well as vitamins and glucose. In fact, a number of studies on silica, ZnO, and TiO_2 NPs, have shown that the composition of the medium and the type of serum (proteins) used, also effect the stability of the particles [271, 272].

It is interesting to note that the UV-Vis spectra for sample AC1 (aged 1 month) in DMEM and water are quite similar, whereas in PBS they show a broader peak overall and a slight blue shift of the tip (Figure 29). It may be that the change in pH and ionic strength of the PBS solution modify the capping agents of the extract surrounding the particles; perhaps causing them to detach and diffuse into the solution. The DMEM on the other hand, would cause a similar detachment; however, it would also create a new coating made of amino acids and proteins. The results from zeta potential measurements, shown in Table 5, confirm this. The zeta potential of the particles increases from -27.5 mV in water to -17.6 mV in PBS and -9.37 in DMEM. As the particles have a negative surface charge by nature, they attract the positive ions, or positive molecules, in the two solutions, leading to an increase in zeta potential. The reason for the more drastic increase in the DMEM solution may have to do with higher charged molecules, or simply the conformation of the interaction [273]. On the other hand, this decrease in zeta potential can also indicate less stability; less surface charge means a lesser ability to repel other particles and may lead to agglomeration [243].

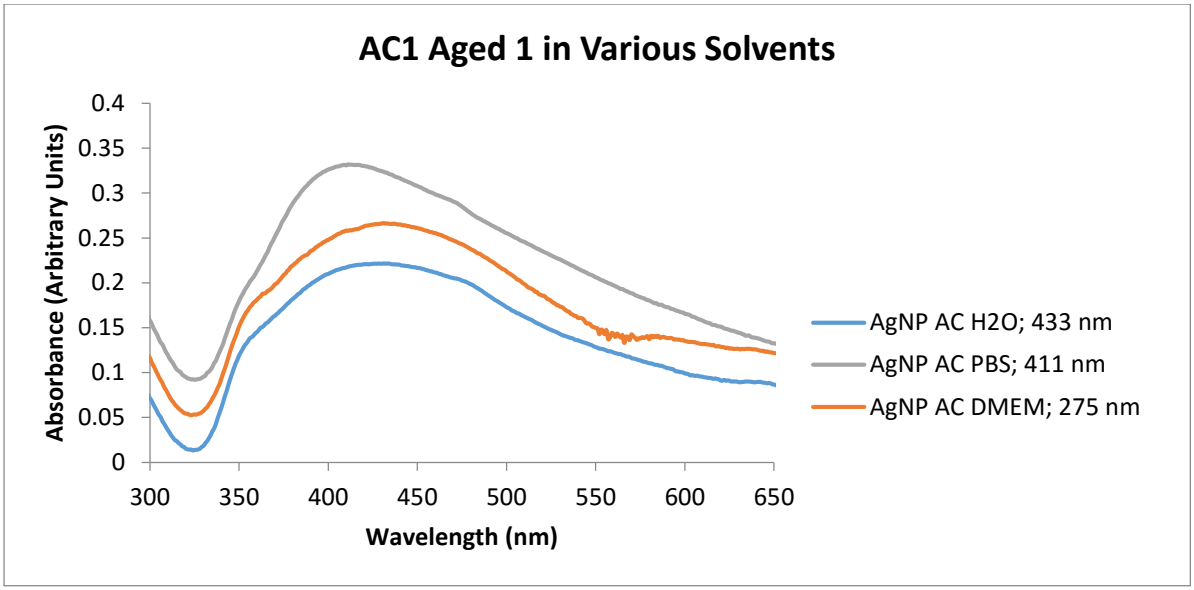

Figure 29: UV-Vis Spectra of AC1 Aged One Month in Various Solvents.

Table 5: Zeta Potential of AgNPs under various condition.

NP	Zeta Potential (mV)
AC1 Post Wash	-30.1
AC1 Aged One Month in Water	-27.5
AC1 Aged One Month in PBS	-17.6
AC1 Aged One Month in DMEM	-9.37
AC1 Aged Two Months	-23.6

The size distribution suggested by the DLS can only be used to compare the distribution curves, and not the suggested diameter values (Figure 30). It shows a bimodal distribution for AgNP in water and PBS, with most of the particles being of the larger size in water, and the majority being of the smaller size in PBS. This suggests that upon dispersion in PBS the particles tend to agglomerate or that their hydrodynamic volume is increased in some other way. The AgNPs in DMEM seem to be a combination of the other two curves; a bimodal distribution shifted towards a smaller particle size, with the smaller particles making up the larger peak. Here perhaps, the instability of the ions and particles in solution is balanced by the stereo-chemical interaction of the surface proteins; thereby reducing the agglomeration [273].

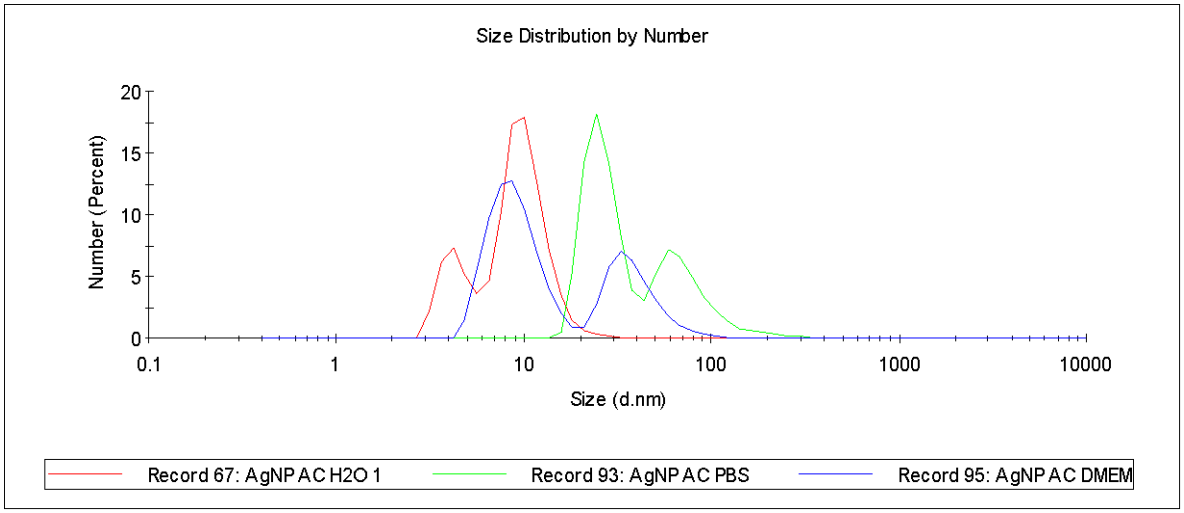

Figure 30: Hydrodynamic Diameter Size Distribution of AC1 sample Aged One Month in Various Solvents (Zetasizer Instrument).

IV.1.5 Effect of Incubation

In order to mimic the conditions of the AgNPs during the cytotoxicity and metabolomics testing, the particles were subject to size distribution analysis by DLS at an initial, as well as 24 and 48 hour time points during which they were incubated at 37 °C. A previous study in our workgroup had shown that the concentration of the AgNP in solution was a factor in their agglomeration state [274]; thus the concentrations that were being tested for the cytotoxicity and metabolomics assays were those chosen for this study. Finally, the particles were tested in both water and DMEM. Figure 31 shows the compilation of this data.

The AgNP dispersed in water showed good stability, both in terms of time and concentration. Indeed, it is only after 48 hours, and only for the lowest concentration of 5 µg/mL, that an increase in hydrodynamic diameter was observed. The AgNPs in DMEM have an overall higher hydrodynamic diameter, as expected, due to the protein corona that envelopes them. However here, we see the diameter increase at every concentration as the incubation time is increased. Moreover, a concentration dependent trend also forms, where at lower concentrations the diameters become increasingly larger. The increase in size due to incubation time can be attributed to the formation of agglomerates; or equally, the slower motion of the particles due to the evaporation of water and a subsequent increase in viscosity, for the instrument's algorithm is based on the particles' motion or velocity [243]. Similarly, the apparent increase in size at low concentrations may also be a consequence of velocity, rather than agglomeration. At low concentrations, the particles collide with each other less often, resulting in decreased motion, equated by the instrument to "larger" particles [275].

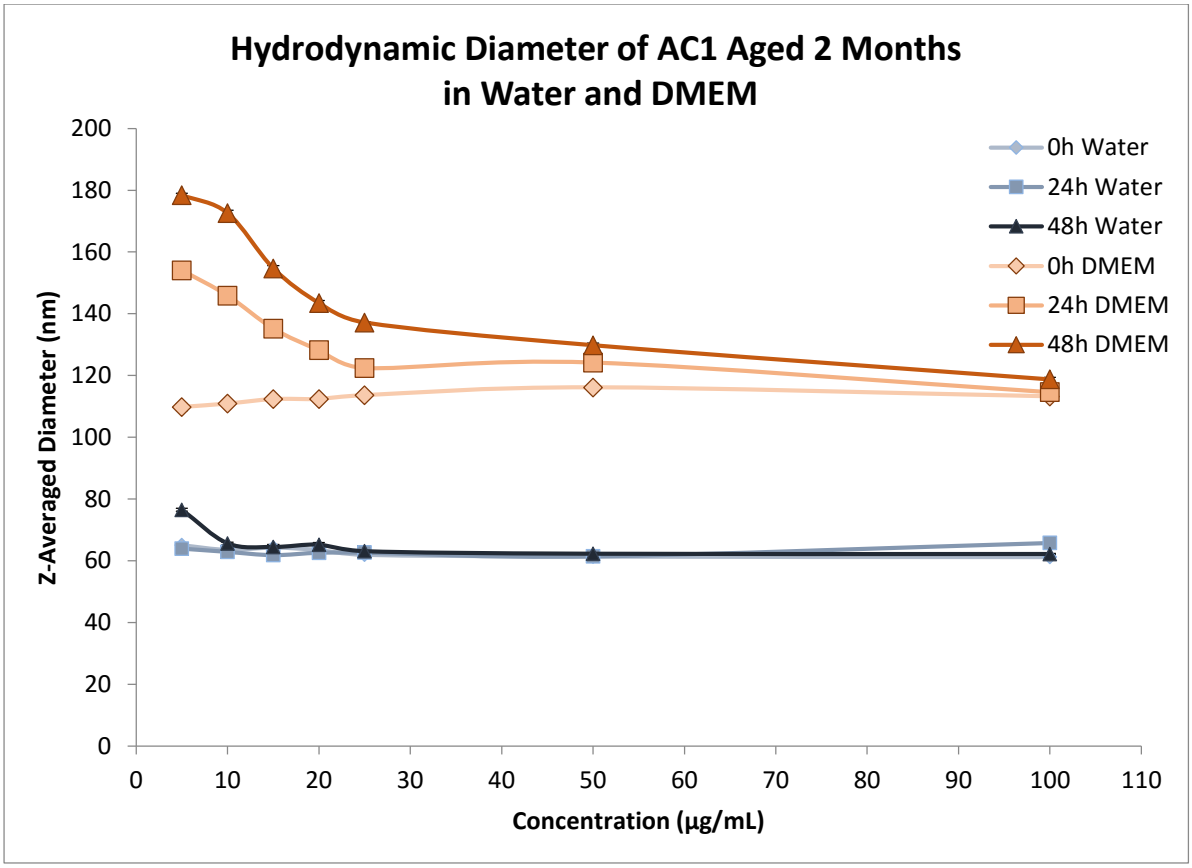

Figure 31: Hydrodynamic Diameter of AC1 sample Aged Two Months in Water and DMEM for Various Concentrations and Three Incubations Times.

IV.2 Characterization of PLAL AgNPs

UV-Vis presents a narrow band (maximum of absorbance at 421 nm) for the PLAL synthesis, indicating a more uniform size distribution as compared to the GS AgNPs (Figure 32). The PLAL, contrary to expectations, showed a broad, almost bimodal, curve around the same diameter as the GS AgNP samples when analyzed by DLS distribution by intensity (Figure 33). However, using the distribution by number, the band becomes narrow, with a peak indicating that it has a much smaller average diameter than the GS AgNPs, confirming the producers' specifications (Figure 34) [239]. Moreover, the particles also showed a more negative zeta-potential of -32.9 mV, indicating their superior stability, as compared to GS AgNPs, in water.

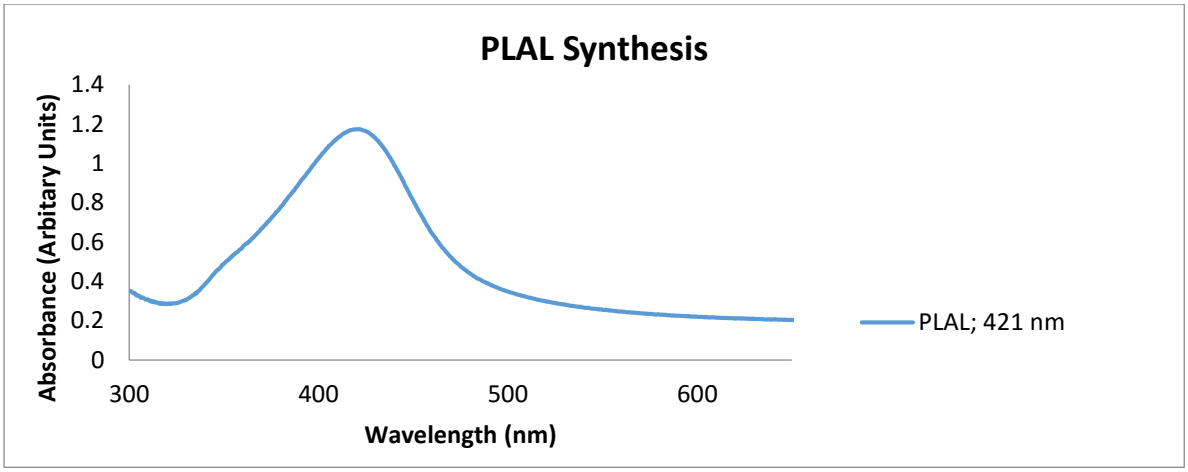

Figure 32: UV-Vis Spectra of PLAL AgNP Synthesis and respective maximum absorbance.

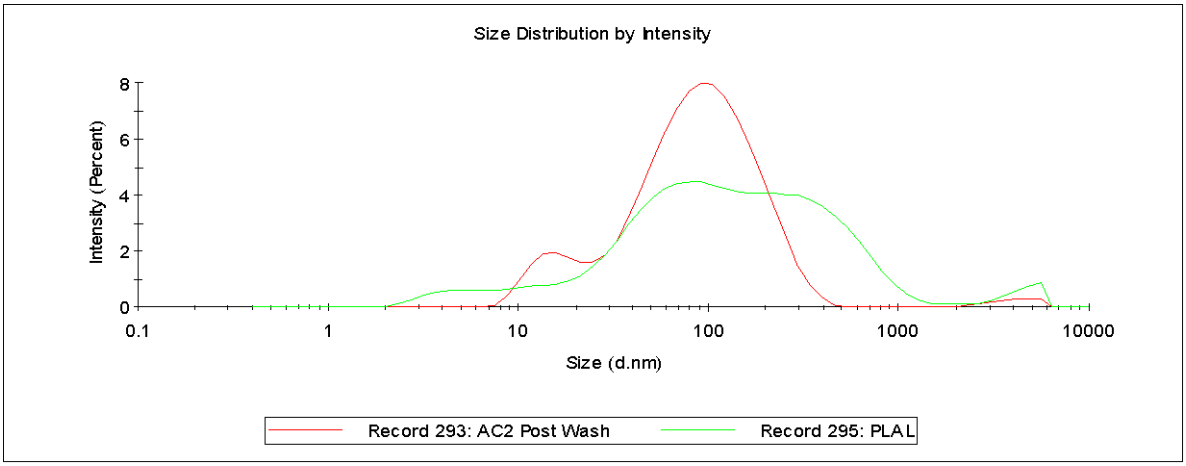

Figure 33: Hydrodynamic size distribution by intensity for PLAL AgNP synthesis (Zetasizer Software).

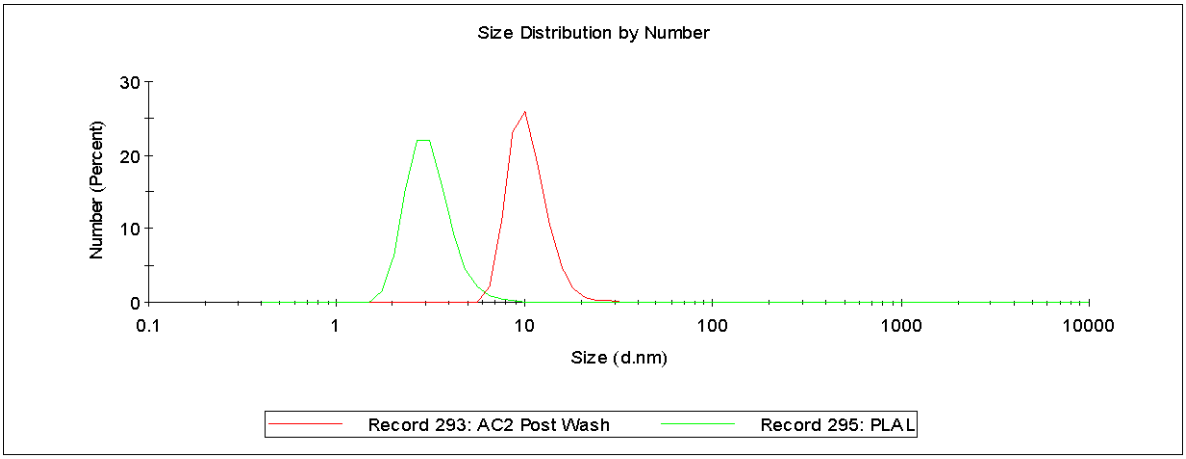

Figure 34: Hydrodynamic size distribution by number for PLAL AgNP synthesis (Zetasizer Software).

Finally, the STEM images as well as the derived size distribution for the PLAL particles are in fact in agreement with the UV-Vis and DLS distribution by number results (Figure 35). As expected, based on the specifications given by the collaborating partners [239], they showed a narrow size distribution, centered at approximately 10 to 15 nm with an average value of 10.84 nm. The only doubt that can be cast is towards the low number of measurements taken as compared to the other images. However, this was also expected for the initial concentration of these AgNPs was much lower.

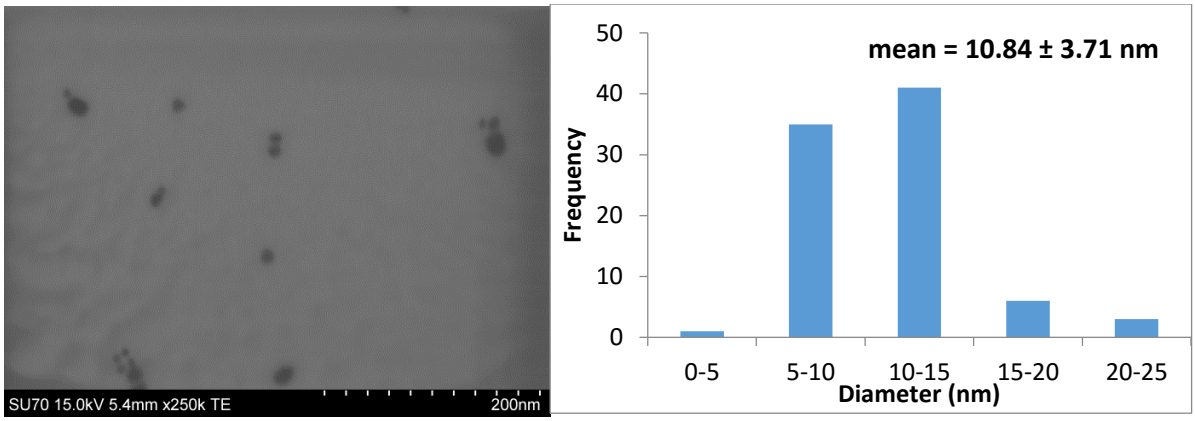

Figure 35: STEM Image of AgNP by PLAL at 250X Magnification and respective size distribution: 2 Images, 86 Measurements.

Chapter V: Cytotoxicity Evaluation of AgNPs in Human Keratinocytes

To characterize the Green Chemical Synthesis (GS) and PLAL AgNPs in terms of their cytotoxicity, HaCaT cells were exposed to them over 24 and 48 hour periods. The change in cells' morphology was observed and recorded, and the cell viability and cell cycle dynamics were also evaluated. A number of control studies were performed before testing of the actual particles. Where applicable, statistical analysis, in the form of the one way ANOVA test, was applied to the data. The IC_{10}, IC_{20}, and IC_{50} values were determined and used for the metabolomics studies (discussed in Chapter 6). As the results for the uptake study were preliminary, they are included in Appendix B. The following section describes and discusses the cytotoxicity results and their significance.

V.1 Exposure to Green Synthesis AgNPs

V.1.1 Cell Viability

The potential cytotoxicity of GS AgNPs was evaluated using the MTT cell viability assay in seven rounds of testing at 24 and 48 hour exposures, as well as two sets of controls; one for the toxicity of the *Eucalyptus globulus* Bark Extract (EGB), and one without cells to test for the interference of AgNPs with the MTT assay reagents.

V.1.1.1 Exposure of Green Synthesis AgNPs to HaCaT Cells

At each of those seven rounds of testing, small adjustments were made to the dose range until an appropriate range was selected. The results from the last round, with three independent assays each having four technical replicates, are presented in Figure 36. The displayed regressions are based on a logistical three parameter equation, previously shown in Chapter 2; where a is the curve's maximum value, b the steepness of the curve, and x_o the x value at the midpoint of the sigmoidal curve. It is in fact this x_o value that is used as the IC_{50}.The regression equation was modified from the one expressed in Chapter 2 by the software to include negative values of x and b.

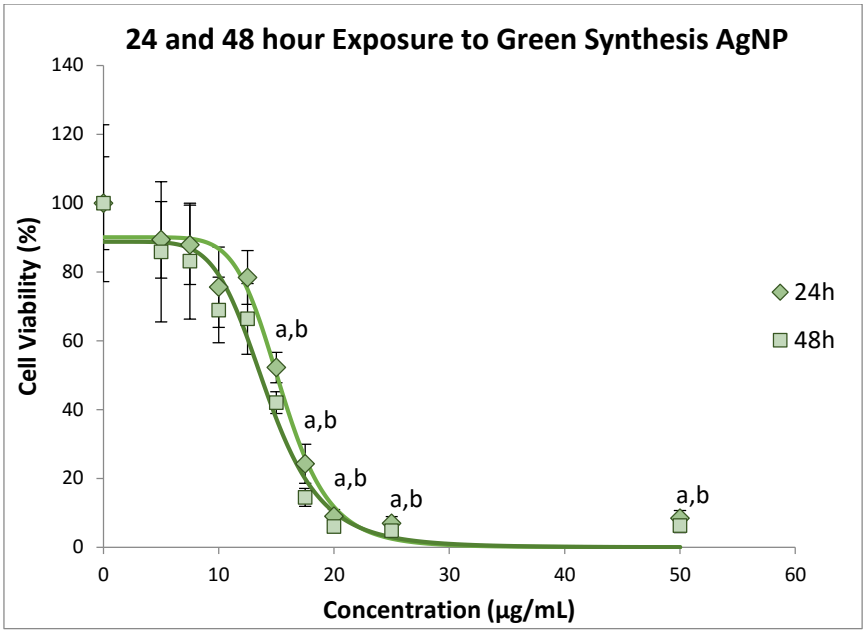

Figure 36: Cell Viability upon 24 and 48 hour Exposure to GS AgNP and the Respective Sigmoidal Logistic Curve Fitting; Where "a" indicates a significant difference as compared to the 24h control, and "b" indicates a significant difference as compared to the 48h control ($p<0.05$).

For the GS AgNPs 24 hour Exposure:

$$y = 90.0435 * \left(\frac{\left|\frac{x}{15.4932}\right|^{|7.4475|}}{1 + \left|\frac{x}{15.4932}\right|^{|7.4475|}} \right)$$

For the GS AgNPs 48 hour Exposure:

$$y = 88.7534 * \left(\frac{\left|\frac{x}{14.2183}\right|^{|5.9769|}}{1 + \left|\frac{x}{14.2183}\right|^{|5.9769|}} \right)$$

Though lacking significance, the lowest concentration tested shows a visible decrease in viability, with the 10 µg/mL and the 12.5 µg/mL concentrations causing a 20% decrease and falling onto the linear region of the sigmoidal curve. The next tested concentration of 15 µg/mL results in a 48% decrease in viability, and is quite influential in the calculation of the IC_{50} value. Moreover, the small standard deviation and homogeneous response for this concentration result in a significant difference as compared to the control for both the 24 and 48 hour exposure periods; therefore the calculation for the IC_{50} value can be considered reliable. A time-dependent effect is also apparent within the results as the cell viability for the 48 hour exposure is lower than that of the 24 hour. Moreover, a slight increase in "cell viability" can be noted for the highest AgNP concentration at 50 µg/mL.

The equations were used to calculate IC_{10}, IC_{20} and IC_{50} values for cell cycle and metabolomics studies, 24 hour durations 24 hour durations only. The calculated values are listed in

Table 6 along with the actual tested values. The actual tested values for the GS AgNPs were adjusted to reflect the decrease in viability based on the averages, as shown on the graphs, rather than the sigmoidal equations.

Table 6: Summary of Calculated Inhibition Concentrations for GS AgNPs.

IC_{10} (µg/mL)		IC_{20} (µg/mL)		IC_{50} (µg/mL)	
Calculated	Tested	Calculated	Tested	Calculated	Tested
11.7072	5.00	13.0838	10.0	15.4932	15.0

V.1.1.2 EGB Extract Control Study

As the AgNPs would be coated with the components of the EGB extract, its potential toxicity was assessed through a series of dilutions with cell culture media for 24 and 48 hour exposures. The cell viability as a function of the dilution factor is shown in Figure 37. The results indicate that the autoclaved EGB extract has little to no toxicity for the 24 hour exposure time, dipping to approximately 60% at the lowest dilution of 1/10 (0.1 on the figure). The toxicity does indeed increase for the longer exposure time of 48 hours, with the viability of the same dilution factor falling to approximately 30%.

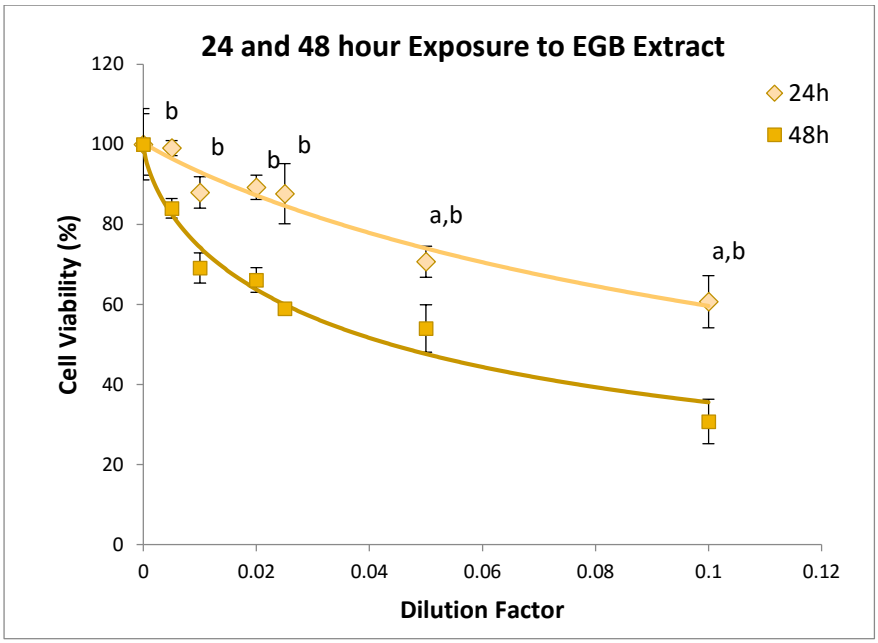

Figure 37: Cell Viability upon 24 and 48 hour Exposure to Various Dilutions of EGB Extract and Respective Sigmoidal Logistic Fits; where "a" indicates a significant difference as compared to the 24h control, and "b" indicates a significant difference as compared to the 48h control ($p<0.05$).

In order to put the extract cytotoxicity into context, the equivalent dilution factors to which the cells would be exposed with the AgNPs were calculated. The synthesis process included a number of dilution factors: with silver nitrate at a 1/4 dilution; during the washing at a 1/15 dilution, consisting of approximately 10 mL of AgNPs and 40 mL of water per wash, performed three times; and finally, the dilution in cell culture media according to the selected exposure concentrations. The AgNP concentrations in cell culture media and the corresponding extract dilution factors are given in Table 7.

Table 7: Equivalent Dilution of EGB Extract during AgNP Exposure

Concentration of Silver	Final Dilution Factor of Extract
100	1/1000
50	3/10 000
25	2/10 000
20	2/10 000
17.5	1/10 000
15	1/10 000
12.5	9/100 000
10	7/100 000
7.5	5/100 000
5	3/100 000

The highest dilution factor in the MTT Assay is 1/200, and shows a 1% decrease in cell viability; whereas even with the highest concentration of AgNPs, the associated amount of extract is equivalent to a 1/1000 dilution, suggesting a residual contribution to the toxicity.

V.1.1.3 AgNP Interference Control Study

As discussed in Chapter 1, some assays are prone to interference from nanoparticles. This was checked by performing five independent MTT assays without any cells, using only the GS AgNPs over a range of concentrations and the assay reagents. Figure 38 shows the averaged absolute absorbance values from these assays, as well as a typical curve from an assay with cells, while the inset shows only the no-cell absorbance curves. From the inset, the results show no increase in absorbance for concentrations below 17.5 µg/mL; from 25 µg/mL to 100 µg/mL there is a slight but steady increase, with a final difference of 0.03 as compared to the control. Statistical analysis on these numbers did not yield any significant difference. Moreover, these differences seem almost insignificant when put into the context of assays with cells. Nevertheless the increase in absorbance at the higher concentrations, above 50 µg/mL, is noticeable in assays with and without cells.

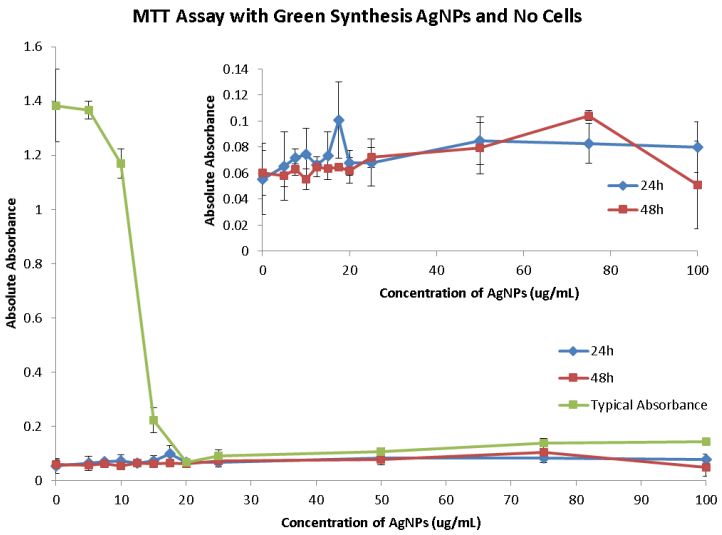

Figure 38: Absolute Absorbance at 570 nm of an MTT Assay performed without cells using the Green Synthesis AgNPs; Statistical analysis failed in finding a significant difference between any of the values.

V.1.2 MORPHOLOGY

HaCaT cells, under normal conditions, are adhering cells of triangular shape that grow into a monolayer. With a light microscope at 10X magnification, the nucleus can be distinguished as the relatively spherical grey outline at the center of each cell, with the smaller darker shapes being various cell organelles. Once seeded, the cells start to grow in colonies that eventually reach each other; the flask or plate is considered fully confluent when the entire surface is covered with cells (Figure 39).

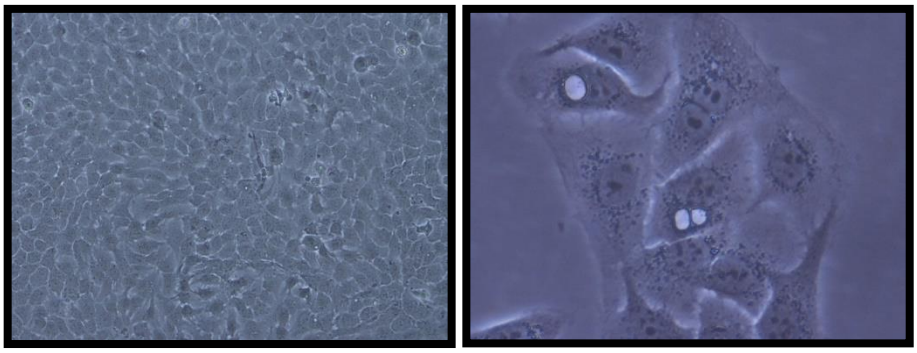

Figure 39: Left, A confluent surface of HaCaT cells at 10X magnification; Right, A colonoy of HaCaT cells at 40X magnification.

The cells were exposed to three concentrations of GS AgNPs; 5 µg/mL, 10 µg/mL and 15 µg/mL. After 24 hours of incubation, the cells exposed to 5 µg/mL were indifferentiable from the control, however, those exposed to 10 µg/mL showed a lower confluence, suggesting slower proliferation. The cells exposed to 15 µg/mL no longer had intact cell membranes; instead, there were a number of circular outlines around and overlapping the cells (Figure 40). Moreover, the cell organelles, as well as a number of round floating cells, could be seen suspended throughout the media. Together, these signs confirm cell death, with the spherical outlines suggesting apoptosis, or programmed cell death. The number of cells per colony was close to the cell density upon exposure, suggesting that the cell cycle was arrested and that they died shortly afterwards.

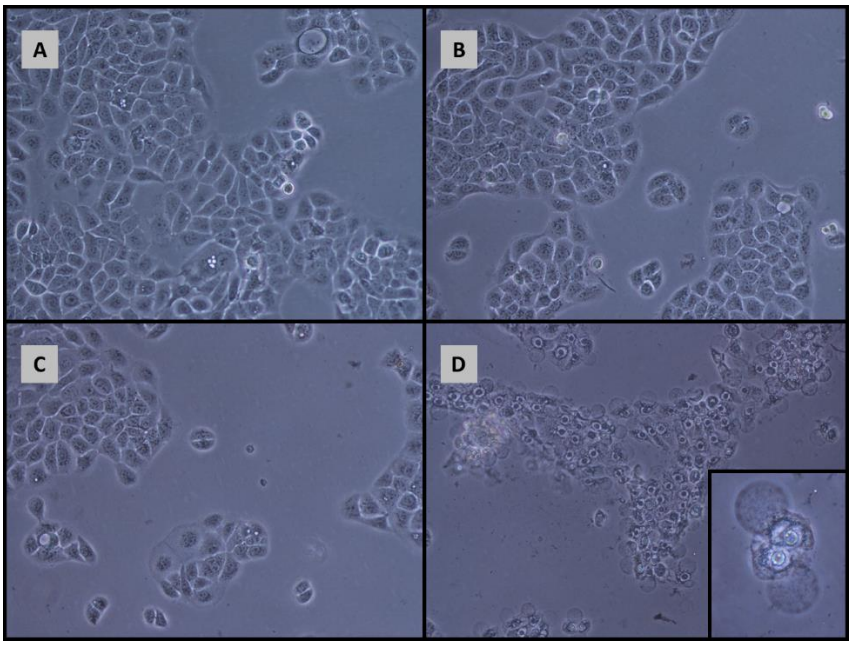

Figure 40: Cell morphology after 24 hours of exposure to GS AgNPs at 10X magnification; A) Control; B) 5 µg/mL; C) 10 µg/mL; D) 15 µg/mL; Inset at 40X magnification.

After 48 hours of exposure, the 5 µg/mL wells were approximately 10 to 15% less confluent than the controls, while the 10 µg/mL wells showed 30 to 40% less confluence, with little or no signs of cell death. This may indicate that while this concentration slows down or stops the regular cell cycle, it does not cause cell death. The 15 µg/mL wells looked just as they had at the 24 hour mark, with all the cells being dead.

V.1.3 Cell Cycle Analysis

Approximately three months after their synthesis, the Green Synthesis AgNPs were used to conduct cell cycle analysis. Three concentrations of 5, 10 and 15 µg/mL were tested against the controls, for both a 24 and 48 hour duration. The number of counted nuclei was plotted against the intensity of fluorescence detected in channel 3 (FL3) as shown in Figure 41 and Figure 42; where the intensity of fluorescence is proportional to the amount of PI bound to the DNA. The boundaries of the peaks were set using the FlowJo software to distinguish nuclei in the G_0/G_1, S, and G_2/M phases, as shown by the green, beige, and blue colours, respectively; the area under each curve was then calculated. The ratio of these areas were determined and plotted in Figure 43. Although a concentration of 15 µg/mL was also tested, the results were omitted as there was not a sufficient number of cells for significant detection by the flow cytometer.

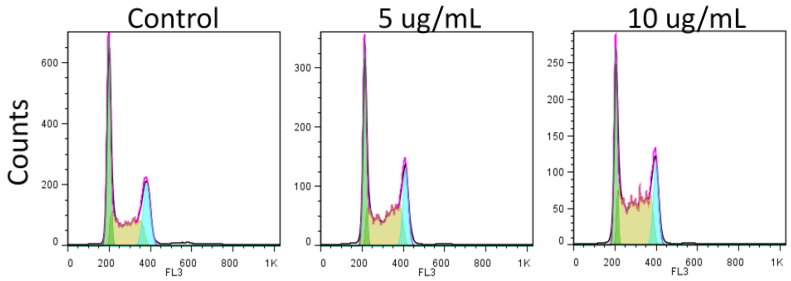

Figure 41: The number of counted nuclei with respect to the intensity of fluorescence detected in channel 3 (FL3) for the 24 hour exposure of HaCaT cells to 0, 5, and 10 µg/mL of Green Synthesis AgNPs.

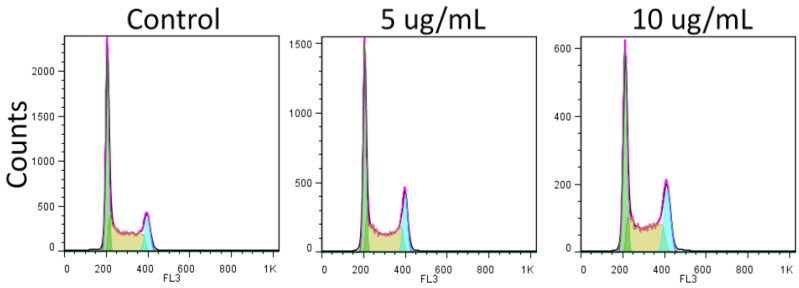

Figure 42: The number of counted nuclei with respect to the intensity of fluorescence detected in channel 3 (FL3) for the 48 hour exposure of HaCaT cells to 0, 5, and 10 µg/mL of Green Synthesis AgNPs.

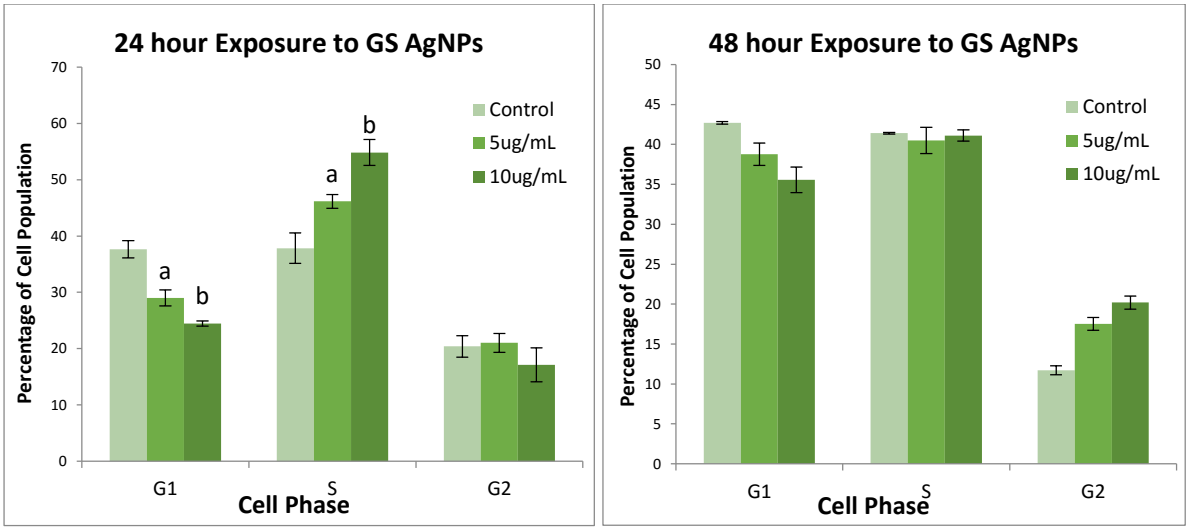

Figure 43: Percent of cells in each phase of the cell cycle upon exposure to GS AgNPs for 24h (Left) and 48h (Right); where "a" and "b" indicate a significant difference as compared to the control sample in that phase, and where "a" is significantly different from "b" as assessed by one way ANOVA.

An asynchronous culture of cells will have a random number of nuclei in each cell cycle phase. In this case, at the end of the 24 hours, the control population had almost an equal number of nuclei in the G_0/G_1 and S phases, with the G_2/M phase at almost half of those values (Figure 43), indicating that the cells are actively proliferating. However, the G_0/G_1 population decreases incrementally for both of the exposure concentrations, while the S phase population increases. The number of cells in G_2/M phase remains at a relatively constant percentage, though slightly less for the 10 µg/mL concentration. The increase in S phase suggests cell cycle delay at the S-phase and the decrease in G_2/M phase confirms this. This in turn shows that that cells are attempting to repair damaged or miscopied DNA.

After 48 hours, the control cells are once again, equally divided between the G_0/G_1 and S phases; however, the population in G_2/M phase is now barely more than a quarter of the others. A decrease in G_0/G_1 phase is evident as the exposure concentration increases, though contrary to the 24 hour duration, it is the population in G_2/M phase that increases incrementally, rather than the S. On the other hand, the 24 and 48 hour G_2/M percentage values for the 5 and 10 µg/mL concentrations have opposite changes; the 5 µg/mL changes from 21.0% to 17.5%, whereas the 10 µg/mL changes from 17.1% to 20.2%. The decrease of the population in G_2/M phase for 5 µg/mL is in line with the change in controls, suggesting that the cells were able to move past the G_2 checkpoint, divide, and are now part of the G_0/G_1 phase. The increase in G_2/M phase for the 10 µg/mL, coupled with the decrease in the S phase, would suggest that the cells that were previously held at the S-phase checkpoint were able to pass, and are now held at the G_2 checkpoint, indicating cell cycle arrest. Furthermore, a possible implication of the altered arrest checkpoint is that the cells were successful in making the repairs, suggesting that cell recovery is possible.

V.2 Exposure to PLAL AgNPs

V.2.1 Cell Viability

The PLAL AgNP, coming from a stock solution of lower concentration, could only be tested up to a concentration of 10 µg/mL; this is because the maximum dilution of media tolerated by the cells is approximately 10%. Moreover, a smaller amount of this stock further lead to limitations in terms of the type of studies that could be employed. On the other hand, the particles were tested with the

original citrate coating, as well as an ubiquitin coating. Similar to the case for GS AgNPs above, a coating toxicity control was also performed, where HaCaT cells were exposed to ubiquitin only.

V.2.1.1 Exposure of HaCaT Cells to PLAL AgNPs

Cell viability was assessed using the MTT assay, as before. Figure 44 and Figure 45 show the resulting cell viabilities for the 24 and 48 hour exposures respectively. Considering the low concentrations tested, a significant decrease in cell viability can be seen for all tested concentrations at 24 hours, including the lowest at 2.5 µg/mL (Figure 44). Furthermore, the shape of the logistic curve fit and respective equations, namely the *b* value, are very different from those of the Green Synthesis AgNPs, having a gradual decrease in viability as oppose to a drop. The precision of the three independent assays is notable, especially considering that they were conducted in a two week period, completely independent of time. Moreover, there is no statistical significance between the particles coated with and without ubiquitin.

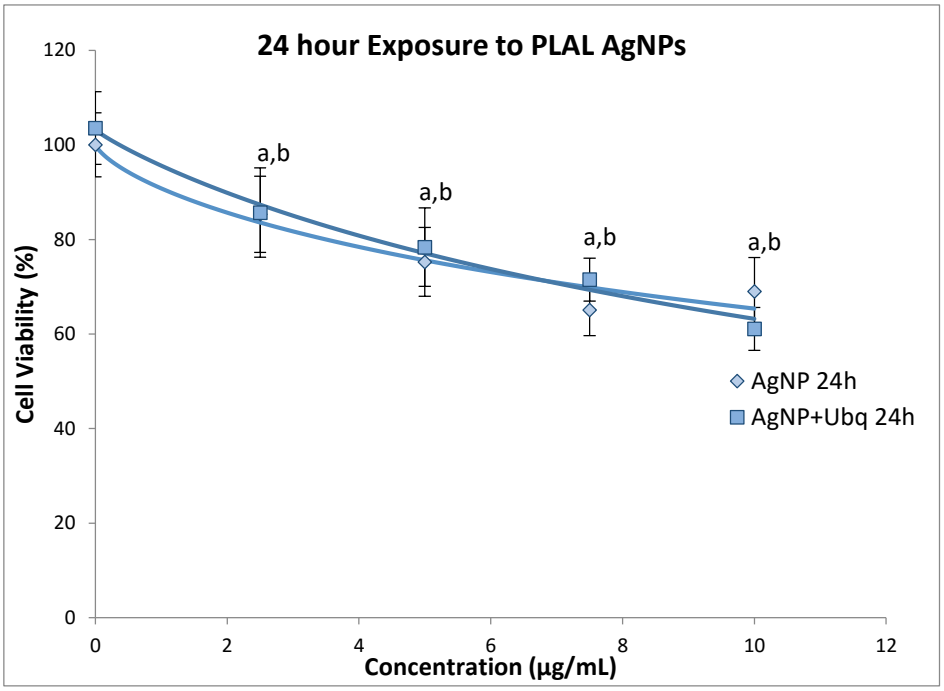

Figure 44: Cell Viability upon 24 Hour Exposure to PLAL AgNP and the Respective Sigmoidal Logistic Curve Fits; where "a" indicates a significant difference as compared to the AgNP control, and "b" indicates a significant difference as compared to the AgNP+Ubq Control ($p<0.05$)

For 24 hour exposure to PLAL AgNPs:

$$y = 100.2524 * \left(\frac{\left|\frac{x}{24.1934}\right|^{|0.7103|}}{1 + \left|\frac{x}{24.1934}\right|^{|0.7103|}} \right)$$

For 24 hour exposure to PLAL AgNPs coated with Ubiquitin:

$$y = 103.2493 * \left(\frac{\left|\frac{x}{16.5899}\right|^{|0.9010|}}{1 + \left|\frac{x}{16.5899}\right|^{|0.9010|}} \right)$$

The 48 hour exposure to PLAL AgNPs showed similar results in terms of curve shape and statistical significance (Figure 45). However, the toxicity does not seem to be dependent on time for the

decrease in viability is minutely different between the 24 and 48 hour exposures. This is reflected in the equations, where the x_o values are greater for the 48 hour exposure than the 24 hour. In fact, the regression curves calculated seem more linear than sigmoidal.

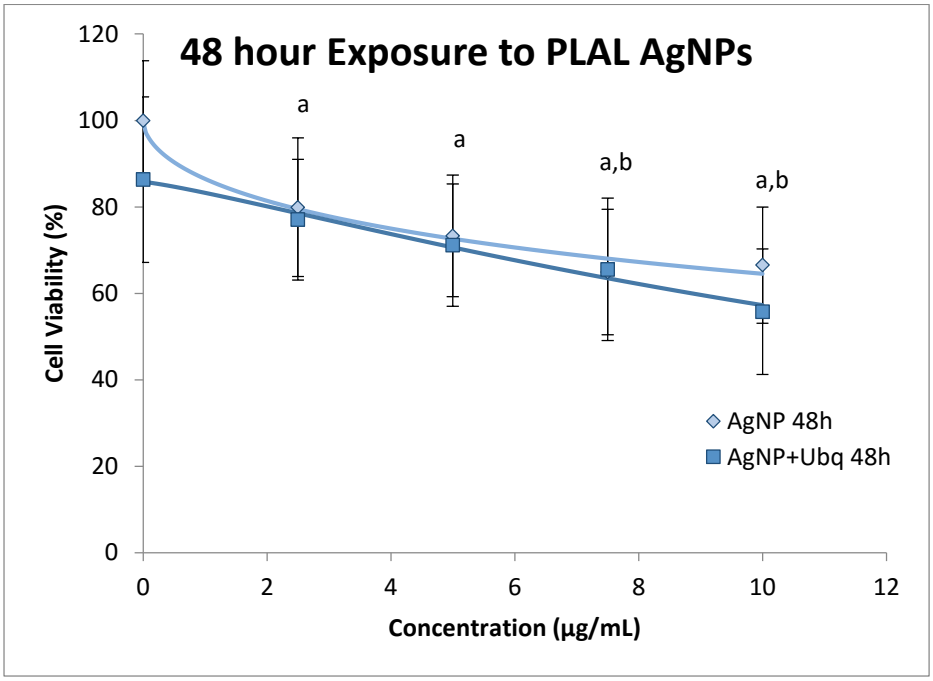

Figure 45: Cell Viability upon 48 hour Exposure to PLAL AgNP and the Respective Sigmoidal Logistic Curve Fits; where "a" indicates a significant variation as compared to the AgNP control, and "b" indicates a significant variance as compared to the AgNP+Ubq Control

For 48 hour exposure to PLAL AgNPs:

$$y = 100.0516 * \left(\frac{\left|\frac{x}{29.8978}\right|^{|0.5446|}}{1 + \left|\frac{x}{29.8978}\right|^{|0.5446|}} \right)$$

For 48 hour exposure to PLAL AgNPs coated with ubiquitin:

$$y = 85.8139 * \left(\frac{\left|\frac{x}{17.7664}\right|^{|1.2146|}}{1 + \left|\frac{x}{17.7664}\right|^{|1.2146|}} \right)$$

The calculated values based on the above equations are listed in Table 8 along with the actual tested values. For the PLAL AgNPs, the actual tested values were based on the AgNPs without the ubiquitin coating, in order to minimize the number of altered parameters.

Table 8: Summary of Inhibition Concentration Values for PLAL AgNPs.

	IC_{10} (µg/mL)		IC_{20} (µg/mL)		IC_{50} (µg/mL)	
	Calculated	**Actual**	**Calculated**	**Actual**	**Calculated**	**Actual**
PLAL AgNPs	1.0928	1.09	3.4210	3.42	24.1934	N/A
PLAL AgNPs+Ubq	1.3920	1.09	3.4075	3.42	16.5899	N/A

V.2.1.2 Ubiquitin Control Study

Similarly, as a portion of the PLAL particles was coated in ubiquitin, an MTT Assay of this protein was also carried out. The stock solution of 500 µM ubiquitin in citric acid underwent a similar dilution series as that of the extract; the results shown below include the conversion from µM to µg/mL (Figure 46).

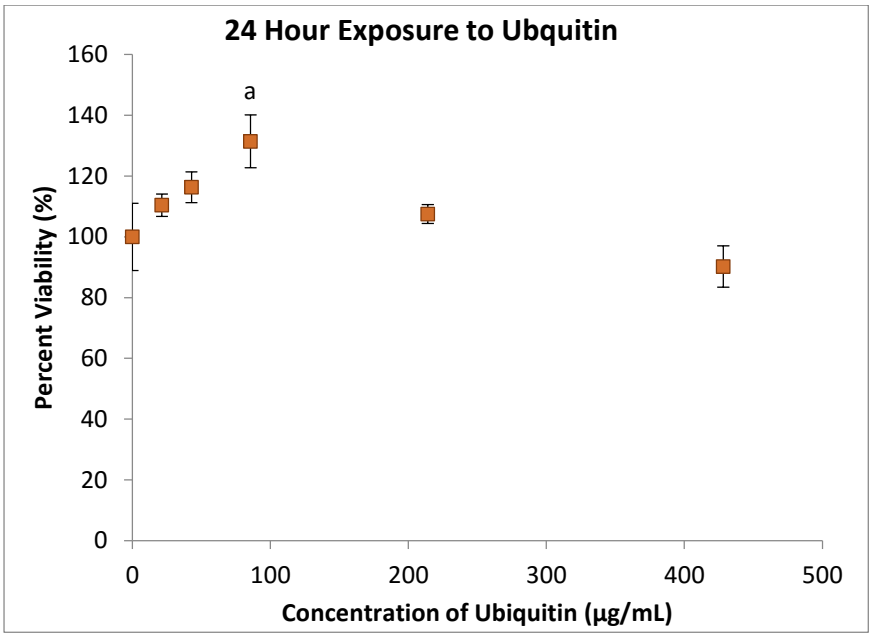

Figure 46: Cell Viability upon 24 hour exposure to various concentrations of ubiquitin; where "a" indicates a significant variation as compared to the control using the Holms-Sidak Method ($p<0.05$).

Here the ubiquitin shows little to no toxicity, with the loss of cell viability at the highest concentration possibly being attributed to the decrease in cell culture media. In fact, at the lower concentrations, an increase in cell viability can be observed. Similar to the extract control, an equivalent concentration of ubiquitin during exposure with AgNPs was calculated. The final concentrations of ubiquitin with AgNPs ranged between 0.12 to 1.0 µg/mL; since the variance between the control and the lowest concentration of 20 µg/mL is not significant, neither an increase nor a decrease in viability due to the ubiquitin coating of particles can be concluded.

V.3 Discussion

The AgNPs synthesized via two green synthesis techniques, one chemical and one physical, were characterized in terms of their cytotoxicity to the HaCaT cell line. Two qualitative and two quantitative methods were chosen; namely the study of morphology and uptake, as well as the MTT cell viability assay and cell cycle analysis. In addition, three control studies were conducted; two to determine the toxicity of the respective coatings, and the last to check for the interference of AgNPs with the MTT assay reagents.

Neither of the coatings revealed an inherent toxicity, except at low dilutions. However, this can also be attributed to the 10% decrease in cell culture media; in other words for low dilution factors, each cell receives less nutrients. The increase in cell viability upon exposure to ubiquitin would correlate with recent studies that have shown the modulation of immune response and inflammation via extracellular ubiquitin [276, 277]. If true, it would suggest that the coating of particles with ubiquitin would in fact lower their effective toxicity. However, this was not reflected when the particles were coated in ubiquitin, as there was no significant difference between any of the tested PLAL AgNP

concentrations with their ubiquitin-coated counterparts. At the same time, the concentration of ubiquitin coating the tested AgNPs was much lower than the concentration that caused the increase in viability. A more appropriate dilution range must be tested in order to derive an exact response.

The precedent of nanoparticle interference with toxicity assays, as discussed in Chapter 1, prompted a control study on whether the AgNPs used for this project would cause a similar interference with the assay reagents. AgNPs have been shown to interfere with the LDH assay [94], as well as more recently the MTS, a viability assay that works similar to the MTT [278]. Moreover, a study comparing three different viability assays using a similar type of control, found that unwashed and carbon-coated AgNPs induced a statistically significant increase in absorbance with the MTT assay reagents [192]. Previous studies in our workgroup had shown that PVP coated AgNPs caused an increase in absorption for the MTT, whereas neither citrate nor PEG coated particles did so [274]. Nevertheless, the MTT continues to be the standard for testing cell viability in literature, though the tendency to confirm the results with other assays has become common [71, 196, 192, 222]. Thus, while our investigation used the MTT assay as the sole method of determining viability, the respective interference study was performed.

The results showed the interference to be negligible at low concentrations, and minimal at even the highest tested concentration. The MTT assays with cells did in fact show an increase in viability at the higher concentrations. The maximum interference detected increased the absorption by approximately 0.03; while it may be visually noticeable as compared to the 0.2 absorption for a well of dead cells, it is almost insignificant as compared to the control wells that retain absorptions of 1.5. The results from this control help explain the increase in signal at high concentrations, where the cells are known to be dead. At the same time, they also show that interference at low concentrations is minimal and that the MTT can be used as a viability assay with AgNPs.

The viability assays revealed an IC_{50} value of 15.49 and 14.21 µg/mL for the GS AgNPs at 24 and 48 hour exposures respectively; while the PLAL AgNPs showed 24.19 and 29.89 µg/mL for 24 and 48 hour exposures, and the PLAL AgNPs with ubiquitin coating showed 16.59 and 17.76 µg/mL, respectively. Based on the IC_{50}s, the GS AgNPs cause the highest decrease in viability. However, the values from the latter type of synthesis cannot be considered reliable as they are extrapolated outside of the tested concentration range.

The overwhelming death response induced by the IC_{50} dose for the morphology and cell cycle studies suggests a discrepancy, or rather a missing factor, that has not been accounted for. In both cases, exposure to the 50% inhibitory concentration caused a greater death response than expected. This discrepancy may be attributed to a number of factors; the steepness of the linear region of the sigmoidal curve; the effects of AgNP storage conditions; and the change in dose per cell.

The steepness of the curve means that even the smallest change in concentration would create a drastic change in cell viability. Regarding storage conditions, other studies have shown that the dissolution of AgNPs is greatly affected by temperature and time [136, 137]. Unlike the PLAL AgNPs, the GS particles were stored in the dark but under ambient condition. The AgNPs become smaller as they dissolve by releasing more and more silver ions, increasing the toxicity in two ways; an increased concentration of silver ions, and smaller particles [192, 136, 224, 196, 198]. This in turn means that over time the same batch of AgNPs, for which a particular IC_{50} had been calculated, becomes more toxic with an actual IC_{50} that is potentially much lower.

Furthermore, the dose per cell value must also be taken into consideration. The IC_{50} is calculated based on the MTT test, performed in 96-well plates, at a cell density of 6 000 seeded cells per well, whereas

the morphology and cell cycle assays are performed in 6-well plates, at a density of 100 000 seeded cells per well. In order for the IC_{50} to be an equivalent dose to those cells, they must be equally confluent at the time of exposure. However, this was not the case as observed by visual inspection, with the larger wells being less confluent 24 hours after seeding. This means that those cells received a higher concentration of AgNPs per cell, leading to their death in greater numbers than expected. Thus, higher inherent toxicity, due to storage conditions, and the lower number of cells, due to the seeding density, are enhanced by the steepness of the curve, ultimately resulting in the drastic effect observed.

This is in part reflected by the changes in morphology and cell cycle. Observation of the cells after 24 hours indicated extensive cell death, likely as apoptosis, for cells exposed to the IC_{50}, while those exposed to the IC_{20} only a showed a slower proliferation, even after 48 hours. This was further confirmed by cell cycle analysis where the IC_{50} samples did not contain enough cells, and the IC_{10} and IC_{20} samples showed first a delay in S phase, then arrest at the G_2/M phase, in a dose dependent manner. Other studies with AgNPs have also shown cell cycle arrest at the S [198] and G_2 phases [200, 197, 71, 205].

Although the IC_{50} value derived for the PLAL AgNPs may not have been reliable, the smaller error bars and the resulting statistical significance as verified by the ANOVA test, suggest that they are more uniform in nature and more stable through time as compared to the GS AgNPs; especially considering that the PLAL assays were conducted throughout a two week period and the GS assays within hours of each other. This is further confirmed by the lack of correlation between cell viability and exposure time; which also indicates particle stability. In contrast, the variable results from the GS AgNPs would suggest a lack of uniformity and stability through time, similarly reported by the physico-chemical characterization (Chapter 4). The GS AgNPs showed an evolution in morphology, size, and size distribution with the passage of time, reflected here in cytotoxicity studies as variability within the same assays. This too, can be attributed to storage conditions and the excessive release of silver ions [136, 137, 279, 224].

The different viability profiles and inhibition concentrations are usually due to the differences in average particle size, size distribution, and surface coating. While both silver ions and AgNPs may damage the cell membrane from the outside, it has been shown that their uptake into the cells, either via endocytosis or diffusion, can have far more devastating effects [196, 225]. The acidic environment of lysosomes has been suggested as the site where the particles are degraded into ions, thus becoming more available to create ROS, or to damage DNA and other organelles directly [225]. Here the smaller particles, PLAL AgNPs, induced a more uniform, almost linear, response. Whereas the larger particles, GS AgNPs, showed a steep drop in cell viability. This difference can be attributed to the uptake dynamics of each type of particle, as well as the ion release kinetics in solution and within the cell. However, without further testing of ionic silver concentrations, localization of particles upon uptake, and more systematic controls, a definite conclusion as to how each particle induces toxicity cannot be derived.

Surface coating of NPs is another important factor in determining cellular response. Previous studies performed at our workgroup showed an IC_{50} value of approximately 40 µg/mL for citrate coated particles and over 50 µg/mL for PEG coated particles [274]. Other studies in literature have also shown the importance of AgNP coating, with citrate coatings reported as having higher toxicity compared to other coatings, namely PVP and L-Lactose. The difference in toxicity stemming from differences in coating can be attributed to two phenomenon: the particles' uptake due to different interactions with the cell membrane; as well as the hindrance or enhancement of silver ion release, modulated by the steric nature of the coating molecules [280].

The toxicity seen for the GS AgNPs may be due to the nature of the saccharide coating. As the capping molecules are small, they provide low steric interaction and may readily detach, therefore allowing higher dissolution rates of silver ions, and thus higher toxicities. A comparison cannot be made to the PLAL particles, for not only does the coating change to citrate, but the size and size distribution are also different. Therefore, without controlling for one parameter or the other, it is not possible to attribute the difference in toxicity to a specific characteristic. Moreover the toxicity of PLAL citrate coated AgNPs cannot be compared to previous studies of the workgroup until higher concentrations are tested and a reliable IC_{50} is established.

Chapter VI: Metabolomics

To further assess toxicity by understanding the alterations in cellular biochemical processes, an NMR-based metabolomics approach was taken. A series of 24 hour assays were conducted comparing controls to a low exposure concentration (IC_{10}), and a higher exposure concentration (IC_{20} or IC_{50}). Each sample was subject to a dual-phase extraction to collect aqueous and organic phases. The results of the aqueous phase for the Green Synthesis AgNPs (GS or GAg) and the PLAL AgNPs (PAg) are given in the following section.

VI.1 Peak Assignments

The averaged ^{1}H NMR spectrum of four aqueous extract obtained from HaCaT cells is shown in Figure 47. Due to the similarity in cell line, composition of particles, and methodology, the spectral peak assignment previously performed by our work group was confirmed on a peak-by-peak basis and subsequently used. Moreover a visual comparison of spectra from the two studies confirmed that there were no significant peaks outside those already assigned. Table 9 shows the compound names and the assigned peak positions.

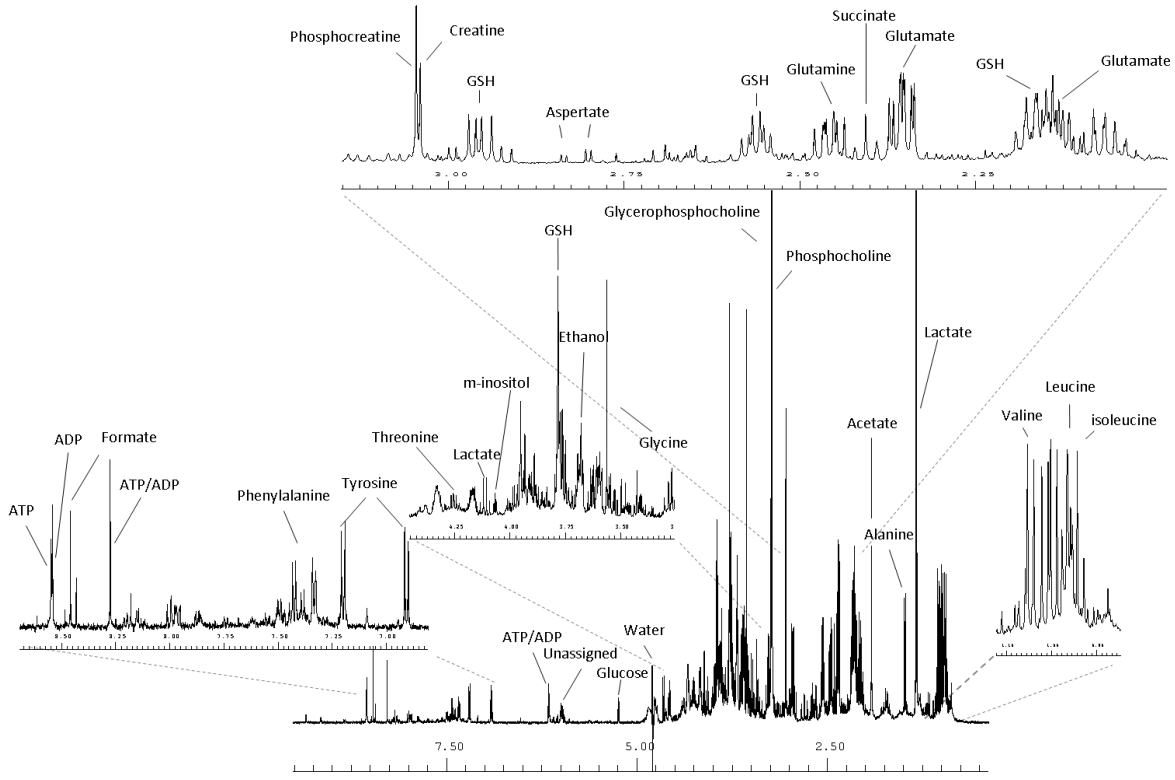

Figure 47: Averaged ^{1}H NMR Spectrum of control aqueous extracts with some peak assignments indicated.

Table 9: Assignment of resonances in the NMR profile of HaCaT cells' aqueous extract (s, singlet; d, doublet; t, triplet; m, multiplet; dd, doublet of doublets); adapted with permission from [237].

No.	Compound	δ ^{1}H in ppm (multiplicity, assignment) / δ ^{13}C in ppm
1	Acetate	1.92 (s, β-CH_3)/26.0
2	ADP	4.22 (m, C5'H, ribose); 4.38 (m, C4'H, ribose); 4.61 (m, C2'H, ribose); 6.15 (d, C1'H, ribose)/89.4; 8.28 (s, C8, ring); 8.54 (s, C2, ring)
3	Alanine	1.49 (d, β-CH_3)/18.9; 3.78 (q, α-CH)

4	Aspartate	2.69 (dd, β-CH); 2.82 (dd, β'-CH); 3.90 (dd, α-CH)
5	ATP	4.22 (m, C5'H, ribose); 4.29 (m, C5''H, ribose); 4.41 (m, C4'H, ribose); 4.62 (m, C2'H, ribose); 6.15 (d, C1'H, ribose)/89.4; 8.28 (s, C2, ring); 8.55 (s, NH, ring)
6	Choline	3.21 (s, $N(CH_3)_3$); 3.53 ($C\mathbf{H_2}NH$)); 4.07 (m, $C\mathbf{H_2}(OH)$)
7	Creatine	3.04 (s, CH_3)/39.6; 3.93 (s, CH_2)/56.6
8	Formate	8.46 (s, CH)
9	Fumerate	6.52 (s, CH)
10	α-Glucose	3.40 (m, C4H)/72.3; 3.55 (dd, C2H)/74.0; 3.71 (m, C3H)/75.5; 3.83 (m, C6H)/63.2; 3.85 (m, C5H)/74.2; 5.24 (d, C1H)/94.8
11	β-Glucose	3.26 (dd, C2H)/76.8; 3.41 (m, C4H)/72.3; 3.47 (m, C5H)/78.6; 3.49 (t, C3H)/78.4; 3.74 (m, C6H)/63.4; 3.90 (dd C6'H)/63.4; 4.66 (d, C1H)/98.6
12	Glutamate	2.06 (m, β-CH)/29.7; 2.13 (m, β'-CH)/29.7; 2.35 (m, γ-CH_2)/36.2
13	Glutamine	2.14 (m, β-CH_2)/29.6; 2.45 (m, γ-CH_2)/33.7
14	Glutathione Reduced (GSH)	2.17 (m, β-CH_2, Glu)/29.1; 2.56 (m, α-CH_2, Cys)/34.2; 2.96 (m, α-CH_2, Gly)/28.4; 3.78 (α-CH)/46.1, 56.8; 4.57 (m, β-CH_2)/58.5; 8.37 (NH, Gly); 8.56 (NH, Cys)
15	Glycerophosphocholine (GPC)	3.235 (s, $N(CH_3)_3$)/56.6; 3.68 (β'-CH_2(N))/68.6; 4.33 (m, α'-CH_2(P))/62.2
	Glycine	3.57 (s, α-CH_2)/ 44.2
16	3-Hydroxybuterate	1.20 (d, γ-CH3); 2.30 (dd, CH2); 2.42 (dd, CH2); 4.16 (m, CH)
17	Isoleucine	0.94 (t, δ-CH_3)/ 13.8; 1.01 (d, β'-CH_3)/17.4; 1.26 (m, γ-CH_2)/27.2; 1.48 (m, γ'-CH_2)/27.2; 1.98 (m, β-CH)/38.7; 3.68 (d, α-CH)/62.0
18	Lactate	1.33 (d, β-CH_3)/22.8; 4.12 (q, α-CH)/71.3
19	Leucine	0.96 (d, δ-CH_3)/23.7; 0.97 (d, δ'-CH_3)/24.9; 1.70 (m, γ-CH)/27.0; 1.72 (m, β-CH_2)/42.4; 3.74 (t, α-CH)
20	Myo-inositol	3.29 (t, C5H)/77.1; 3.54 (C1H, C3H)/73.8; 3.63 (dd, C4H, C6H)/75.2; 4.07 (t, C2H)/74.9
21	NAD+	4.23 (m, A5'); 4.36 (m, A4'); 4.39 (m, A4'/N5'); 4.42 (dd, N3'); 4.50 (m, A3'); 4.54 (m, N2'); 6.04 (d, N1'); 6.10 (d, A1'); 8.18 (s, A2); 8.19 (N5); 8.43 (s, A8); 8.83 (d, N4); 9.14 (d, N6); 9.34 (s, N2)
22	Phenylalanine	3.14 (m, β-CH); 3.27 (dd, β'-CH); 4.00 (m, α-CH); 7.33 (d, C2H, C6H, ring)/131.9; 7.39 (d, C4H, ring); 7.43 (t, C3H, C5H, ring)/131.7
23	Phosphocholine (PC)	3.226 (s, $N(CH_3)_3$)/56.6; 3.62 (m, N-CH_2)/69.3; 4.17 (m, PO_3-CH_2)/60.7
24	Phosphocreatine (PCr)	3.05 (s, CH_3); 3.95 (s, CH_2)/63.2
25	Succinate	2.41 (s, CH_2)
26	Threonine	1.34 (d, γ-CH_3)/22; 3.59 (d, α-CH)/63.1; 4.26 (m, β-CH)/68
27	Tyrosine	3.07 (m, β'-CH); 3.21 (m, β-CH); 3.96 (m, α-CH); 6.91 (d, C3H, C5H, ring)/118.6; 7.20 (d, C2H, C6H, ring)/133.6
28	UDP	4.23 (m, C5'H, ribose); 4.27 (m, C4'H, ribose); 4.40 (t, C2'H, ribose); 4.44 (t, C3'H, ribose); 5.97 (s, C1'H, ribose); 5.98 (d, C6, ring); 8.00 (d, C5, ring)
29	UTP	4.26 (m, C5'H, ribose); 4.30 (m, C4'H, ribose); 4.42 (t, C2'H, ribose); 4.45 (t, C3'H, ribose); 5.97 (s, C1'H, ribose); 5.99 (d, C6, ring); 7.98 (d, C5, ring)
30	Valine	0.99 (d, γ-CH_3)/ 19.5; 1.05 (d, γ'-CH_3)/20.7; 2.28 (m, β-CH)/31.7; 3.62 (d, α-CH)/63.0

VI.2 METABOLIC EFFECTS OF GREEN SYNTHESIS AgNPS

The spectra from different groups (control and exposed) were initially compared using Amix-Viewer software. Visual inspection suggested a dose dependent pattern of changes. This was explored further using multivariate analysis (MVA) and the results are discussed in the following section.

The data were first analysed using the unsupervised PCA method in order to uncover any outliers and inherent trends in sample grouping. The initial PCA score plot of the three sample classes, control, IC_{10} and IC_{50}, shows a clear separation of the IC_{50} samples (Figure 48). Moreover, the Controls and the IC_{10}s appear in distinct clusters, though close together, indicating their similarity, while the IC_{50}s have looser grouping tendencies.

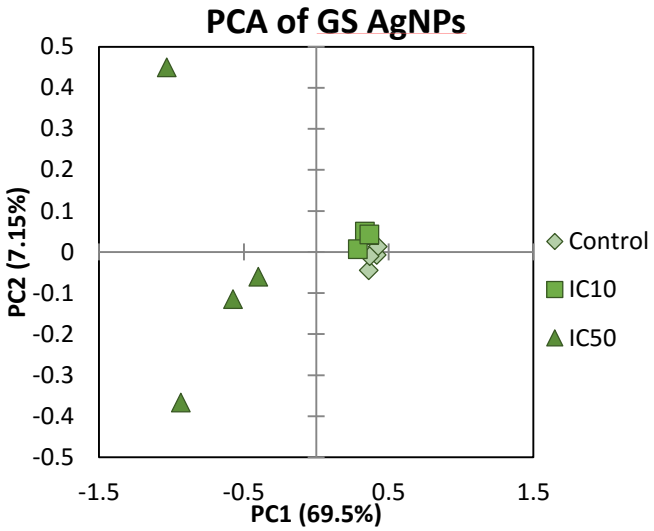

Figure 48: PC1 vs PC2 scores scatter plot obtained by PCA of ^{1}H NMR spectra from aqueous extracts of control cells and cells exposed to GS AgNPs at IC_{10} and IC_{50} concentrations.

Table 10: Summary of MVA parameters.

Model Fit	PCA	PLS-DA		
	R^2X	R^2X	R^2Y	Q^2
GAg CT v Exposed	0.766	0.758	0.996	0.96
GAg CT v IC_{10}	0.625	0.562	1	0.943
GAg CT v IC_{50}	0.83	0.805	0.994	0.935
GAg IC_{10} v IC_{50}	0.835	0.809	0.995	0.939

PLS-DA was then applied to each pair of groups, to maximize class separation and further interpret the variables accounting for that separation. The resulting R^2 and Q^2 values, indicating respectively the explained variance and predictive power, are shown in Table 10. The IC_{50}s also show a spread in this model, though here they separate along the axis of LV2, suggesting that there is another factor that distinguishes them.

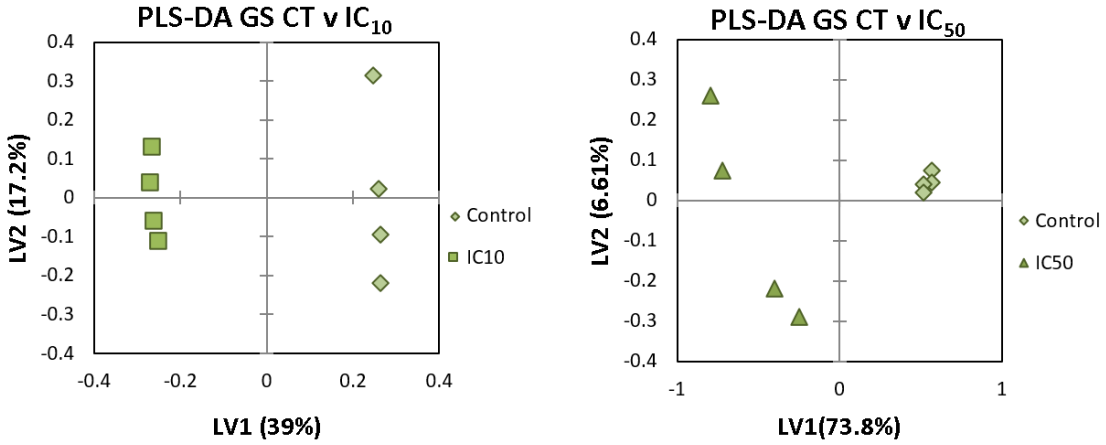

Figure 49: LV1 vs LV2 scores scatter plot obtained by PLS-DA of ^{1}H NMR spectra from aqueous extracts of control cells and cells exposed to GS AgNPs; Left, Control versus IC_{10} Samples; Right, Control versus IC_{50} Samples.

The PLS-DA LV1 loadings were then used to create plots that show the spectra in terms of the weight and variable importance (VIP) of those loadings. In practical terms, the variables, or peaks, most responsible for the separation along the LV1 axis have "hotter" colours in the loading plots, allowing for the identification of compounds that cause these variations (Figure 50 and Figure 51). The results show some dose dependent changes, such as the decrease in lactate, glycine, creatine, phosphocreatine (PCr), phosphocholine (PC) and glycerophosphocholine (GPC), which are more pronounced at the higher dose than the lower. However, there are also some dose specific alterations; for example the IC_{10} samples show an increase in GSH, whereas the IC_{50}s show a decrease. The IC_{50}s additionally show an increase in succinate, formate, phenylalanine, isoleucine and valine.

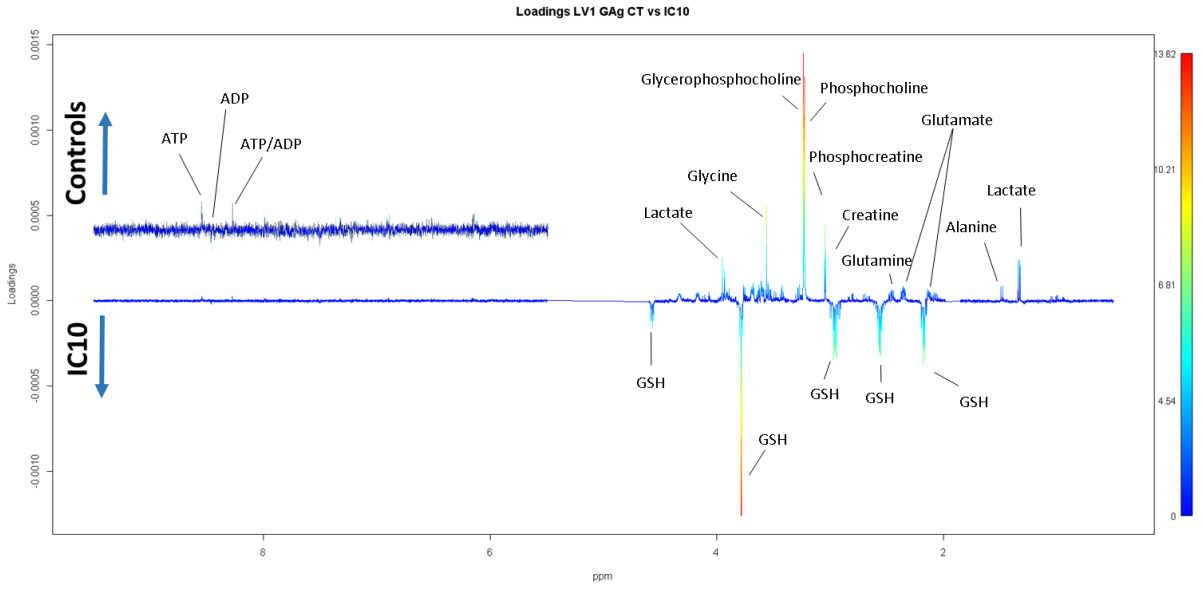

Figure 50: LV1 Loadings coloured as a function of Variable Importance in Projection (VIP) for Pareto scaled PLS-DA model of controls and cells treated with the IC_{10} dose of GS AgNPs.

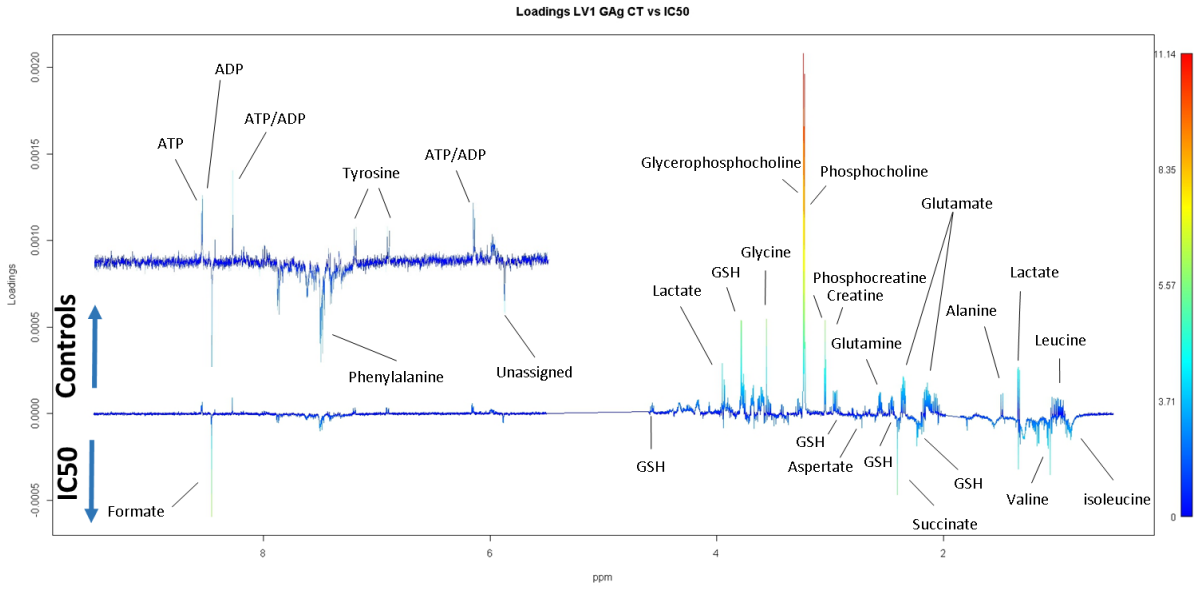

Figure 51: LV1 Loadings coloured as a function of Variable Importance in Projection (VIP) for Pareto scaled PLS-DA model of controls and cells treated with the IC_{50} dose of GS AgNPs.

Peaks that showed a greater VIP, as well as those chosen based on earlier visual inspection, were also subject to univariate analysis. The integrated peaks were averaged, and their standard deviation, percent variation compared to control, corresponding error and effect size were calculated and are tabulated below (Table 11). The results for these metabolites are also graphically presented in Figure 52. The highest effect size for the IC_{10} dose are GSH, PC, GPC, glutamine, and glycine, all with corresponding significant differences. For the IC_{50} dose, the highest effect sizes are seen for PCr, creatine, m-inositol, PC, and glutamate, also with statistical significance. It is interesting to note that the metabolites with the highest variation percent values, i.e. acetate, succinate, and formate, while statistically significant, did not have correspondingly high effect size values.

Table 11: Percent Variation and Effect Size of Selected Metabolites in the Aqueous Extracts of HaCaT Cells Exposed to Green Synthesis AgNPs.

Compound	IC_{10}		IC_{50}	
	%Variation of Control	Effect Size	% Variation of Control	Effect Size
Acetate	7.95 ± 6.958	0.68 ± 0.638	371.61 ± 18.41	4.34 ± 1.248
ADP	-	-	-77.6 ± 13.641	-5.72 ± 1.555
Alanine	-11.29 ± 5.103	-1.44 ± 0.713	-18.33 ± 8.677	-1.43 ± 0.711
Aspartate	-25.26 ± 4.538	-3.92 ± 1.156	-50.15 ± 9.641	-4.27 ± 1.232
ATP	-10.82 ± 6.038	-1.16 ± 0.68	-74.88 ± 18.917	-3.89 ± 1.151
Creatine	-32.69 ± 5.306	-4.53 ± 1.288	-78.19 ± 7.505	-10.52 ± 2.7
Formate	6.67 ± 5.551	0.71 ± 0.64	391.54 ± 21.687	3.75 ± 1.122
Glucose	-13.72 ± 12.904	-0.7 ± 0.639	49.79 ± 15.128	1.62 ± 0.736
Glutamate	-12.24 ± 2.268	-3.53 ± 1.077	-50.6 ± 5.999	-6.94 ± 1.842
Glutamine	-14.83 ± 1.962	-5.02 ± 1.398	-31.88 ± 5.79	-4.03 ± 1.18
GPC	-20.09 ± 2.634	-5.21 ± 1.441	-62.56 ± 11.631	-3.62 ± 1.093
Glycine	-30.47 ± 4.802	-4.6 ± 1.305	-62.04 ± 15.296	-4.81 ± 1.351
GSH1	78.44 ± 2.76	12.55 ± 3.198	-62.39 ± 15.51	-3.59 ± 1.089
GSH2	85.66 ± 2.682	13.75 ± 3.493	-81.51 ± 20.296	-4.17 ± 1.21
Isoleucine	-	-	-21.75 ± 7.861	-1.91 ± 0.778
Lactate	-3.5 ± 2.667	-0.82 ± 0.648	-	-
Leucine	-	-	-23.06 ± 7.663	-2.09 ± 0.807
m-inositol	-19.38 ± 4.266	-3.09 ± 0.988	-67.69 ± 7.154	-8.79 ± 2.283
Phosphocholine	-25.21 ± 3.283	-5.4 ± 1.484	-78.61 ± 11.36	-7.01 ± 1.857
Phosphocreatine	-34.02 ± 5.962	-4.23 ± 1.223	-87.12 ± 7.208	-13.17 ± 3.349
Succinate	-	-	194.41 ± 15.19	3.99 ± 1.172
Threonine	-	-	-62.52 ± 10.486	-5.33 ± 1.468
Tyrosine	-	-	-48.43 ± 8.818	-4.46 ± 1.272
Valine	-	-	-20.69 ± 6.854	-2.07 ± 0.804

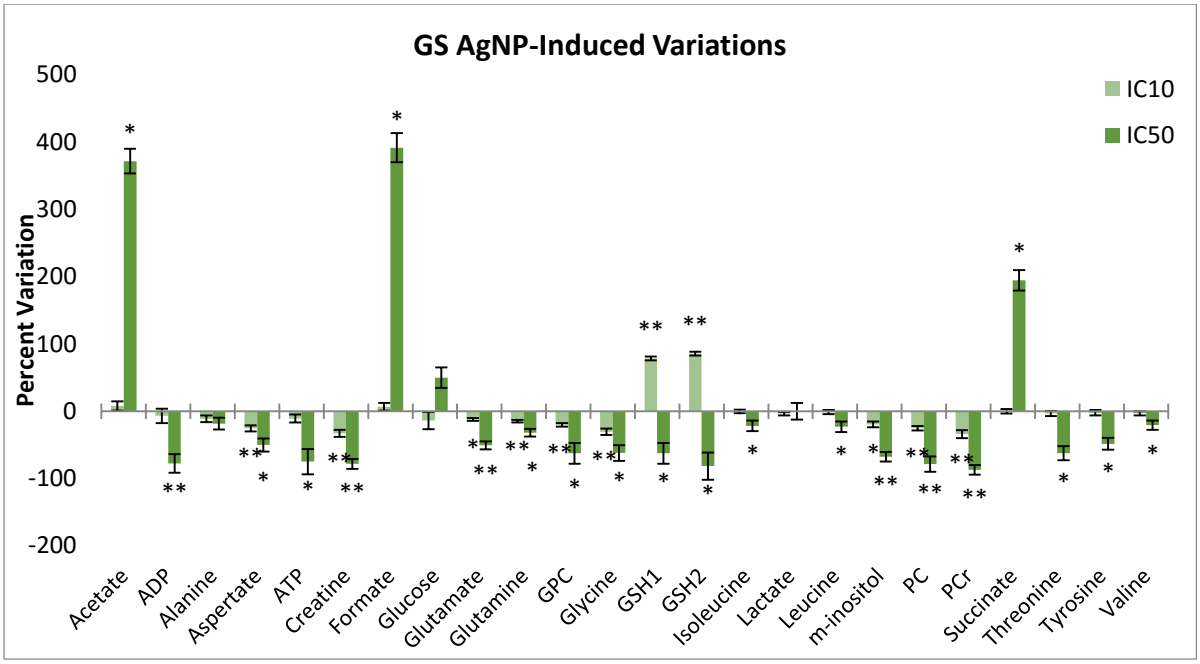

*Figure 52: Average Percent variation of metabolites in Green Synthesis AgNP-exposed samples as compared to their controls. Error bars show the standard error; significance was calculated based on the Student's t-test: * indicates p<0.05 and ** indicates p<0.001.*

VI.3 METABOLIC EFFECTS OF PLAL AgNPS

The initial PCA for the PLAL AgNPs included the controls, ubiquitin controls, IC_{10} with and without ubiquitin, and IC_{20} with and without ubiquitin. It is recalled that IC_{20} was the maximum dose tested due to the quantity of AgNPs available, and the low concentration of the initial stock solution. The results showed a clear separation between IC_{20} samples and the other groups (Figure 53); with a slight overlap between the IC_{10} and controls and almost a complete overlap between the control samples and those exposed only to ubiquitin. It is also interesting to note that there is no consistent separation between samples exposed to AgNPs coated in ubiquitin (shown with lighter markers on the score plot) and their bare counterparts. In fact, the IC_{10} samples coated in ubiquitin have the most separation within their group, and the IC_{20} samples with ubiquitin are both within the cluster of their class.

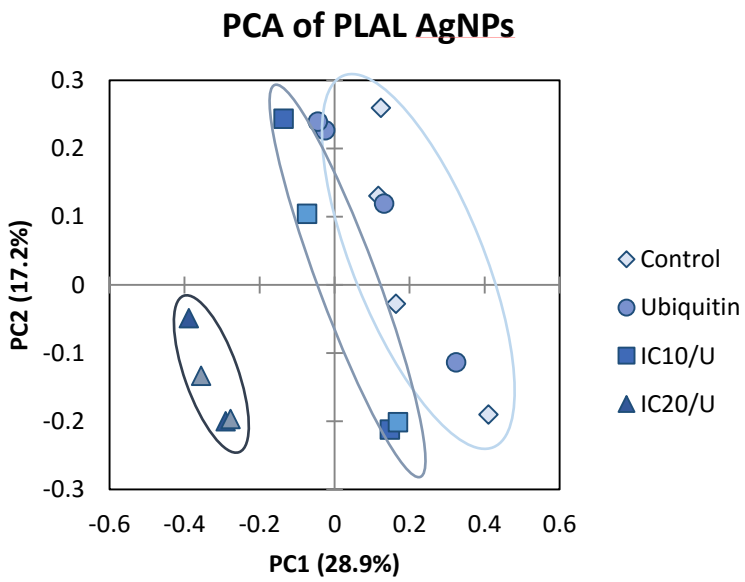

Figure 53: PC1 vs PC2 scores scatter plot obtained by PCA of ^{1}H NMR spectra from aqueous extracts of control cells and cells exposed to PLAL AgNPs at IC_{10} and IC_{50} concentrations.

Each of the group pairings was then analysed using PLS-DA; pairings that provided a low R^2 and Q^2 values, redundant information, that were found to have too little variation, or that were not sufficiently separated on the score plot were excluded from further analysis. As the controls and the ubiquitin controls show little to no variation, they are hereon grouped together for proceeding analyses. Similarly, a lack of distinction between the particles coated with and without ubiquitin also lead to their combination. Figure 54 shows the PLS-DA score plots that provide the most relevant information for the PLAL AgNPs. Table 12 provides a summary of the resulting fit for the corresponding models.

Table 12: Summary of MVA Parameters for PLAL AgNPs.

Model Fit	PCA	PLS-DA		
	R^2X	R^2X	R^2Y	Q^2
PAg CT v Exposed	0.46	0.412	0.911	0.629
PAg 10+U v 20+U	0.589	0.587	0.999	0.97
PAg CT+U v 10+U	0.436	0.366	0.977	0.422
PAg CT+U v 20+U	0.504	0.496	0.994	0.963

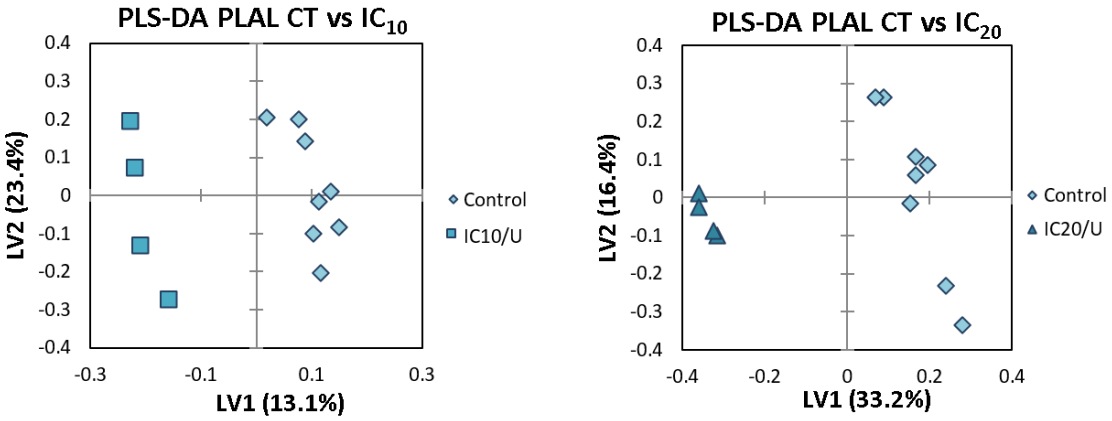

Figure 54: : LV1 vs LV2 scores scatter plot obtained by PLS-DA of ^{1}H NMR spectra from aqueous extracts of control cells and cells exposed to PLAL AgNPs; Left, Control versus IC_{10} Samples; Right, Control versus IC_{50} Samples

The separations across the LV1 axes were further used to create the loading plots, allowing for the metabolites responsible for those separations to be visualized (Figure 55 and Figure 56). As the two doses tested are much closer in concentration, their induced effects are rather similar; both show an increase in GSH and decreases in glycine, lactate, PC and GPC. However, as the increase in GSH and decrease in PC and GPC become more prominent at the higher dose, the decrease in lactate and glycine diminishes. It is also interesting to note the ratio of ADP to ATP almost reverses from one dose to the other.

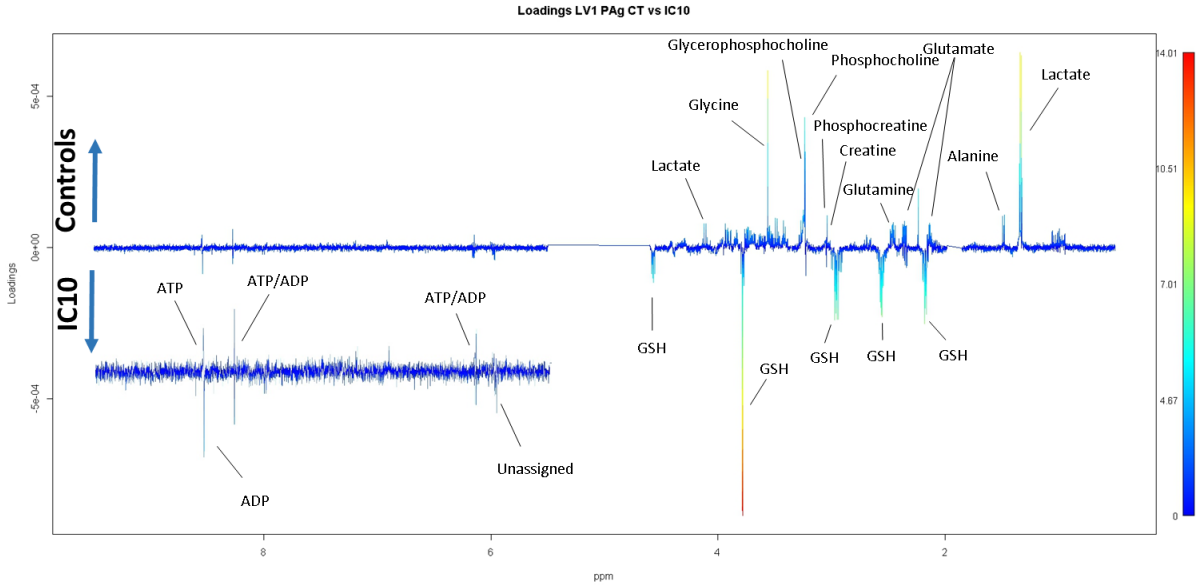

Figure 55: LV1 Loadings coloured as a function of Variable Importance in Projection (VIP) for Pareto scaled PLS-DA model of controls and cells treated with the IC_{10} dose of PLAL AgNPs.

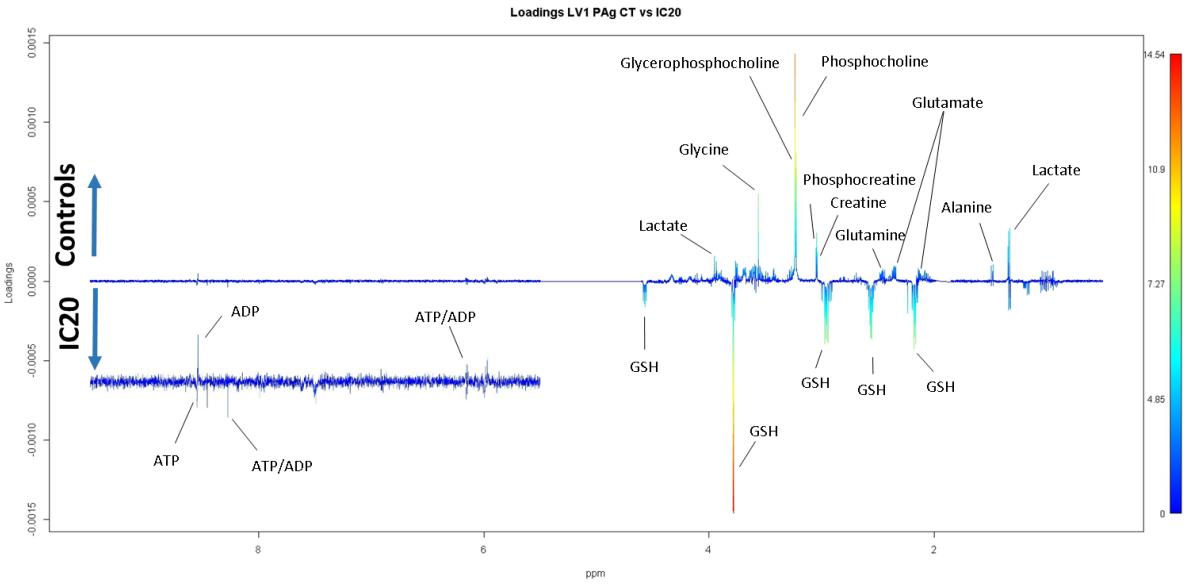

Figure 56: LV1 Loadings coloured as a function of Variable Importance in Projection (VIP) for Pareto scaled PLS-DA model of controls and cells treated with the IC_{20} dose of PLAL AgNPs.

The same peak regions as those of the Green Synthesis AgNPs were integrated to obtain the univariate analysis; percent variation from the controls with the corresponding error, as well as effect size and its respective error are tabulated below in Table 13. The percent variation is also graphically presented in Figure 57. Here, the greatest effect size for the IC_{10} dose is also seen for GSH, glutamine and glycine. For the IC_{50} dose however, the highest value is for GSH, followed by GPC, aspartate, glutamate, and m-inositol.

Table 13: Percent Variation and Effect Size of Selected Metabolites in the Aqueous Extracts of HaCaT Cells Exposed to PLAL AgNPs.

	IC_{10}		IC_{20}	
Compound	**%Variation of Control**	**Effect Size**	**% Variation of Control**	**Effect Size**
Acetate	6.7 ± 2.724	1.34 ± 0.628	-	-
ADP	26.73 ± 12.715	0.8 ± 0.588	-25.98 ± 14.472	-0.78 ± 0.587
Alanine	-7.03 ± 2.181	-1.48 ± 0.641	-6.85 ± 3.013	-1.28 ± 0.623
Aspartate	-9.64 ± 4.396	-1.22 ± 0.618	-20.71 ± 3.215	-2.95 ± 0.827
ATP	-16.47 ± 11.409	-0.72 ± 0.584	10.46 ± 8.336	-
Creatine	-6.46 ± 3.054	-1 ± 0.601	-19.17 ± 4.15	-2.69 ± 0.788
Formate	-	-	7.35 ± 4.154	0.84 ± 0.591
Glucose	-19.72 ± 6.608	-1.59 ± 0.652	-9.33 ± 4.907	-0.81 ± 0.589
Glutamate	-3.02 ± 1.5	-0.88 ± 0.593	-10.9 ± 1.99	-2.92 ± 0.822
Glutamine	-8.12 ± 1.789	-2.01 ± 0.698	-8.96 ± 1.814	-2.21 ± 0.723
GPC	-3.49 ± 2.212	-0.74 ± 0.585	-18.94 ± 1.993	-4.22 ± 1.03
Glycine	-17.44 ± 3.165	-2.34 ± 0.739	-20.18 ± 3.97	-2.55 ± 0.769
GSH1	25.54 ± 3.057	4.54 ± 1.086	69.18 ± 1.808	14.4 ± 2.993
GSH2	27.05 ± 4.79	2.88 ± 0.816	71.96 ± 3.279	8.43 ± 1.812
Isoleucine	-3.13 ± 1.244	-1 ± 0.601	-	-
Lactate	-10.28 ± 3.789	-1.45 ± 0.638	-3.67 ± 3.007	-
Leucine	-1.73 ± 1.115	-0.67 ± 0.581	-	-

m-inositol	-	-	-17.12 ± 3.016	-2.7 ± 0.789
Phosphocholine	-	-	-13.07 ± 2.595	-2.38 ± 0.745
Phosphocreatine	-	-	-16.23 ± 5.038	-1.85 ± 0.68
Succinate	-	-	-9.04 ± 3.511	-1.23 ± 0.619
Threonine	-	-	-	-
Tyrosine	-5.07 ± 3.003	-0.78 ± 0.587	-	-
Valine	-3.1 ± 1.39	-0.99 ± 0.6	-	-

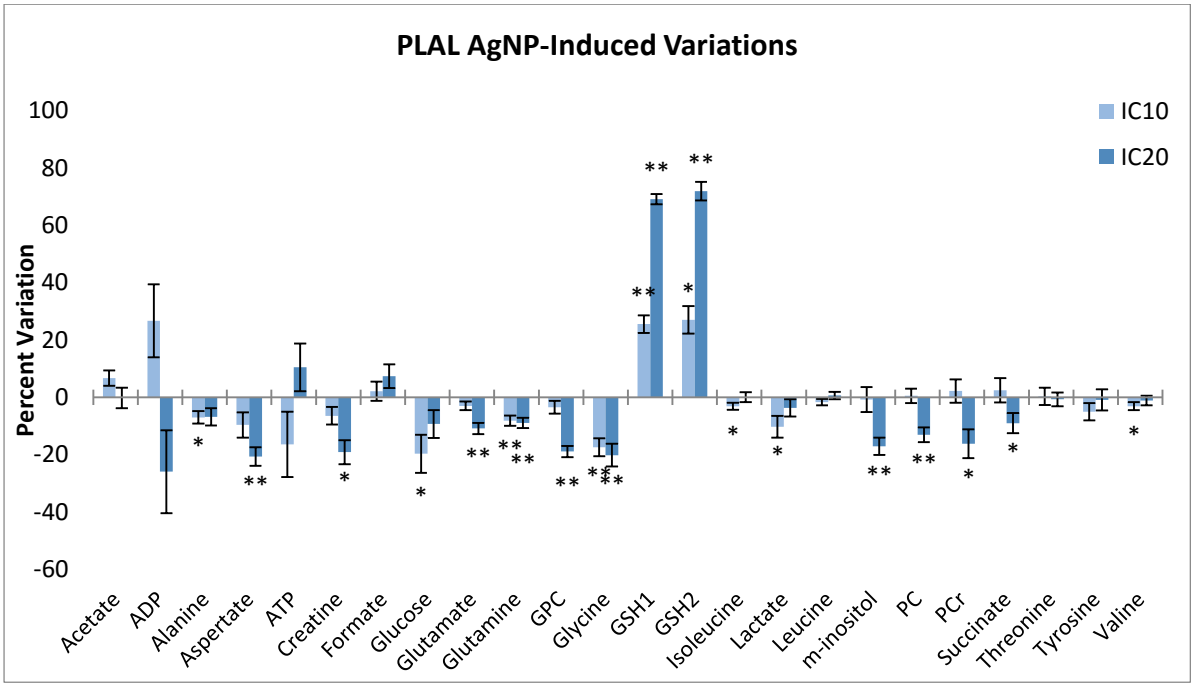

*Figure 57: Average Percent variation of metabolites in PLAL AgNP-exposed samples as compared to their controls. Error bars show the standard error; significance was calculated based on the Student's t-test: * indicates p<0.05 and ** indicates p<0.001.*

VI.4 A Comparison of the Metabolic Effects of GS and PLAL AgNPs

Univariate analysis was chosen to compare the Green Synthesis (GS) AgNPs with the Pulsed Laser Ablation in Liquid (PLAL) AgNPs for those doses that induced the same decrease in cell viability, i.e. the IC_{10}s, and those metabolites that had shown a statistically significant variation as compared to their controls. The multivariate analysis was not followed through in this case, as an initial PCA of all control and IC_{10}s separated not only the IC_{10}s of the two synthesis methods, but also the controls of each synthesis from each other. This suggested that there exists some difference between the controls of each data set, preventing the data from being compared directly. Therefore, the percent variations of each IC_{10} set, as compared to their respective controls, were plotted for metabolites that had previously shown to have significant variations (Figure 58). Both types of particles tend to cause the same direction of response, however, aside from glucose and lactate, the GS AgNPs induce a much stronger response.

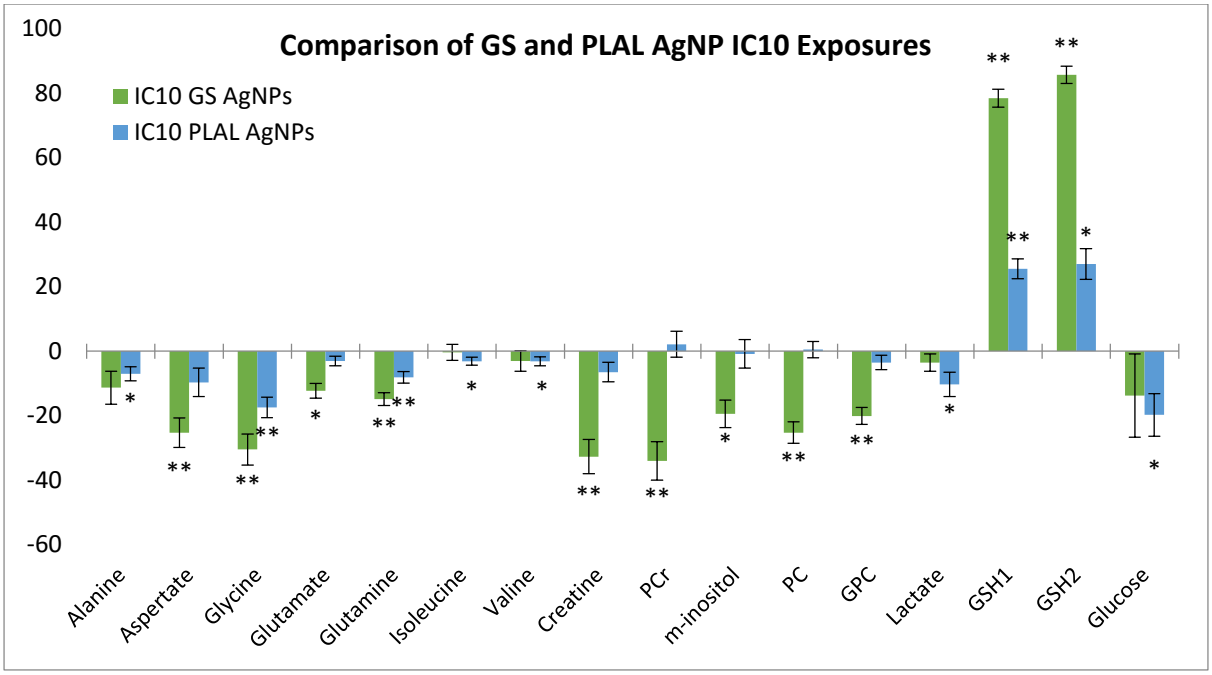

*Figure 58: Percent variation of IC_{10} samples as compared to their respective controls for metabolites of statistically significant variation for GS and PLAL AgNPs; where * indicates p<0.05 and ** indicates p<0.001.*

VI.5 Discussion on Cellular Implications

The biological effects of AgNPs synthesized via a chemical and a physical route were further evaluated at toxic and sub-toxic concentrations using an NMR based metabolomics approach. Aqueous extracts of HaCaT cells exposed to a low (IC_{10}) and a higher concentration (IC_{20} or IC_{50}) of each type of particle were analyzed using MVA and compared to their respective controls and each other. The results showed dose-dependent changes in a number of metabolites, as well as particle-specific biochemical responses.

Before delving into results from the metabolomics, it is worth mentioning a note from the sample preparation. Observation of cells before the extraction process revealed the IC_{50} dose to have killed more than the expected 50% of cells, leaving only a small percentage for extraction. This is consistent with the dose response obtained for the morphology and cell cycle studies, as discussed in the previous chapter. It specifically effects the metabolomics study in two ways: as there are a fewer number of cells receiving the same concentration of AgNPs, a more extreme response can be expected; moreover, fewer cells in total means less intense signals, and therefore low signal to noise ratios. This was indeed the case for the IC_{50} samples, and consequently their need for longer acquisition times.

GSH is an antioxidant molecule capable of modulating the reactive oxygen species (ROS) produced during regular cell metabolism, as well as excessive ROS resulting from stress factors. In conventional toxicology various reagents are used to measure the depletion of GSH as an endpoint indicating oxidative stress [65]. The majority of toxicity and metabolomics studies report a depletion of GSH upon exposure of various cell lines, including keratinocytes, to AgNPs [208, 204, 223, 203, 281]. However, in this study, the results showed a statistically significant increase in GSH levels for the low concentration doses of IC_{10} and IC_{20} as compared to the controls, and a decrease only for the IC_{50} dose.

An increase in GSH has also been reported by our workgroup for HaCaT cells exposed to citrate coated AgNPs [237]; and elsewhere for lung cells exposed to gold nanorods [282].

Here, the increase in GSH was mirrored with a decrease in both glycine and glutamate, which are precursor compounds of GSH [283, 282]. The increase in GSH levels may also explain why cells pretreated with sub-toxic doses of AgNPs show less damage upon exposure to UVB radiation; as UVB radiation is also a source of ROS production, the GSH in excess would be able to modulate this new source of stress [143]. Thus, it is suggested that cells respond to AgNPs exposure through upregulation of GSH production in order to cope with NP-mediated oxidative stress [237]. However, at higher NP concentrations, it is possible that GSH is consumed at higher rate than it is produced or recycled, due to an even higher increase in ROS, thus leading to an overall decrease of GSH pools.

Amino acids are essentially used in two ways in the human body; for the synthesis of proteins and enzymes, or for the release of energy via amino acid catabolism [105]. A decrease in amino acids such as leucine, isoleucine, valine, alanine, and threonine is seen in a dose-dependent manner for both particle types, though only with statistical significance at the highest dose of IC_{50}. Their decrease suggests the catabolic pathway, where their by-products are fed into the tricarboxylic acid (TCA) cycle for the release of energy, or used for gluconeogenesis. The two fold increase of succinate at the IC_{50} exposure seems to confirm the former pathway, suggesting the entry of threonine, isoleucine, and valine into the TCA cycle by conversion to succinyl-CoA, which is then converted to succinate along with the release of one ATP or equivalent. The alterations in energy metabolism in the cell can be related to the activity of the TCA cycle and the energy needs of the cell at a particular point [284]. These energy needs can also be associated with cell cycle arrest and apoptosis [285, 286].

At the same time, the accumulation of succinate may imply that the next step of the cycle, one that requires ubiquinone, may have faltered. Ubiquinone or Coenzyme Q (CoQ) is a component of the electron transport chain, aiding the generation of ATP in mitochondria; its ability to exist at a fully reduced form also allows it to act as an antioxidant [287]. The breakdown of this process further suggests oxidative stress and the eventual transition to apoptosis.

Acetate is also a component of Acetyl Coenzyme A (CoA), part of the TCA cycle, as well as a building block of fatty acids. The trifold increase in formate and acetate may indeed be linked, as the former is typically a by-product in the latter's production; with pyruvate as the substrate, pyruvate formate-lyase as the enzyme, and acetyl-CoA and formate as the products [265]. The increase of acetate may indicate the breakdown of fatty acids in the lipid membrane of the cell, however, coupled with an increase in formate, it may also suggest the previously noted alterations to energy metabolism, i.e. the intensification of the TCA cycle to maintain energy levels in response to oxidative stress, cell cycle arrest and apoptosis.

Cholines serve a number of functions throughout the body, with the most common being as the head group of phospholipids in biological membranes, in the form of phosphotidylcholine (PTC) [288]. The drastic decrease in PC and GPC may indicate synthesis or modification of cellular membranes, as the cells prepare for apoptosis [289, 290]. Since apoptosis is a type of programmed cell death, the constituents of the cells are lysed and divided between vesicles, as observed in the morphology of cells when the high dose of IC_{50} was applied. However, this cannot be confirmed until the organic extracts, where PTC would be detected, are analyzed.

Normally, PCr acts as an energy reservoir for tissues and cells that consume ATP rapidly, such as skeletal muscles or the brain. In times of need, creatine kinase uses PCr in a reversible enzymatic reaction, to regenerate ATP from ADP, with creatine as the product [291]. Here, the cells show a

decrease in creatine and PCr for all tested doses as compared to the controls. The decrease in PCr is in agreement with the increased energy needs of the cell, as discussed above, for the TCA cycle, DNA repair, and eventually apoptosis. However, the lack of an accompanying increase in creatine suggests either that this pathway is not the cause for the decrease in PCr, or that the degradation of PCr to creatine is followed by another reaction that then consume creatine.

The comparison of the data from the two types of particles revealed a much stronger response in the samples exposed to GS AgNPs than PLAL AgNPs. Although this difference can be attributed to a number of differences in the particles' characterization, namely size, size distribution, and coating, it is possible that the difference in storage conditions is the main cause. The GS AgNPs were previously shown to induce a drop in cell viability with the MTT assay (Chapter 5), and to have an evolution in morphology and size distribution with time (Chapter 4). It was proposed earlier that the storage condition, ambient temperature and pressure, are likely to have caused the particles' dissolution, leading to a higher amount of silver ions in solution, and therefore a higher toxicity. If this is true, it would also explain the greater metabolic response found here for these particles as compared to the PLAL ones.

Chapter VII: Conclusions and Future Perspectives

In this work, two types of silver nanoparticles (AgNPs) were compared in terms of their physico-chemical properties and biological effects. The PLAL AgNPs presented a more uniform size distribution, having a narrow band in UV-Vis spectra, and similarly narrow distributions in DLS and STEM measurements. The GS AgNPs were found to have a larger particle size and broader distributions. Modifications to the GS synthesis process showed the use of MilliQ water to be more favourable, while the "one pot synthesis" was deemed as a plausible potential for the synthesis of sterile AgNPs with a narrower size distribution than the other biosynthesis iterations. The washing and centrifugation step were found to inflict noticeable changes to the size distribution. Though stable up to 48 hours, the dispersion of AgNPs in cell culture media induced an overall increase in hydrodynamic diameter.

Though DLS provides a general idea of the diameter and size distribution, it is not a reliable method for calculating the average diameter or size distribution of poly dispersed NPs. This is in part due to the very concept of the hydrodynamic diameter, one that includes the hard corona of solvent molecules bound to the particle, but more so because of the way the speckle pattern intensity fluctuations are used to calculate the average size. The average sizes derived based on intensity, volume, and number often have very different values, and can only be used in a qualitative manner to compare similar particles under similar conditions. It is suggested that alternative analysis methods, such as Nanoparticle Tracking Analysis (NTA) [56] or Analytical Centrifugation (AUC) [266], be explored in the long term. Moreover, for comparing the GS coating to other particles, a better understanding of the surface coating is required, especially considering that the extract is modified, most likely oxidized, during the autoclaving process. A study comparing the extract before and after autoclavation can be conducted using HPLC-MS or NMR; while coating displacement, coupled with NMR, can be used *in-situ* to determine the nature of the surface coating.

In terms of cytotoxicity, neither particle coating, EGB nor ubiquitin, induced cytotoxicity at the concentrations tested. In light of the reported proliferative effects of extracellular ubiquitin, it is suggested that further testing be conducted on ubiquitin alone in order to determine this hypothesis' validity. Furthermore, the interference of AgNPs was ruled as residual based on the experiments conducted. It is suggested that a similar experiment, with a modified protocol where the bottom of the wells are coated in agarose, also be performed in order to mimic the extracellular matrix to which the particles may potentially attach [292]. Another potential control study is testing for endotoxins, lipopolysaccharides released from the cell wall of Gram negative bacteria [293, 294, 295]. This control is particularly relevant for the GS AgNPs as they are synthesized using a biomass extract and such toxins would remain in solution even after autoclaving.

The IC_{50} of the GS AgNPs was determined to be 15.49 and 14.21 µg/mL for 24 and 48 hour exposure times respectively; while that of the PLAL was extrapolated based on the regression to be 24.19 and 29.89 µg/mL for the citrate coated, and 16.59 and 17.76 µg/mL for the ubiquitin coated, respectively. In order to obtain a reliable IC_{50} for the PLAL AgNPs, the range must be such that the IC_{50} value falls within; therefore it is recommended that higher concentrations be tested for the PLAL in future studies.

The drastic changes in results from the GS AgNP IC_{50} dose for the morphology and cell cycle sample preparation suggested that particles' toxicity is changing over time; this was confirmed by the physico-

chemical changes encountered by UV-Vis, DLS, and STEM and attributed to the storage conditions and silver ion release. Therefore, it is recommended that the standard condition chosen for the storage of AgNPs include low temperatures so as to minimize dissolution. Furthermore, due to a lack of time and resources, a study on the concentration of silver ions was not conducted for this work. However, going forward, it is highly recommended that this parameter be included as part of the physico-chemical characterization. The most common method for performing this study is the use of centrifugation and ICP analysis of the supernatant [136].

For the GS AgNPs, changes in morphology showed dose and time dependent trends; with the low concentrations causing slower proliferation and the higher concentrations causing extensive cell death, visually resembling apoptosis. Similarly cell cycle analysis showed a delay, followed by arrest, for the sub-toxic concentrations. Going forward, the type of cell death may be further investigated using Annexin V assay and the quantification of cell nuclei in the sub-G_1 phase. Moreover, the work on uptake and localization in this thesis has been minimal due to time constraints. However, a thorough study can be performed using either TEM, fluorescence or Raman microscopies for localization visualization, and ICP and flow cytometry for uptake quantification.

Based on the metabolomics results, it can be concluded that exposure to sub-toxic concentrations causes important and statistically significant alterations in the metabolome. Specifically, an increase in GSH for the lower doses was detected and attributed to antioxidant protection; while its depletion at the high concentration was attributed to extensive oxidative stress. Upregulation of TCA cycle activity was derived from a decrease in amino acids, phosphocreatine and creatine. TCA cycle activity can also be investigated further by measuring the consumption and excretion of metabolites from and into the extracellular media; it is recommended that the data acquired from these samples be analyzed and combined with the aqueous extract results. Decreases in phosphocholine, choline, and glycerophosphocholine suggested membrane modification; similarly, it is recommended that the acquired data from the organic extracts be analyzed and combined, in order to determine if there exist links between these precursors and the actual membrane compounds.

In comparing the two sets of particles, the GS AgNPs induced a stronger metabolic response from the cells. This can be attributed to the difference in size, size distribution, surface coating, or storage conditions. Going forward, it is recommended that future experiments be performed in comparable pairs with relevant controls. In order to determine the cell response at toxic concentrations, a higher dose of PLAL AgNPs should also be tested; at the same time, it may be interesting to also investigate the suggested beneficial effects of ubiquitin at higher concentrations with metabolomics.

It is also recommended that a control study, similar to that of the AgNP interference be conducted for the metabolomics. The cell-free samples, though with a layer of agarose to mimic cellular biofilm, would help determine whether the coating is release into the media, and its potential concentration. This is particularly useful when the coating is comprised of a molecule that is endogenous to the cell or cellular metabolism; in this case all three coatings, citrate, ubiquitin, and the EGB extract saccharides fall into this category.

Finally, it can be concluded that metabolomics is a sensitive and high-throughput approach, capable of detecting alterations in cellular pathways at sub-toxic doses, and thus a complementary technique to the conventional battery of cytotoxicity assays.

While beneficial in retrospect, the conclusions reached through the physico-chemical characterization could not be utilized in the toxicity or metabolomics testing, as they were being conducted in parallel.

Furthermore, it may be interesting to investigate the bactericide efficacy of each particle type, in one or more antibiotic-resistant strains.

Chapter VIII: References

[1] ISO/IEC, "ISO/TS 80004-2:2015 Nanotechnologies -- Vocabulary -- Part 2: Nano-objects," ISO/IEC, Geneva, 2015.

[2] Z. Aguilar, Nanomaterials for Medical Applications, 1st Edition, Oxford, UK: Elsevier , 2012.

[3] SCENIHR (Scientific Committee on Emerging and Newly Identified Health Risks), "Opinion on the scientific basis for the definition of the term “nanomaterial”," SCENIHR, Europe, 8 December 2010.

[4] E. Commission, "REACH - European Commission," European Commission, 10 June 2015. [Online]. Available: http://ec.europa.eu/growth/sectors/chemicals/reach/index_en.htm. [Accessed 28 July 2015].

[5] A. Keller, S. McFerran, A. Lazareva and S. Suh, "Global life cycle releases of engineered nanomaterials," *J. Nanoparticle Res.,* vol. 15, p. 1692–1709, 2013.

[6] K. D. Drexler and C. Peterson, "Nanotechnology and Enabling Technologies: Foresight Briefing #2," The Foresight Institute, California, 1989.

[7] V. G. Dubrovskii, Nucleation Theory and Growth of Nanostructures, Hiedelberg: Springer-Verlag, 2014.

[8] D. Oxtoby, "Nucleation of First-Order Phase Transitions," *Accounts of Chemical Research,* vol. 31, no. 2, pp. 91-97, 1998.

[9] N. Thanh, N. Maclean and S. Mahiddine, "Mechanisms of Nucleation and Growth of Nanoparticles in Solution," *Chem Rev,* vol. 114, p. 7610−7630, 2014.

[10] W. C. Carter, "Lecture 24," MIT, 12 4 2002. [Online]. Available: http://pruffle.mit.edu/~ccarter/3.21/Lecture_24/. [Accessed 1 9 2015].

[11] V. K. LaMer and R. H. Dinegar, "Theory, Production and Mechanism of Formation of Monodispersed Hydrosols," *J. Am. Chem. Soc.,* vol. 72, no. 11, p. 4847–4854, 1950.

[12] W. Ostwald, "Volume 2, Part 1," in *Lehrbuch der allgemeinen chemie [Textbook of General Chemistry]*, Germany, Liepzig, 1896.

[13] R. Viswanatha and D. Sarma, "Chapter 4. Growth of Nanocrystals in Solution," in *Nanomaterials Chemistry: Recent Developments and New Directions*, Weinheim, Germany, Wiley-VCH Verlag GmbH & Co., 2007.

[14] P. T. Anastas and J. C. Warner, Green Chemistry: Theory and Practice, New York: Oxford University Press, 1998.

[15] L. Lin, W. Wang, J. Huang, Q. Li, D. Sun, X. Yang, H. Wang, N. He and Y. Wang, "Nature factory of silver nanowires: plant synthesis using broth of Cassia fistula leaf," *Chem Eng J,* vol. 162, no. 2, p. 852–858, 2010.

[16] D. Leff, P. Ohara, J. Heath and W. Gelbart, "Thermodynamic control of gold nanocrystal size: experiment and theory," *J Phys Chem,* vol. 99, no. 18, p. 7036–7041, 1995.

[17] M. Pileni, "Nanosized particles made in colloidal assemblies," *Langmuir,* vol. 13, no. 13, p. 3266–3276, 1997.

[18] M. Adlim, M. Abu Bakar, K. Liew and J. Ismail, "Synthesis of chitosan-stabilized platinum and palladium nanoparticles and their hydrogenation activity," *J Mol Catal A Chem,* vol. 2012, no. 1-2, p. 141–149, 2004.

[19] N. Kotelnikova, G. Wegener, M. Stoll and V. Demidov, "Comparative study of intercalation of zero-valent silver into the cellulose matrix by raster and transmission microscopy," *Russ J Appl Chem,* vol. 76, no. 1, p. 117–123, 2003.

[20] E. Egorova and A. Revina, "Synthesis of metallic nanoparticles in reverse micelles in the presence of quercetin," *Colloids Surf A,* vol. 168, no. 1, p. 87–96, 2000.

[21] K. Vijayaraghavan and S. Nalini, "Biotemplates in the green synthesis of silver nanoparticles," *Biotechnol J,* vol. 5, no. 10, p. 1098–1110, 2010.

[22] S. Shankar, A. Rai, A. Ahmad and M. Sastry, "Rapid synthesis of Au, Ag, and bimetallic Au core-Ag shell nanoparticles using Neem (Azadirachta indica) leaf broth," *J Colloid Interface Sci ,* vol. 275, no. 2, p. 496–502, 2004.

[23] P. P. Gan and S. Fong Yau Li, "Potential of plant as a biological factory to synthesize gold and silver nanoparticles and their applications," *Rev Environ Sci Biotechnol,* vol. 11, p. 169–206, 2012.

[24] R. Sweeney, C. Mao, X. Gao, J. Burt, A. Belcher, G. Georgiou, Iverson and B.L., "Bacterial biosynthesis of cadmium sulfide nanocrystals," *Chem Biol. ,* vol. 11, no. 11, pp. 1553-1559, 2004.

[25] K. Narayanan and N. Sakthivel, "Biological synthesis of metal nanoparticles by microbes," *Adv Colloid Interface Sci.,* vol. 156, no. 1-2, pp. 1-13, 2010.

[26] A. Ahmad, P. Mukherjee, S. Senapati, D. Mandal, M. Khan, R. Kumar and M. Sastry, "Extracellular biosynthesis of silver nanoparticles using the fungus Fusarium oxysporum," *Colloids Surf B,* vol. 28, no. 4, pp. 313-318, 2003.

[27] G. Singaravelu, J. Arockiamary, V. Kumar and K. Govindaraju, "A novel extracellular synthesis of monodisperse gold nanoparticles using marine alga, Sargassum wightii Greville," *Colloids Surf B Biointerfaces.,* vol. 57, no. 1, pp. 97-101, 2007.

[28] R. Jonas and L. F. Farah, "Production and application of microbial cellulose," *Polymer Degradation and Stability,* vol. 59, no. 1-3, p. 101–106, 1998.

[29] P. Rauwel, S. Küünal, S. Ferdov and E. Rauwel, "A Review on the Green Synthesis of Silver Nanoparticles and Their Morphologies Studied via TEM," *Advances in Materials Science and Engineering,* vol. 2015, p. ID 682749, 2015.

[30] M. R. Bruins, S. Kapil and F. W. Oehme, "Microbial resistance to metals in the environment," *Ecotoxicol. Environ. Saf.,* vol. 45, p. 198–207, 2000.

[31] A. Prakash, S. Sharma, N. Ahmad, A. Ghosh and P. Sinha, "Bacteria mediated extracellular synthesis of metallic nanoparticles.," *Int Res J. Biotechnol.,* vol. 1, pp. 71-79, 2010.

[32] N. Pugazhenthiran, S. Anandan, G. Kathiravan, N. Udaya Prakash, S. Crawford and M. Ashok Kumar, "Microbial synthesis of silver nanoparticles by Bacillus sp.," *J. Nanopart. Res.,* vol. 11, pp. 1811-1815, 2009.

[33] N. Krumov, S. Oder, I. Perner-Nochta, A. Angelov and C. Posten, "Accumulation of CdS nanoparticles by yeasts in a fed-batch bioprocess," *J Biotechnol. ,* vol. 132, no. 4, pp. 481-486, 2007.

[34] N. D.H., "Microbial heavy-metal resistance," *Appl Microbiol Biotechnol.,* vol. 51, no. 6, pp. 730-750, 1999.

[35] D. R. N. V. L. Jaysankar, "Detoxification of Toxic Heavy Metals by Marine Bacteria Highly Resistant to Mercury," *Mar Biotechnol,* vol. 10, pp. 471-477, 2008.

[36] Y. Nangia, N. Wangoo, N. Goyal, G. Shekhawat and C. Suri, "A novel bacterial isolate Stenotrophomonas maltophilia as living factory for synthesis of gold nanoparticles," *Microb Cell Fact,* vol. 8, p. 52, 2009.

[37] R. Slawson, M. Van Dyke, H. Lee and J. Trevor, "Germanium and silver resistance, accumulation, and toxicity in microorganisms.," *Plasmid,* vol. 27, no. 1, pp. 72-79, 1992.

[38] S. Minaeian, R. Shahverdi, S. Nohi and R. Shahverdi, "Extracellular biosynthesis of silver nanoparticles by some bacteria.," *JSci IAU,* vol. 17, pp. 1-4, 2008.

[39] A. Bankar, B. Joshi, A. Ravi Kumar and S. Zinjarde, "Banana peel extract mediated synthesis of gold nanoparticles," *Colloids Surf B,* vol. 80, no. 1, p. 45–50, 2010.

[40] C. Girling, P. Peterson and H. Warren, "Plants as indicators of gold mineralization at Watson bar, British Columbia, Canada," *Economic Geol Lancaster Pa,* vol. 74, no. 4, p. 902–907, 1979.

[41] J. L. Gardea-Torresdy, J. G. Parsons, E. Gomez, P. Videa, H. E. Troiani, P. Santiago and M. Jos'e-Yacam'an, "Formation and Growth of Au Nanoparticles inside Live Alfalfa Plants," *Nano Lett.,* vol. 2, no. 4, p. 397–401, 2002.

[42] R. Herrera-Becerra, C. Zorrilla, J. L. Rius and J. A. Ascencio, "Electron microscopy characterization of biosynthesized iron oxide nanoparticles," *Appl. Phys. A: Mater. Sci. Process.,* vol. 91, no. 2, p. 241–246, 2008.

[43] P. Schabes-Retchkiman, G. Canizal, R. Herrera-Becerra, C. Zorrilla, H. Liu and J. Ascencio, "Biosynthesis and characterization of Ti/Ni bimetallic nanoparticles," *Opt. Mater,* vol. 29, no. 1, pp. 95-99, 2006.

[44] V. Armendariz, M. Joseyacaman, A. Duarte Moller, J. Peralta-Videa, H. Troiani, I. Herrera and J. L. Gardea-Torresdey, "HRTEM characterization of gold nanoparticles production," *Rev. Mex Fis. Suppl,* vol. 50, pp. 7-11, 2004.

[45] V. Armendariz, I. Herrera, J. R. Peralta-Videa, M. Jos'e-Yacam'an, H. Troiani, S. P. and J. L. Gardea-Torresdey, "Size controlled gold nanoparticle formation by Avena sativa biomass: use of plants in nanobiotechnology," *J. Nanopart. Res.,* vol. 6, no. 4, p. 377–382, 2004.

[46] R. Bali and A. Harris, "Biogenic synthesis of Au nanoparticles using vascular plants," *Ind Eng Chem Res,* vol. 49, no. 24, p. 12762–12772, 2010.

[47] N. C. Sharma, S. V. Sahi, S. Nath, J. G. Parsons, J. L. Gardea-Torresdey and T. Pal, "Synthesis of plant-mediated gold nanoparticles and catalytic role of biomatrix-embedded nanomaterials.," *Environ Sci Technol.,* vol. 41, no. 14, pp. 5137-5142, 2007.

[48] J.-F. Manen, O. Sinitsyna, L. Aeschbach, A. V. Markov and A. Sinitsyn, "A fully automatable enzymatic method for DNA extraction from plant tissues," *BMC Plant Biol.,* vol. 5, p. 23, 2005.

[49] S. Shankar, A. Ahmad and M. Sastry, "Geranium leaf assisted biosynthesis of silver nanoparticles," *Biotechnol Prog,* vol. 19, no. 6, p. 1627–1631, 2003.

[50] J. Spencer, "Flavonoids: modulators of brain function?," *Br J Nutr,* vol. 99, no. E-SUPPL. 1, p. ES60–ES77, 2008.

[51] R. Haverkamp and A. Marshall, "The mechanism of metal nanoparticle formation in plants: limits on accumulation," *J Nanopart Res,* vol. 11, no. 6, p. 1453–1463, 2009.

[52] ANSES, "Évaluation des risques liés aux nanomatériaux," ANSES, Maisons-Alfort, 2014.

[53] *ISO/TR 13014:2012 Nanotechnologies - Guidance on physico-chemical characterization of engineered nanoscale materials for toxicologic assessment..*

[54] Y. Leng, Materials Characterization: Introduction to Microscopic and Spectroscopic Methods, Singapore: Wiley & Sons (Asia), 2008.

[55] B. Chu and T. Liu, "Characterization of Nanoparticles by Scattering Techniques," *Journal of Nanoparticle Research,* vol. 2, no. 1, pp. 29-41, 2000.

[56] V. Filipe, A. Hawe and W. Jiskoot, "Critical Evaluation of Nanoparticle Tracking Analysis (NTA) by NanoSight for the Measurement of Nanoparticles and Protein Aggregates," *Pharm Res,* vol. 27, no. 5, pp. 796-810, 2010.

[57] H. Gunther, NMR Spectroscopy: Basic Principles, Concepts and Applications in Chemistry, 3rd Edition, Singapore: Wiley-VCH, 2013.

[58] S. M. Moghimi, "Long-Circulating and Target-Specific Nanoparticles: Theory to Practice," *Pharmacological Reviews,* vol. 53, no. 2, pp. 283-318, June 2001.

[59] E. Hodgson, A Textbook of Modern Toxicology; 4th Edition, Hoboken, NJ: Wiley, 2010.

[60] C. Nantasenamat, C. Isarankura-Na-Ayudhya, T. Naenna and V. Prachayasittikul, "A practical overview of quantitative structure-activity relationship," *Excli J.,* vol. 8, p. 74–88, 2009.

[61] J. P. Griffin, J. Posner and G. R. Barker, The Textbook of Pharmaceutical Medicine, 7th Edition, Belfast: Wiley-Blackwell, 2013.

[62] C. o. t. E. U. European Parliament, "Directive 2010/63/EU of the European Parliament and of the Council of 22 September 2010 on the protection of animals used for scientific purposes," European Union, Europe, 2010.

[63] W. Russell and R. Burch, The Principles of Humane Experimental Technique, London: Mathuen, 1959.

[64] G. Oberdörster, E. Oberdörster and J. Oberdörster, "Nanotoxicology: An Emerging Discipline Evolving from Studies of Ultrafine Particles," *Environ Health Perspect.,* vol. 113, no. 7, p. 823–839, 2005.

[65] S. A. Love, M. A. Maurer-Jones, J. W. Thompson, Y.-S. Lin and C. L. Haynes, "Assessing Nanoparticle Toxicity," *Annu. Rev. Anal. Chem.,* vol. 5, p. 181–205, 2012.

[66] A. Kroll, M. H. Pillukat, D. Hahn and J. Schnekenburger, "Current in vitro methods in nanoparticle risk assessment: Limitations and challenges," *Eur J Pharm Biopharm,* vol. 72, pp. 370-377, 2009.

[67] T. Puck and P. Marcus, "Action of x-rays on mammalian cells," *J Exp Med,* vol. 103, no. 5, p. 653–666, 1956.

[68] Q. Mu, G. Du, T. Chen, B. Zhang and B. Yan, "Suppression of human bone morphogenetic protein signaling by carboxylated single-walled carbon nanotubes," *Am. Chem. Soc. Nano,* vol. 3, p. 1139–1144, 2009.

[69] T. Zhang, J. Stilwell, D. Gerion, L. Ding, O. Elboudwarej, P. Cooke, J. Gray, A. Ailvisatos and F. Chen, "Cellular Effect of High Doses of Silica-Coated Quantum Dot Profiled with High Throughput Gene Expression Analysis and High Content Cellomics Measurements," *Nano Lett,* vol. 6, no. 4, pp. 800-808, 2006.

[70] P. Twentyman and M. Luscombe, "A study of some variables in a tetrazolium dye (MTT) based assay for cell growth and chemosensitivity.," *Br J Cancer,* vol. 56, no. 3, pp. 279-285, 1987.

[71] P. AshaRani, G. Low Kah Mun, M. Hande and S. Valiyaveettil, "Cytotoxicity and genotoxicity of silver nanoparticles in human cells," *Am. Chem. Soc. Nano,* vol. 3, pp. 279-290, 2009.

[72] H. Oliveira, C. Monteiro, F. Pinho, S. Pinho, J. Ferreira de Oliveira and C. Santos, "Cadmium-induced genotoxicity in human osteoblast-like cells.," *Mutat Res Genet Toxicol Environ Mutagen,* Vols. 775-776, no. December, p. 38–47, 2014.

[73] B. J. Marquis, S. A. Love, K. L. Braun and C. L. Haynes, "Analytical methods to assess nanoparticle toxicity," *Analyst,* vol. 134, p. 425–439, 2009.

[74] M. Vendrell, K. Maiti, K. Dhaliwal and Y. Chang, "Surface-enhanced Raman scattering in cancer detection and imaging," *Trends Biotechnol,* vol. 31, no. 4, pp. 249-257, 2013.

[75] V. S. Kalambur, E. K. Longmire and J. C. Bischof, "Cellular Level Loading and Heating of Superparamagnetic Iron Oxide Nanoparticles," *Langmuir,* vol. 23, no. 24, p. 12329–12336, 2007.

[76] W. Strober, "Trypan blue exclusion test of cell viability," *Curr Protoc Immunol.,* vol. Appendix, p. Appendix 3B, 2001.

[77] K. Mascotti, J. McCullough and S. Burger, "HPC viability measurement: trypan blue versus acridine orange and propidium iodide," *Transfusion,* vol. 40, p. 693–696, 2000.

[78] G. Repetto, A. del Peso and J. L. Zurita, "Neutral red uptake assay for the estimation of cell viability/cytotoxicity," *Nature Protocols,* vol. 3, pp. 1125 - 1131, 2008.

[79] D. B. Mitchell, K. S. Santone and D. Acosta, "Evaluation of cytotoxicity in cultured cells by enzyme leakage," *J Tissue Cult Meth,* vol. 6, no. 3-4, pp. 113-116, 1980.

[80] M. Fenech, "Cytokinesis-block micronucleus cytome assay," *Nat Protoc,* vol. 2, no. 5, pp. 1084-1104, 2007.

[81] A. Collins, "The comet assay for DNA damage and repair: principles, applications, and limitations," *Mol Biotechnol,* vol. 26, no. 3, pp. 249-261, 2004.

[82] L. Bregoli, F. Chiarini, A. Gambarelli, G. Sighinolfi, A. Gatti, P. Santi, A. Martelli and L. Cocco, "Toxicity of antimony trioxide nanoparticles on human hematopoietic progenitor cells and comparison to cell lines," *Toxicology,* vol. 362, no. 2, pp. 121-129, 2009.

[83] T. Hauck, A. Ghazani and W. Chan, "Assessing the effect of surface chemistry on gold nanorod uptake, toxicity, and gene expression in mammalian cells," *Small,* vol. 4, p. 153–159, 2008.

[84] J. Veranth, E. Kaser, M. Veranth, M. Koch and Y. GS., "Cytokine responses of human lung cells (BEAS-2B) treated with micron-sized and nanoparticles of metal oxides compared to soil dusts," *Part Fibre Toxicol,* vol. 4, p. 2, 2007.

[85] G. Oostingh, E. Casals, P. Italiani, R. Colognato, R. Stritzinger, J. Ponti, T. Pfaller, Y. Kohl, D. Ooms, F. Favilli, H. Leppens, D. Lucchesi, F. Rossi, I. Nelissen, H. Thielecke, V. Puntes, A. Duschl and D. Boraschi, "Problems and challenges in the development and validation of human cell-based assays to determine nanoparticle-induced immunomodulatory effects," *Part Fibre Toxicol,* vol. 8, no. 1, p. 8, 2011.

[86] E. Eruslanov and S. Kusmartsev, "Identification of ROS Using Oxidized DCFDA and Flow-Cytometry," *Advanced Protocols in Oxidative Stress II, Methods in Molecular Biology,* vol. 594, pp. 57-72, 2010.

[87] C. Sharma, S. Sarkar, A. Periyakaruppan, J. Barr, K. Wise, R. Thomas, B. Wilson and G. Ramesh, "Single-walled carbon nanotubes induces oxidative stress in rat lung epithelial cells," *J Nanosci Nanotechnol,* vol. 7, no. 7, pp. 2466-2472, 2007.

[88] I. Rahman, A. Kode and S. Biswas, "Assay for quantitative determination of glutathione and glutathione disulfide levels using enzymatic recycling method," *Nat Protoc,* vol. 1, no. 6, pp. 3159-3165, 2006.

[89] S. Moghimi and J. Szebeni, "Stealth liposomes and long circulating nanoparticles: critical issues in pharmacokinetics, opsonization and protein-binding properties," *Prog Lipid Res,* vol. 42, no. 6, pp. 463-478, 2003.

[90] L. Guo, A. Von Dem Bussche, M. Buechner, A. Yan, A. Kane and R. Hurt, "Adsorption of essential micronutrients by carbon nanotubes and the implications for nanotoxicity testing," *Small,* vol. 4, p. 721–727, 2008.

[91] J. Worle-Knirsch, K. Pulskamp and H. Krug, "Oops, they did it again! Carbon nanotubes hoax scientists in viability assays," *Nano Lett,* vol. 6, p. 1261–1268, 2006.

[92] T. Laaksonen, H. Santos, H. Vihola, J. Salonen, J. Riikonen, T. Heikkilä, L. Peltonen, N. Kumar, D. Murzin, V. Lehto and J. Hirvonen, "Failure of MTT as a toxicity testing agent for mesoporous silicon microparticles," *Chem Res Toxicol,* vol. 20, no. 12, pp. 1913-1918, 2007.

[93] I. Bravo-Osuna, G. Millotti, C. Vauthier and G. Ponchel, "In vitro evaluation of calcium binding capacity of chitosan and thiolated chitosan poly(isobutylcyanoacrylate) core-shell nanoparticles," *Int. J. Pharm,* vol. 338, p. 284, 2007.

[94] S. Oh, H. Kim, Y. Liu, H. Han, K. Kwon, K. Chang, K. Park, Y. Kim, K. Shim, S. An and M. Lee, "Incompatibility of silver nanoparticles with lactate dehydrogenase leakage assay for cellular viability test is attributed to protein binding and reactive oxygen species generation," *Toxicol Lett,* vol. 225, no. 3, pp. 422-432, 2014.

[95] K. Pulskamp, S. Diabate and H. Krug, "Carbon nanotubes show no sign of acute toxicity but induce intracellular reactive oxygen species in dependence on contaminants," *Toxicol. Lett.,* vol. 168, p. 58–74, 2007.

[96] R. Davis, P. Lockwood, D. Hobbs, R. Messer, R. Price, J. Lewis and J. Wataha, "In vitro biological effects of sodium titanate materials," *J. Biomed Mater. Res. B Appl. Biomater.,* vol. 83, p. 2007, 505–511.

[97] E. Dulkeith, M. Ringler, T. Klar, J. Feldmann, A. Munoz Javier and W. Parak, "Gold nanoparticles quench fluorescence by phase induced radiative rate suppression," *Nano Lett,* vol. 5, p. 585–589, 2005.

[98] E. Meulenkamp, "Size dependence of the dissolution of ZnO nanoparticles," *J Phys. Chem. B,* vol. 102, p. 7764–7769, 1998.

[99] J. Plumb, R. Milroy and S. Kaye, "Effects of the pH dependence of 3-(4,5-dimethylthiazol-2-yl)-2,5-diphenyl-tetrazolium bromide-formazan absorption on chemosensitivity determined by a novel tetrazolium-based assay," *Cancer Res,* vol. 49, p. 4435–4440, 1989.

[100] A. Babson and G. Phillips, "A rapid colorimetric assay for serum lactic dehyrogenase," *Clin. Chim. Acta,* vol. 12, p. 210, 1965.

[101] L. Belyanskaya, P. Manser, P. Spohn, A. Bruinink and P. Wick, "The reliability and limits of the MTT reduction assay for carbon nanotubes–cell interaction," *Carbon,* vol. 45, p. 2643–2648, 2007.

[102] V. W. Davis, O. F. Bathe, D. E. Schiller, C. M. Slupsky and M. B. Sawyer, "Metabolomics and surgical oncology: Potential role for small molecule biomarkers," *J. Surg. Oncol.,* vol. 103, p. 451–459, 2011.

[103] Office of Biological and Environmental Research of the U.S. Department of Energy Genomic Science, "Categories of Global Omics Measurements," U.S. Department of Energy Office of Science, 2009. [Online]. Available: http://genomicscience.energy.gov. [Accessed 1 9 2015].

[104] R. Goodacre, "Metabolomics – the way forward," *Metabolomics,* vol. 1, no. 1, pp. 1-2, 2005.

[105] J. Berg, J. Tymoczko and L. Stryer, Biochemistry 5th Edition, New York: W H Freeman, 2002.

[106] D. Nelson and M. Cox, Lehninger Principles of Biochemistry 5th Edition, New York: W.H. Freeman and Company, 2008.

[107] The Global Resource, "Silver in History|The Silver Institute," The Silver Institute, 2011. [Online]. Available: https://www.silverinstitute.org/site/silver-essentials/silver-in-history/. [Accessed 18 08 2015].

[108] A. D. Russell and W. B. Hugo, "7 Antimicrobial activity and action of silver," *Progress inMedicinal Chemistry,* vol. 31, p. 351–370, 1994.

[109] Y. Liu, D. Zhang, E. C. Alocilja and S. Chakrabartty, "Biomolecules Detection Using a Silver-Enhanced Gold Nanoparticle-Based Biochip," *Nanoscale Res Lett,* vol. 5, no. 3, p. 533–538, 2010.

[110] P. Wu, Y. Gao, Y. Lu, H. Zhang and C. Cai, "High specific detection and near-infrared photothermal therapy of lung cancer cells with high SERS active aptamer–silver–gold shell–core nanostructures," *Analyst,* vol. 138, pp. 6501-6510, 2013.

[111] K. Y. Yoon, J. H. Byeon, C. W. Park and J. Hwang, "Antimicrobial Effect of Silver Particles on Bacterial Contamination of Activated Carbon Fibers," *Environ. Sci. Technol.,* vol. 42, no. 4, p. 1251–1255, 2008.

[112] Y. Lv, H. Liu, Z. Wang, S. Liu, L. Hao, Y. Sang, D. Liu, J. Wang and R. I. Boughton, "Silver nanoparticle-decorated porous ceramic composite for water treatment," *J Memr Sci,* vol. 336, no. 1-2, p. 50–56, 2009.

[113] L. Mpenyana-monyatsi, N. H. Mthombeni and M. S. Onyango, "Cost-Effective Filter Materials Coated with Silver Nanoparticles for the Removal of Pathogenic Bacteria in Groundwater," *Int. J. Environ. Res. Public Health,* vol. 9, no. 1, pp. 244-271, 2012.

[114] A. Kumar, P. K. Vemula, P. M. Ajayan and G. John, "Silver-nanoparticle-embedded antimicrobial paints based on vegetable oil," *Nature Mater,* vol. 7, pp. 236 - 241, 2008.

[115] S. Wijnhoven, W. Peijnenburg, C. Herberts, W. Hagens, A. Oomen, E. Heugens, B. Roszek, J. Bisschops, I. Gosens, D. V.D. Meent, S. Dekkers, W. De Jong, M. van Zijverden, A. Sips and R.

Geertsma, "Nano-silver – a review of available data and knowledge gaps in human and environmental risk assessment," *Nanotoxicology,* vol. 2, no. 3, pp. 109-138, 2009.

[116] L. G. Ovington, "The truth about silver," *Ostomy Wound Management,* vol. 50, no. 9 supplement, p. 1s–10s, 2004.

[117] K. Chaloupka, Y. Malam and A. M. Seifalian, "Nanosilver as a new generation of nanoproduct in biomedical applications," *Trends in Biotechnology,* vol. 28, no. 11, p. 580–588, 2010.

[118] G. L. Grunkemeier, R. Jin and A. Starr, "Prosthetic heart valves: objective performance criteria versus randomized clinical trial," *Annals ofThoracic Surgery,* vol. 82, no. 3, p. 776–780, 2006.

[119] D. Roe, B. Karandikar, N. Bonn-Savage, B. Gibbins and J. Roullet, "Antimicrobial surface functionalization of plastic catheters by silver nanoparticles," *Journal of Antimicrobial Chemotherapy,* vol. 61, no. 4, p. 869–876, 2008.

[120] A. Akhavan, A. Sodagar, F. Mojtahedzadeh and K. Sodagar, "Investigating the effect of incorporating nanosilver/nanohydroxyapatite particles on the shear bond strength of orthodontic adhesives," *Acta Odontologica Scandinavica,* vol. 71, no. 5, p. 1038–1042, 2013.

[121] A. Magalhães, R. Santos, L. Lopes, C. Araújo Estrela, C. Estrela, E. Torres, A. Bakuzis, P. Cardoso and M. Carriao, "Nanosilver Application in Dental Cements," *ISRN Nanotechnology,* p. Article ID 365438, 2012.

[122] V. Alt, T. Bechert, P. Steinrücke, M. Wagener, P. Seidel, E. Dingeldein, E. Domann and R. Schnettler, "An in vitro assessment of the antibacterial properties and cytotoxicity of nanoparticulate silver bone cement," *Biomaterials,* vol. 25, no. 18, pp. 4383-4391, 2004.

[123] Z. Zheng, W. Yin, J. Zara, W. Li, J. Kwak, R. Mamidi, M. Lee, D. Siu, R. Ngo, J. Wang, D. Carpenter, X. Zhang, B. Wu, K. Ting and C. Sooa, "The use of BMP-2 coupled – Nanosilver-PLGA composite grafts to induce bone repair in grossly infected segmental defects," *Biomaterials,* vol. 31, no. 35, pp. 9293-9300, 2010.

[124] A. I. Freeman, L. J. Halladay and P. Cripps, "The effect of silver impregnation of surgical scrub suits on surface bacterial contamination," *Vet J,* vol. 192, no. 3, p. 489–493, 2012.

[125] M. Murphy, K. Ting, X. Zhang, C. Soo and Z. Zheng, "Current Development of Silver Nanoparticle Preparation, Investigation, and Application in the Field of Medicine," *Journal of Nanomaterials,* p. Article ID 696918, 2015.

[126] V. Amendola and M. Meneghetti, "Laser ablation synthesis in solution and size manipulation of noble metal nanoparticles," *Physical Chemistry Chemical Physics,* vol. 11, no. 20, pp. 3805-3821, 2009.

[127] D. Tien, K. Tseng, C. Liao and T. Tsung, "Colloidal silver fabrication using the spark discharge system and its antimicrobial effect on Staphylococcus aureus," *Medical Engineering and Physics,* vol. 30, no. 8, p. 948–952, 2008.

[128] D. Carpenter, "Method and apparatus for forming nano-particles". USA Patent US 7282167 B2, 16 October 2007.

[129] D. Cruz, P. Fale, A. Mourato, P. Vaz, S. M. Luisa and A. Lino, "Preparation and physicochemical characterization of Ag nanoparticles biosynthesized by Lippia citriodora (Lemon Verbena)," *Colloids Surf B,* vol. 81, no. 1, p. 67–73, 2010.

[130] H. M. Ibrahim, "Green synthesis and characterization of silver nanoparticles using banana peel extract and their antimicrobial activity against representative microorganisms," *Journal of Radiation Research and Applied Sciences,* vol. 8, no. 3, p. 265–275, 2015.

[131] M. M. Khalila, E. H. Ismaila, K. Z. El-Baghdady and D. Mohamed, "Green synthesis of silver nanoparticles using olive leaf extract and its antibacterial activity," *Arabian Journal of Chemistry,* vol. 7, no. 6, p. 1131–1139, 2014.

[132] T. Santhoshkumar, A. Rahuman, G. Rajakumar, S. Marimuthu, A. Bagavan, C. Jayaseelan, A. Abduz Zahir, G. Elango and C. Kamaraj, "Synthesis of silver nanoparticles using Nelumbo nucifera leaf extract and its larvicidal activity against malaria and filariasis vectors," *Parasitology Research,* vol. 108, no. 3, pp. 693-702, 2011.

[133] M. Faramarzi and A. Sadighi, "Insights into biogenic and chemical production of inorganic nanomaterials and nanostructures," *Advances in Colloid and Interface Science,* Vols. 189-190, pp. 1-20, 2013.

[134] S. Iravani, "Green synthesis of metal nanoparticles using plants," *Green Chem,* vol. 13, p. 2638–2650, 2011.

[135] X. Li, J. Lenhart and H. Walker, "Dissolution-accompanied aggregation kinetics of silver nanoparticles," *Langmuir,* vol. 26, no. 22, pp. 16690-16698, 2010.

[136] C. Beer, R. Foldbjerg, Y. Hayashi, D. Sutherland and H. Autrup, "Toxicity of silver nanoparticles - nanoparticle or silver ion?," *Toxicol Lett.,* vol. 208, no. 3, pp. 286-292, 2012.

[137] S. Kittler, C. Greulich, J. Diendorf, M. Köller and M. Epple, "Toxicity of Silver Nanoparticles Increases during Storage Because of Slow Dissolution under Release of Silver Ions," *Chem Mater,* vol. 22, no. 16, p. 4548–4554, 2010.

[138] K. Kim, W. Sung, S. Moon, J. Choi, J. Kim and D. Lee, "Antifungal effect of silver nanoparticles on dermatophytes," *J Microbiol Biotechnol,* vol. 18, no. 8, pp. 1482-1484, 2008.

[139] S. Gaikwad, A. Ingle, A. Gade, M. Rai, A. Falanga, N. Incoronato, L. G. S. Russo and M. Galdiero, "Antiviral activity of mycosynthesized silver nanoparticles against herpes simplex virus and human parainfluenza virus type 3," *International Journal of Nanomedicine,* vol. 8, pp. 4303-4314, 2013.

[140] P. L. Nadworny, J. Wang, E. E. Tredget and R. E. Burrell, "Antiinflammatory activity of nanocrystalline silver in a porcine contact dermatitis model," *Nanomedicine: Nanotechnology, Biology, Medicine,* vol. 4, no. 3, p. 241–251, 2008.

[141] K. K. Wong, S. O. Cheung, L. Huang, J. Niu, C. Tao, C. Ho, C. Che and P. K. Tam, "Further Evidence of the Anti-inflammatory Effects of Silver Nanoparticles," *ChemMedChem,* vol. 4, p. 1129–1135, 2009.

[142] L. Wei, J. Lu, H. Xu, A. Patel and Z.-S. Chen, "Silver nanoparticles: synthesis, properties, and therapeutic applications," *Drug Discovery Today,* vol. 20, no. 5, p. 595–601, 2015.

[143] S. Arora, N. Tyagi, A. Bhardwaj, L. Rusu, R. Palanki, K. Vig, S. R. Singh, A. P. Singh, S. Palanki, M. E. Miller, J. E. Carter and S. Singh, "Silver nanoparticles protect human keratinocytes against UVB radiation-induced DNA damage and apoptosis: potential for prevention of skin carcinogenesis," *Nanomedicine: Nanotechnology, Biology, and Medicine,* vol. 11, no. 5, p. 1265–1275, 2015.

[144] C. M. Jones and E. M. V. Hoek, "A review of the antibacterial effects of silver nanomaterials and potential implications for human health and the environment," *J. Nanopart. Res.,* vol. 12, no. 5, pp. 1531-1551, 2010.

[145] Q. H. Tran, V. Q. Nguyen and A.-T. Le, "Silver nanoparticles: synthesis, properties, toxicology, applications and perspectives," *Adv. Nat. Sci.: Nanosci. Nanotechnol.,* vol. 4, no. 3, p. 033001, 2013.

[146] S. Agnihotria, S. Mukherjiabc and S. Mukherji, "Size-controlled silver nanoparticles synthesized over the range 5–100 nm using the same protocol and their antibacterial efficacy," *RSC Adv,* vol. 4, pp. 3974-3983, 2014.

[147] B. Sadeghi, F. S. Garmaroudi, M. Hashemi, H. R. Nezhad, A. Nasrollahi and S. Ardalan, "Comparison of the anti-bacterial activity on the nanosilver shapes: Nanoparticles, nanorods and nanoplates," *Advanced Powder Technology,* vol. 23, no. 1, pp. 22-26, 2012.

[148] S. Pal, Y. K. Tak and J. M. Song, "Does the Antibacterial Activity of Silver Nanoparticles Depend on the Shape of the Nanoparticle? A Study of the Gram-Negative Bacterium Escherichia coli," *Appl. Environ. Microbiol.,* vol. 73, no. 6, pp. 1712-1720, 2007.

[149] C. Lok, C. Ho, R. Chen, Q. He, W. Yu, H. Sun, P. Tam, J. Chiu and C. Che, "Silver nanoparticles: Partical oxidation and antibacterial activities.," *J. Biol. Inorg. Chem.,* vol. 12, p. 527–534, 2007.

[150] I. Sondi and B. Salopek-Sondi, "Silver nanoparticles as antimicrobial agent: a case study on E. coli as a model for Gram-negative bacteria," *Journal of Colloid and Interface Science,* vol. 275, p. 177–182, 2004.

[151] M. Raffi, F. Hussain, T. Bhatti, J. Akhter, A. Hameed and M. Hasan, "Antibacterial Characterization of Silver Nanoparticles against E. Coli ATCC-15224," *J. Mater. Sci. Technol.,* vol. 24, no. 2, pp. 192-196, 2008.

[152] H. Xu, F. Qu, H. Xu, W. Lai, Y. Andrew Wang, Z. Aguilar and H. Wei, "Role of reactive oxygen species in the antibacterial mechanism of silver nanoparticles on Escherichia coli O157:H7.," *Biometals,* vol. 25, no. 1, pp. 45-53, 2012.

[153] Q. Feng, J. Wu, G. Chen, F. Cui, T. Kim and J. Kim, "A mechanistic study of the antibacterial effect of silver ions on Escherichia coli and Staphylococcus aureus," *J Biomed Mater Res.,* vol. 52, no. 4, pp. 662-668, 2000.

[154] W. Lee, K. Kim and D. Lee, "A novel mechanism for the antibacterial effect of silver nanoparticles on Escherichia coli.," *Biomaterials,* vol. 27, no. 6, pp. 1191-1201, 2014.

[155] H. Rosenkranz, J. Coward, T. Wlodkowski and H. Carr, "Properties of silver-sulfadiazine-resistant Enterobacter cloacae," *Antimicrob Agents Chemother,* vol. 5, no. 2, pp. 199-201, 1974.

[156] D. Marx and D. Barillo, "Silver in medicine: the basic science," *Burns,* vol. 40, no. Sup, pp. S9-S18, 2014.

[157] R. Warriner and R. Burrell, "Infection and the chronic wound: a focus on silver," *Adv Skin Wound Care,* vol. 18, no. S1, pp. 2-12, 2005.

[158] H. J. Johnston, G. Hutchison, F. M. Christensen, S. Peters, S. Hankin and V. Stone, "A review of the in vivo and in vitro toxicity of silver and gold particulates: Particle attributes and biological mechanisms responsible for the observed toxicity.," *Critical Reviews in Toxicology,* vol. 40, no. 4, p. 328–346, 2010.

[159] M. Munger, P. Radwanski, G. Hadlock, G. Stoddard, A. Shaaban, J. Falconer, D. Grainger and C. Deering-Rice, "In vivo human time-exposure study of orally dosed commercial silver nanoparticles," *Nanomedicine,* vol. 10, no. 1, pp. 1-9, 2014.

[160] J. Lee, J. Mun, J. Park and I. Yu, "A health surveillance case study on workers who manufacture silver nanomaterials," *Nanotoxicology,* vol. 6, no. 6, pp. 667-669, 2012.

[161] A. Wadhera and M. Fung, "Systemic argyria associated with ingestion of colloidal silver," *Dermatology Online Journal,* vol. 11, no. 1, p. 12, 2005.

[162] A. Chang, V. Khosravi and B. Egbert, "A case of argyria after colloidal silver ingestion," *J Cutan Pathol,* vol. 33, p. 809–811, 2006.

[163] E.-J. V. Dunn K., "The role of Acticoat with nanocrystalline silver in the management of burns," *Burns,* vol. 30, no. Sup, pp. S1-9, 2004.

[164] E. Vlachou, E. Chipp, E. Shale, Y. Wilson, R. Papini and N. Moiemen, "The safety of nanocrystalline silver dressings on burns: a study of systemic silver absorption," *Burns,* vol. 33, no. 8, pp. 979-985, 2007.

[165] Y. Huang, X. Li, Z. Liao, G. Zhang, Q. Liu, J. Tang, Y. Peng, X. Liu and Q. Luo, "A randomized comparative trial between Acticoat and SD-Ag in the treatment of residual burn wounds, including safety analysis," *Burns,* vol. 33, no. 2, pp. 161-166, 2007.

[166] M. Trop, M. Novak, S. Rodl, B. Hellbom, W. Kroell and W. Goessler, "Silver-coated dressing acticoat caused raised liver enzymes and argyria-like symptoms in burn patient," *J Trauma,* vol. 60, no. 3, pp. 648-652, 2006.

[167] J. Chen, C. Han, X. Lin, Z. Tang and S. Su, "[Effect of silver nanoparticle dressing on second degree burn wound] [Article in Chinese]," *Zhonghua Wai Ke Za Zhi,* vol. 44, no. 1, pp. 50-52, 2006.

[168] J. Ji, J. Jung, S. Kim, J. Yoon, J. Park, B. Choi, Y. Chung, I. Kwon, J. Jeong, B. Han, J. Shin, J. Sung, K. Song and I. Yu, "Twenty-eight-day inhalation toxicity study of silver nanoparticles in Sprague-Dawley rats," *Inhal Toxicol,* vol. 19, no. 10, pp. 857-871, 2007.

[169] J. Hyun, B. Lee, H. Ryu, J. Sung, K. Chung and I. Yu, "Effects of repeated silver nanoparticles exposure on the histological structure and mucins of nasal respiratory mucosa in rats," *Toxicol Lett,* vol. 182, no. 1-3, pp. 24-28, 2008.

[170] J. Sung, J. Ji, J. Yoon, D. Kim, M. Song, J. Jeong, B. Han, J. Han, Y. Chung, J. Kim, T. Kim, H. Chang, E. Lee, J. Lee and I. Yu, "Lung function changes in Sprague-Dawley rats after prolonged inhalation exposure to silver nanoparticles," *Inhal Toxicol,* vol. 20, no. 6, pp. 567-574, 2008.

[171] J. Sung, J. Ji, J. Park, J. Yoon, D. Kim, K. Jeon, M. Song, J. Jeong, B. Han, J. Han, Y. Chung, H. Chang, J. Lee, M. Cho, B. Kelman and I. Yu, "Subchronic inhalation toxicity of silver nanoparticles," *Toxicol Sci,* vol. 108, no. 2, pp. 452-461, 2009.

[172] S. J. J. J. S. K. L. J. K. C. Y. I. Kim JS, "In vivo Genotoxicity of Silver Nanoparticles after 90-day Silver Nanoparticle Inhalation Exposure," *Saf Health Work. ,* vol. 2, no. 1, p. 34–38, 2011.

[173] H. Cho, J. Sung, S. Song, J. Kim, J. Ji, J. Lee, H. Ryu, K. Ahn and I. Yu, "Genotoxicity of Silver Nanoparticles in Lung Cells of SpragueDawley Rats after 12 Weeks of Inhalation Exposure," *Toxics,* vol. 1, pp. 36-45, 2013.

[174] L. Stebounova, A. Adamcakova-Dodd, J. Kim, H. Park, P. O'Shaughnessy, V. Grassian and P. Thorne, "Nanosilver induces minimal lung toxicity or inflammation in a subacute murine inhalation model," *Part Fibre Toxicol,* vol. 8, no. 1, p. 5, 2011.

[175] C. Y. J. E. Y. H. K. J. K. J. I. H. Lee HY, M. Cho, J. Kim, H. Kim and B. Lee, "Genomics-based screening of differentially expressed genes in the brains of mice exposed to silver nanoparticles via inhalation," *Journal of Nanoparticle Research,* vol. 12, no. 5, pp. 1567-1578, 2010.

[176] N. Yin, Y. Zhang, Z. Yun, Q. Liu, G. Qu, Q. Zhou, L. Hu and G. Jiang, "Silver nanoparticle exposure induces rat motor dysfunction through decrease in expression of calcium channel protein in cerebellum," *Toxicol Lett,* vol. 237, no. 2, pp. 112-120, 2015.

[177] N. Yin, X. Yao, Q. Zhou, F. Faiola and G. Jiang, "Vitamin E attenuates silver nanoparticle-induced effects on body weight and neurotoxicity in rats," *Biochem Biophys Res Commun,* vol. 458, no. 2, p. 2015, 405-410.

[178] J. Tang, L. Xiong, S. Wang, J. Wang, L. Liu, J. Li, Z. Wan and T. Xi, "Influence of silver nanoparticles on neurons and blood-brain barrier via subcutaneous injection in rats," *Applied Surface Science,* vol. 255, p. 502–504, 2008.

[179] M. Rahman, J. Wang, T. Patterson, U. Saini, B. Robinson, G. Newport, R. Murdock, J. Schlager, H. SM and S. Ali, "Expression of genes related to oxidative stress in the mouse brain after exposure to silver-25 nanoparticles," *Toxicol Lett,* vol. 187, no. 1, pp. 15-21, 2009.

[180] P. Liu, Z. Huang and N. Gu, "Exposure to silver nanoparticles does not affect cognitive outcome or hippocampal neurogenesis in adult mice," *Ecotoxicol Environ Saf,* vol. 87, pp. 124-130, 2013.

[181] D. Lankveld, A. Oomen, P. Krystek, A. Neigh, A. Troost-de Jong, C. Noorlander, J. Van Eijkeren, R. Geertsma and W. De Jong, "The kinetics of the tissue distribution of silver nanoparticles of different sizes," *Biomaterials,* vol. 31, no. 32, pp. 8350-8361, 2010.

[182] D. Tiwari, T. Jin and J. Behari, "Dose-dependent in-vivo toxicity assessment of silver nanoparticle in Wistar rats," *Toxicol Mech Methods,* vol. 21, no. 1, pp. 13-24, 2011.

[183] Y. Xue, S. Zhang, Y. Huang, T. Zhang, X. Liu, Y. Hu, Z. Zhang and M. Tang, "Acute toxic effects and gender-related biokinetics of silver nanoparticles following an intravenous injection in mice," *J Appl Toxicol,* vol. 32, no. 11, pp. 890-899, 2012.

[184] W. De Jong, L. Van Der Ven, A. Sleijffers, M. Park, E. Jansen, H. Van Loveren and R. Vandebriel, "Systemic and immunotoxicity of silver nanoparticles in an intravenous 28 days repeated dose toxicity study in rats.," *Biomaterials,* vol. 34, no. 33, pp. 8333-8343, 2013.

[185] R. Vandebriel, E. Tonk, L. de la Fonteyne-Blankestijn, E. Gremmer, H. Verharen, L. van der Ven, H. van Loveren and d. J. WH, "Immunotoxicity of silver nanoparticles in an intravenous 28-day repeated-dose toxicity study in rats," *Part Fibre Toxicol,* vol. 11, p. 21, 2014.

[186] C. A. Austin, "Intravenous Exposure of Pregnant Mice to Silver Nanoparticles: Silver Tissue Distribution and Effects in Maternal and Extra-Embryonic Tissues and Embryos," The George Washington University, DC, USA, 2013.

[187] A. Ashraf, R. Sharif, M. Ahmad, M. Masood, A. Shahid, D. Anjum, M. Rafique and S. Ghani, "In vivo evaluation of the biodistribution of intravenously administered naked and functionalised silver nanoparticles in rabbit," *IET Nanobiotechnology,* vol. 9, p. 7, 2015.

[188] Y. Kim, J. Kim, H. Cho, D. Rha, J. Kim, J. Park, B. Choi, R. Lim, H. Chang, Y. Chung, I. Kwon, J. Jeong, B. Han and I. Yu, "Twenty-eight-day oral toxicity, genotoxicity, and gender-related tissue distribution of silver nanoparticles in Sprague-Dawley rats," *Inhal Toxicol,* vol. 20, no. 6, pp. 575-583, 2008.

[189] Y. Kim, M. Song, J. Park, K. Song, H. Ryu, Y. Chung, H. Chang, O. K. Lee JH, B. Kelman, I. Hwang and I. Yu, "Subchronic oral toxicity of silver nanoparticles," *Part Fibre Toxicol,* vol. 7, p. 20, 2010.

[190] J. Skalska, M. Frontczak-Baniewicz and L. Strużyńska, "Synaptic degeneration in rat brain after prolonged oral exposure to silver nanoparticles," *Neurotoxicology,* vol. 46, pp. 145-154, 2015.

[191] X. Wang, M. Kempf, J. Mott, H. Chang, R. Francis, P. Liu, L. Cuttle, H. Olszowy, O. Kravchuk, J. Mill and R. Kimble, "Silver absorption on burns after the application of Acticoat: data from pediatric patients and a porcine burn model," *J Burn Care Res,* vol. 30, no. 2, pp. 341-348, 2009.

[192] M. Samberg, S. Oldenburg and N. Monteiro-Riviere, "Evaluation of silver nanoparticle toxicity in skin in vivo and keratinocytes in vitro," *Environ Health Perspect,* vol. 118, no. 3, pp. 407-413, 2010.

[193] P. Maneewattanapinyo, W. Banlunara, C. Thammacharoen, S. Ekgasit and T. Kaewamatawong, "An evaluation of acute toxicity of colloidal silver nanoparticles," *J Vet Med Sci,* vol. 73, no. 11, pp. 1417-1423, 2011.

[194] S. Lue, W. Gao and H. Gu, "Construction, application and biosafety of silver nanocrystalline chitosan wound dressing," *Burns,* vol. 34, no. 5, p. 623–628, 2008.

[195] P. D. Marcato, L. B. De Paula, P. Melo, I. R. Ferreira, A. B. A. Almeida, A. S. Torsoni and O. L. Alves, "In Vivo Evaluation of Complex Biogenic Silver Nanoparticle and Enoxaparin in Wound Healing," *Journal of Nanomaterials,* p. Article ID 439820, 2015.

[196] A. Gliga, S. Skoglund, I. Wallinder, B. Fadeel and H. Karlsson, " Size-dependent cytotoxicity of silver nanoparticles in human lung cells: the role of cellular uptake, agglomeration and Ag release," *Part Fibre Toxicol,* vol. 11, p. 11, 2014.

[197] R. Foldbjerg, E. Irving, Y. Hayashi, D. Sutherland, K. Thorsen, H. Autrup and C. Beer, "Global gene expression profiling of human lung epithelial cells after exposure to nanosilver," *Toxicol Sci,* vol. 130, no. 1, pp. 145-157, 2012.

[198] W. Liu, Y. Wu, C. Wang, H. Li, T. Wang, C. Liao, L. Cui, Q. Zhou, B. Yan and G. Jiang, "Impact of silver nanoparticles on human cells: effect of particle size," *Nanotoxicology,* vol. 4, no. 3, pp. 319-330, 2010.

[199] Y. A. Suliman, D. Ali, S. Alarifi, A. Harrath, L. Mansour and S. Alwasel, "Evaluation of cytotoxic, oxidative stress, proinflammatory and genotoxic effect of silver nanoparticles in human lung epithelial cells," *Environ Toxicol,* vol. 30, no. 2, pp. 149-160, 2015.

[200] R. Foldbjerg, D. Dang and H. Autrup, "Cytotoxicity and genotoxicity of silver nanoparticles in the human lung cancer cell line, A549," *Arch Toxicol,* vol. 85, no. 7, pp. 743-50, 2011.

[201] A. Huk, E. Izak-Nau, B. Reidy, M. Boyles, A. L. I. Duschl and M. Dušinska, "Is the toxic potential of nanosilver dependent on its size," *Part Fibre Toxicol,* vol. 11, p. 65, 2014.

[202] I. Sur, M. Altunbek, M. Kahraman and M. Culha, "The influence of the surface chemistry of silver nanoparticles on cell death," *Nanotechnology,* vol. 23, p. 375102, 2012.

[203] M. Piao, K. Kang, I. Lee, H. Kim, S. Kim, J. Choi, J. Choi and J. Hyun, "Silver nanoparticles induce oxidative cell damage in human liver cells through inhibition of reduced glutathione and induction of mitochondria-involved apoptosis," *Toxicol Lett,* vol. 201, no. 1, pp. 92-100, 2011.

[204] P. Liu, R. Guan, X. Ye, J. Jiang, M. Liu, G. Huang and X. Chen, "Toxicity of nano- and micro-sized silver particles in human in hepatocyte cell line L02," *J. Phys. Conf. Ser.,* vol. 304, p. 012036., 2011.

[205] Y. Xue, T. Zhang, B. Zhang, F. Gong, Y. Huang and M. Tang, "Cytotoxicity and apoptosis induced by silver nanoparticles in human liver HepG2 cells in different dispersion media," *J. Appl. Toxicol.,* p. [Epub ahead of print], 2015.

[206] K. Kawata, M. Osawa and S. Okabe, "In vitro toxicity of silver nanoparticles at noncytotoxic doses to HepG2 human hepatoma cells," *Environ Sci Technol,* vol. 43, no. 15, pp. 6046-6051, 2009.

[207] R. Prasad, J. McGee, M. Killius, D. Suarez, C. Blackman, D. DeMarini and S. Simmons, "Investigating oxidative stress and inflammatory responses elicited by silver nanoparticles using high-throughput reporter genes in HepG2 cells: effect of size, surface coating, and intracellular uptake," *Toxicol In Vitro,* vol. 27, no. 6, pp. 2013-2021, 2013.

[208] A. Avalos, A. Haza, D. Mateo and P. Morales, "Cytotoxicity and ROS production of manufactured silver nanoparticles of different sizes in hepatoma and leukemia cells," *J Appl Toxicol.,* vol. 34, no. 4, pp. 413-423, 2014.

[209] S. Sahu, J. Njoroge, S. Bryce, J. Yourick and R. Sprando, "Comparative genotoxicity of nanosilver in human liver HepG2 and colon Caco2 cells evaluated by a flow cytometric in vitro micronucleus assay," *J Appl Toxicol,* vol. 34, no. 11, pp. 1226-1234, 2014.

[210] S. Sahu, J. Zheng, J. Yourick, R. Sprando and X. Gao, "Toxicogenomic responses of human liver HepG2 cells to silver nanoparticles," *J. Appl. Toxicol.,* vol. 35, p. 1160–1168, 2015.

[211] S. Kim, J. Choi, J. Choi, K. Chung, K. Park, J. Yi and D. Ryu, "Oxidative stress-dependent toxicity of silver nanoparticles in human hepatoma cells," *Toxicol In Vitro,* vol. 23, no. 6, pp. 1076-1084, 2009.

[212] F. Larese Filon, F. D'Agostin, M. Crosera, G. Adami, N. Renzi, M. Bovenzi and G. Maina, "Human skin penetration of silver nanoparticles through intact and damaged skin," *Toxicology,* vol. 255, no. 1-2, pp. 33-37, 2009.

[213] C. Bianco, G. Adami, M. Crosera, F. Larese, S. Casarin, C. Castagnoli, M. Stella and G. Maina, "Silver percutaneous absorption after exposure to silver nanoparticles: a comparison study of three human skin graft samples used for clinical applications," *Burns,* vol. 40, no. 7, pp. 1390-1396, 2014.

[214] F. Larese Filon, M. Mauro, G. Adami, M. Bovenzi and M. Crosera, "Nanoparticles skin absorption: New aspects for a safety profile evaluation," *Regul Toxicol Pharmacol,* vol. 72, no. 2, pp. 310-322, 2015.

[215] P. Lam, E. Chan, W. Ho and C. Liew, "In vitro cytotoxicity testing of a nanocrystalline silver dressing (Acticoat) on cultured keratinocytes," *Br J Biomed Sci,* vol. 61, no. 3, pp. 125-127, 2004.

[216] J. Paddle-Ledinek, Z. Nasa and H. Cleland, "Effect of different wound dressings on cell viability and proliferation," *Plast Reconstr Surg,* vol. 117, no. 7(Sup), pp. 110S-120S., 2006.

[217] C. Rigo, L. Ferroni, I. Tocco, M. Roman, I. Munivrana, C. Gardin, W. Cairns, V. Vindigni, B. Azzena, C. Barbante and B. Zavan, "Active Silver Nanoparticles for Wound Healing," *Int J Mol Sci. ,* vol. 14, no. 3, p. 4817–4840, 2013.

[218] S. Arora, J. Jain, J. Rajwade and K. Paknikar, "Cellular responses induced by silver nanoparticles: In vitro studies," *Toxicol Lett,* vol. 179, no. 2, pp. 93-100, 2008.

[219] R. Szmyd, A. Goralczyk, L. Skalniak, A. Cierniak, B. Lipert, F. Filon, M. Crosera, J. Borowczyk, E. Laczna, J. Drukala, A. Klein and J. Jura, "Effect of silver nanoparticles on human primary keratinocytes," *Biol Chem,* vol. 394, no. 1, pp. 113-123, 2013.

[220] K. Tomankova, J. Horakova, M. Harvanova, L. Malina, J. Soukupova, S. Hradilova, K. Kejlova, J. Malohlava, L. Licman, M. Dvorakova, D. Jirova and H. Kolarova, "Cytotoxicity, cell uptake and microscopic analysis of titanium dioxide and silver nanoparticles in vitro," *Food Chem Toxicol.,* vol. 82, pp. 106-115, 2015.

[221] C. Zanette, M. Pelin, M. Crosera, G. Adami, M. Bovenzi, F. Larese and C. Florio, "Silver nanoparticles exert a long-lasting antiproliferative effect on human keratinocyte HaCaT cell line," *Toxicol In Vitro,* vol. 25, no. 5, pp. 1053-1060, 2011.

[222] B. Boonkaew, M. Kempf, R. Kimble and L. Cuttle, "Cytotoxicity testing of silver-containing burn treatments using primary and immortal skin cells," *Burns,* vol. 40, no. 8, pp. 1562-1569, 2014.

[223] S. Mukherjee, N. O'Claonadh, A. Casey and G. Chambers, "Comparative in vitro cytotoxicity study of silver nanoparticle on two mammalian cell lines," *Toxicol In Vitro,* vol. 26, no. 2, pp. 238-251, 2012.

[224] S. Ahlberg, M. Meinke, L. Werner, M. Epple, J. Diendorf, U. Blume-Peytavi, J. Lademann, A. Vogt and F. Rancan, "Comparison of silver nanoparticles stored under air or argon with respect to the induction of intracellular free radicals and toxic effects toward keratinocytes," *Eur J Pharm Biopharm,* vol. 88, no. 3, pp. 651-657, 2014.

[225] V. De Matteis, M. Malvindi, A. Galeone, V. Brunetti, E. De Luca, S. Kote, P. Kshirsagar, S. Sabella, G. Bardi and P. Pompa, "Negligible particle-specific toxicity mechanism of silver nanoparticles: the role of Ag+ ion release in the cytosol," *Nanomedicine,* vol. 11, no. 3, pp. 731-739, 2015.

[226] G. Karp, Cell and Molecular Biology: Concepts and Experiments, 6th Edition, John Wiley & Sons, 2010.

[227] S. Sahu, J. Zheng, L. Graham, L. Chen, J. Ihrie, J. Yourick and R. Sprando, "Comparative cytotoxicity of nanosilver in human liver HepG2 and colon Caco2 cells in culture," *J Appl Toxicol,* vol. 34, no. 11, pp. 1155-1166, 2014.

[228] K. A, B. Gaiser, G. Hutchison and V. Stone, "An in vitro liver model--assessing oxidative stress and genotoxicity following exposure of hepatocytes to a panel of engineered nanomaterials," *Part Fibre Toxicol,* vol. 9, p. 28, 2012.

[229] V. Christen and K. Fent, "Silica nanoparticles and silver-doped silica nanoparticles induce endoplasmatic reticulum stress response and alter cytochrome P4501A activity," *Chemosphere,* vol. 87, no. 4, pp. 423-434, 2012.

[230] R. Amooaghaei, M. Saeri and M. Azizi, "Synthesis, characterization and biocompatibility of silver nano particles synthesized from Nigella sativa leaf extract in comparison with chemical silver nanoparticles," *Ecotoxicology and Environmental Safety,* vol. 120, pp. 400-408, 2015.

[231] R. Gengan, K. Anand, A. Phulukdaree and A. Chuturgoon, "A549 lung cell line activity of biosynthesized silver nanoparticles using Albizia adianthifolia leaf," *Colloids and Surfaces B: Biointerfaces,* vol. 105, p. 87–91, 2013.

[232] M. Ahmed, M. Khan, M. Siddiqui, M. Alsalhi and S. Alrokayan, "Green synthesis, characterization and evaluation of biocompatibility of silver nanoparticles," *Physica E: Low-dimensional Systems and Nanostructures,* vol. 43, p. 1266–1271, 2011.

[233] M. Moulton, L. Braydich-Stolle, M. Nadagouda, S. Kunzelman, S. Hussain and R. Varma, "Synthesis, characterization and biocompatibility of "green" synthesized silver nanoparticles using tea polyphenols," *Nanoscale,* vol. 2, no. 5, pp. 763-770, 2010.

[234] L. David, B. Modovan, A. Vulcu, L. Olenic, M. Perde-Schrepler, E. Fischer-Fodor, A. Florea, M. Crisan, I. Chiorean, S. Clichici and G. Filip, "Green synthesis, characterization and anti-inflammatory activity ofsilver nanoparticles using European black elderberry fruits extract," *Colloids and Surfaces B: Biointerfaces,* vol. 122, pp. 767-777, 2014.

[235] N. Hadrup, H. Lam, K. Loeschner, A. Mortensen, E. Larsen and H. Frandsen, "Nanoparticulate silver increases uric acid and allantoin excretion in rats, as identified by metabolomics," *J Appl Toxicol,* vol. 32, no. 11, pp. 929-933, 2012.

[236] S. Kim, S. Kim, S. Lee, B. Kwon, J. Choi, J. Hyun and S. Kim, "Characterization of the Effects of Silver Nanoparticles on Liver Cell Using HR-MAS NMR Spectroscopy," *Bull. Korean Chem. Soc.,* vol. 32, no. 6, p. 2021–2026, 2011.

[237] J. Carrola, V. Bastos, J. M. P. Ferreira de Oliveira, H. Oliveira, C. Santos, A. M. Gil and I. F. Duarte, "Insights into the impact of silver nanoparticles on human keratinocytes metabolism through NMR metabolomics," *Archives of Biochemistry and Biophysics ,* p. (In Press), 2015.

[238] S. Santos, R. Pinto, S. Rocha, P. Marques, N. C. Pascoal, A. Silvestre and C. Freire, "Unveiling the chemistry behind the green synthesis of metal nanoparticles," *ChemSusChem,* vol. 7, no. 9, pp. 2704-2711, 2014.

[239] V. Mangini, M. Dell'Aglio, A. De Stradis, A. De Giacomo, O. De Pascale, G. Natile and F. Arnesano, "Amyloid Transition of Ubiquitin on Silver Nanoparticles Produced by Pulsed Laser Ablation in Liquid as a Function of Stabilizer and Single-Point Mutations," *Chem Eur. J.,* vol. 20, pp. 10745-10751, 2014.

[240] P. Jain, X. Huang, I. El-Sayed and M. EL-Sayed, "Review of some interesting surface plasmon resonance-enhanced properties of noble metal nanoparticles and their applications to biosystems," *Plasmonics,* vol. 2, no. 3, pp. 107-118, 2007.

[241] T. Huanga and X.-H. N. Xu, "Synthesis and characterization of tunable rainbow colored colloidal silver nanoparticles using single-nanoparticle plasmonic microscopy and spectroscopy," *J. Mater. Chem.,* vol. 20, pp. 9867-9876, 2010.

[242] Thermo Fisher Scientific, Evolution 200 series UV-Visible Spectrophotometer Users Manual, WI, USA: Thermo Fisher Scientific, 2011.

[243] Malvern Instruments Ltd., Zetasizer Nano Series Users Manual, England: Malvern Instruments Ltd., 2004.

[244] R. Byron Bird, W. E. Stewart and E. N. Lightfoot, Transport Phenomena, Revised 2nd Edition, USA: Wiley & Sons Inc., 2007.

[245] J. A. McGrath and J. Uitto, "Chapter 3: Anatomy and Organization of Human Skin," in *Rook's Textbook of Dermatology, Eighth Edition* , West Sussex, UK, Blackwell, 2010, pp. 1-53.

[246] P. Boukamp, R. T. Petrussevska, D. Breitkreutz, J. Hornung, A. Markham and N. E. Fusenig, "Normal keratinization in a spontaneously immortalized aneuploid human keratinocyte cell line," *J Cell Biol,* vol. 106, no. 3, pp. 761-71, 1988.

[247] University of UTAH Health Care, "Nonmelanoma Skin Cancer," 2015. [Online]. Available: http://healthcare.utah.edu/huntsmancancerinstitute/cancer-information/cancer-types-and-topics/nonmelanoma-skin-cancer.php. [Accessed 2015].

[248] T. Mosmann, "Rapid colorimetric assay for cellular growth and survival: application to proliferation and cytotoxicity assays," *J Immunol Methods,* vol. 65, no. 1-2, pp. 55-63, 1983.

[249] N. Marshall, C. Goodwin and S. Holt, "A critical assessment of the use of microculture tetrazolium assays to measure cell growth and function," *Growth Regul,* vol. 5, no. 2, pp. 69-84, 1995.

[250] C. F. Chin and F. M. Yeong, "Safeguarding Entry into Mitosis: the Antephase Checkpoint," *Molecular and Cellular Biology,* vol. 30, no. 1, p. 22–32, 2010.

[251] M. G. Ormerod, Flow Cytometry - A Basic Introduction, UK: De Novo Software, 2008.

[252] R. Duggan, "How a Flow Cytometer Works: A Look Inside the Magic Box," 2009. [Online]. Available: https://static.abdserotec.com/thumbnails/signal1.jpg. [Accessed 01 09 2015].

[253] F. Dieterle, B. Riefke, G. Schlotterbeck, A. Ross, H. Senn and A. Amberg, "NMR and MS methods for metabonomics," *Methods Mol Biol,* vol. 691, pp. 385-415, 2011.

[254] B. Worley and R. Powers, "Multivariate Analysis in Metabolomics," *Current Metabolomics,* vol. 1, pp. 92-107, 2013.

[255] K. Veselkov, L. Vingara, P. Masson, S. Robinette, E. Want, J. Li, R. Barton, C. Boursier-Neyret, B. Walther, T. Ebbels, I. Pelczer, E. Holmes, J. Lindon and J. Nicholson, "Optimized preprocessing of ultra-performance liquid chromatography/mass spectrometry urinary metabolic profiles for improved information recovery.," *Anal Chem,* vol. 83, no. 15, pp. 5864-5872, 2011.

[256] Umetrics, SIMCA –P and Multivariate Analysis; FAQ Handbook, Sweden: Umetrics MKS Company, Version 1.01.

[257] J. Trygg, E. Holmes and T. Lundstedt, "Chemometrics in metabonomics," *J Proteome Res,* vol. 6, no. 2, pp. 469-479, 2007.

[258] S. Wold, K. Esbensen and P. Geladi, "Principal component analysis," *Chemometrics and Intelligent Laboratory Systems,* vol. 2, pp. 37-52, 1987.

[259] R. Rosipal and N. Krämer, "Overview and Recent Advances in Partial Least Squares," in *Subspace, Latent Structure and Feature Selection*, Heidelberg, Springer-Verlag Berlin, 2006, pp. 34-51.

[260] J. N. Miller and J. C. Miller, Statistics and Chemometrics for Analytical Chemistry, 6th Edition, Pearson Education : Canada, 2010.

[261] G. Sullivan and R. Feinn, "Using Effect Size-or Why the P Value Is Not Enough," *J Grad Med Educ,* vol. 4, no. 3, pp. 279-282, 2012.

[262] L. Berben, S. M. Sereika and S. Engberg, "Effect size estimation: Methods and examples," *International Journal of Nursing Studies,* vol. 49, p. 1039–1047, 2012.

[263] Q. Teng, W. Huang, T. W. Collette, D. R. Ekman and C. Tan, "A direct cell quenching method for cell-culture based metabolomics," *Metabolomics,* vol. 5, pp. 199-208, 2009.

[264] J. Carrola, T. Pedrosa, A. Gil, A. Barros, I. Jarak, J. G. Jones, H. Oliveira and I. Duarte, "NMR metabolic profiling of the effects of silver nanoparticles on human epidermis keratinocytes.," in *Metabomeeting 2014*, London, 10-12 September 2014.

[265] D. Wishart, T. Jewison, A. Guo, M. Wilson, C. Knox, Y. Liu, Y. Djoumbou, R. Mandal, F. Aziat, E. Dong, S. Bouatra, I. Sinelnikov, D. Arndt, J. Xia, P. Liu, F. Yallou, T. Bjorndahl, R. Perez-Pineiro, R. Eisner, F. Allen, V. Neveu, R. Greiner and S. A., "HMDB 3.0--The Human Metabolome Database in 2013," *Nucleic Acids Res,* vol. 41(Database issue), pp. D801-807, 2013.

[266] W. Mächtle, "Centrifugation in Particle Size Analysis," in *Encyclopedia of Analytical Chemistry.*, Germany, BASF Aktiengesellschaft, 2006.

[267] T. Beelders, D. de Beer and E. Joubert, "Thermal Degradation Kinetics Modeling of Benzophenones and Xanthones during High-Temperature Oxidation of Cyclopia genistoides (L.) Vent. Plant Material.," *J Agric Food Chem.,* vol. 63, no. 22, pp. 5518-5527, 2015.

[268] R. Vasiliev, D. Dirin, M. Sokolikova, V. Roddatis, A. Vasiliev, A. Vitukhnovsky and A. Gaskov, "Facet-selective growth and optical properties of CdTe/CdSe tetrapod-shaped nanocrystal heterostructures," *J. Mater. Res.,* vol. 26, no. 13, pp. 1621-1626, 2011.

[269] M. Pavlin and V. Bregar, "Stability of Nanoparticle Suspensions in Different Biologically Relavent Media," *Digest Journal of Nanomaterials and Biostructures ,* vol. 7, no. 4, pp. 1389-1400, 2012.

[270] T. Meißner, A. Potthoff and V. Richter, "Suspension characterization as important key for toxicological investigations," *Journal of Physics: Conference Series,* vol. 170, p. 012012, 2009.

[271] E. Izak-Nau, M. Voetz, S. D. A. Eiden and V. F. Puntes, "Altered characteristics of silica nanoparticles in bovine and human serum: the importance of nanomaterial characterization prior to its toxicological evaluation," *Particle and Fibre Toxicology,* vol. 10, p. 56, 2013.

[272] T. Meißner, K. Oelschlagel and A. Potthoff, "Implications of the stability behavior of zinc oxide nanoparticles for toxicological studies," *Int Nano Lett,* vol. 4, p. 116, 2014.

[273] M. A. Wells, A. Abid, I. M. Kennedy and A. I. Barakat, "Serum proteins prevent aggregation of Fe2O3 and ZnO nanoparticles," *Nanotoxicology,* vol. 6, pp. 837-846, 2012.

[274] F. Rosario, "Effect of Silver Nanoparticles on Osteosarcoma and Lung Cell Lines," University of Aveiro Departmetn of Biology, Aveiro, 2012.

[275] M. Tomšič, M. Bešter-Rogač, A. Jamnik, W. Kunz, D. Touraud, A. Bergmann and O. Glatter, "Nonionic Surfactant Brij 35 in Water and in Various Simple Alcohols: Structural Investigations by Small-Angle X-ray Scattering and Dynamic Light Scattering," *The Journal of Physical Chemistry B,* vol. 108, no. 22, pp. 7021-7032, 2004.

[276] M. Majetschak, "Extracellular ubiquitin: immune modulator and endogenous opponent of damage-associated molecular pattern molecules," *Journal of Leukocyte Biology,* vol. 89, no. 2, pp. 205-219, 2011.

[277] M. Patel, K. Proctor and M. Majetschak, "Extracellular Ubiquitin Increases in Packed Red Blood Cell Units During Storage," *Journal of Surgical Research,* vol. 135, no. 2, pp. 226-232, 2006.

[278] L. Liang, M. Cui, M. Zhang, P. Zheng, Z. Deng, S. Gao, X. Wang, X. Zhang, C. Wang, Y. Liu and L. Xie, "Nanoparticles' interference in the evaluation of in vitro toxicity of silver nanoparticles," *Royal Society of Chemistry Advances,* vol. 5, pp. 67327-67334, 2015.

[279] K. Loza, J. Diendorf, C. Sengstock, L. Ruiz-Gonzalez, J. M. Gonzalez-Calbet, M. Vallet-Regi, M. Köllerb and M. Epple, "The dissolution and biological effects of silver nanoparticles in biological media," *J. Mater. Chem. B,* vol. 2, pp. 1634-1643, 2014.

[280] X. Yang, A. Gondikas, S. Marinakos, M. Auffan, J. Liu, H. Hsu-Kim and J. Meyer, "Mechanism of silver nanoparticle toxicity is dependent on dissolved silver and surface coating in caenorhabditis elegans," *Environ. Sci. Technol,* vol. 46, p. 1119–1127, 2012.

[281] Y. A. Suliman, D. Ali, S. Alarifi, A. Harrath, L. Mansour and S. Alwasel, "Evaluation of cytotoxic, oxidative stress, proinflammatory and genotoxic effect of silver nanoparticles in human lung epithelial cells," *Environ Toxicol,* vol. 30, no. 2, pp. 149-160, 2013.

[282] L. Zhang, L. Wang, Y. Hu, Z. Liu, Y. Tian, X. Z. Y. Wu, H. Tang, C. Chen and Y. Wang, "Selective metabolic effects of gold nanorods on normal and cancer cells and their application in anticancer drug screening," *Biomaterials,* vol. 34, pp. 7117-7126, 2013.

[283] I. García-Álvarez, A. Fernández-Mayoralas and L. Garrido, "Effect of Drugs in Cells and Tissues by NMR Spectroscopy," *Current Topics in Medicinal Chemistry,* vol. 11, pp. 27-42, 2011.

[284] Y. Chen, Z. Wang, M. Xu, X. Wang, R. Liu, Q. Liu, Z. Zhang, T. Xia, J. Zhao, G. Jiang, Y. Xu and S. Liu, "Nanosilver incurs an adaptive shunt of energy metabolism mode to glycolysis in tumor and nontumor cells.," *ACS Nano,* vol. 8, no. 6, pp. 5813-5825, 2014.

[285] M. Triba, A. Starzec, N. Bouchemal, E. Guenin, G. Perret and L. Le Moyec, "Metabolomic profiling with NMR discriminates between biphosphonate and doxorubicin effects on B16 melanoma cells.," *NMR Biomed,* vol. 23, no. 9, pp. 1009-1016, 2010.

[286] L. Mirbahai, M. Wilson, C. Shaw, C. McConville, R. Malcomson, J. Griffin, R. Kauppinen and A. Peet, "1H magnetic resonance spectroscopy metabolites as biomarkers for cell cycle arrest and cell death in rat glioma cells.," *Int J Biochem Cell Biol.,* vol. 43, no. 7, pp. 990-1001, 2011.

[287] L. Ernster and G. Dallner, "Biochemical, physiological and medical aspects of ubiquinone function.," *Biochim Biophys Acta.,* vol. 1271, no. 1, pp. 195-204, 1995.

[288] D. Vance, "Role of phosphatidylcholine biosynthesis in the regulation of lipoprotein homeostasis.," *Curr Opin Lipidol.,* vol. 19, no. 3, pp. 229-234, 2008.

[289] L. Wei, P. Liao, H. Wu, X. Li, F. Pei, W. Li and Y. Wu, "Metabolic profiling studies on the toxicological effects of realgar in rats by (1)H NMR spectroscopy," *Toxicol Appl Pharmacol.,* vol. 234, no. 3, pp. 314-325, 2009.

[290] Q. Chen, Y. Xue and J. Sun, "Kupffer cell-mediated hepatic injury induced by silica nanoparticles in vitro and in vivo.," *Int J Nanomedicine.,* vol. 8, pp. 1129-1140, 2013.

[291] T. Wallimann, M. Wyss, D. Brdiczka, K. Nicolay and H. Eppenberger, "Intracellular compartmentation, structure and function of creatine kinase isoenzymes in tissues with high and fluctuating energy demands: the 'phosphocreatine circuit' for cellular energy homeostasis.," *Biochem J. ,* vol. 281, no. P1, p. 21–40, 1992.

[292] N. Monteiro-Riviere, A. Inman and L. Zhang, "Limitations and relative utility of screening assays to assess engineered nanoparticle toxicity in a human cell line," *Toxicol Appl Pharmacol. ,* vol. 234, no. 2, pp. 222-235, 2009.

[293] G. Oberdorster, A. Maynard, K. Donaldson, V. Castranova, J. Fitzpatrick, K. Ausman, J. Carter, B. Karn, W. Kreyling, D. Lai, S. Olin, N. Monteiro-Riviere, D. Warheit and H. Yang, "Principles for characterizing the potential human health effects from exposure to nanomaterials: elements of a screening strategy," *Part. Fibre Toxicol.,* vol. 2, p. 8, 2005.

[294] C. Schulze, A. Kroll, C. Lehr, U. B. K. Schäfer, J. Schnekenburger, C. Schulze Isfort, R. Landsiedel and W. Wohleben, "Not ready to use – overcoming pitfalls when dispersing nanoparticles in physiological media," *Nanotoxicology,* vol. 2, p. 51–61, 2008.

[295] S. Smulders, J.-P. Kaiser, S. Zuin, K. L. Van Landuyt, L. Golanski, J. Vanoirbeek, P. Wick and P. H. Hoet, "Contamination of nanoparticles by endotoxin: evaluation of different test methods," *Particle and Fibre Toxicology,* vol. 9, p. 41, 2012.

[296] S. El-Mashtoly, D. Niedieker, D. Petersen, S. Krauss, E. Freier, A. Maghnouj, A. Mosig, S. Hahn, C. Kötting and K. Gerwert, "Automated identification of subcellular organelles by coherent anti-stokes Raman scattering.," *Biophys J.,* vol. 106, no. 9, pp. 1910-1920, 2014.

[297] K. Tomankova, J. Horakova, M. Harvanova, L. Malina, J. Soukupova, S. Hradilova, K. Kejlova, J. Malohlava, L. Licman, M. Dvorakova, D. Jirova and H. Kolarova, "Cytotoxicity, cell uptake and

microscopic analysis of titanium dioxide and silver nanoparticles in vitro," *Food and Chemical Toxicology,* vol. 82, pp. 106-115, 2015.

[298] A. Egorov, V. Egorova, H. Grushevskaya, V. Krot, N. Krylova, I. Lipnevich, T. Orekhovskaya and B. Shulitsky, "Enhancement of Raman Light Scattering in Dye-Labeled Rat Glioma Cells by Langmuir-Blodgett CNT-Bundles Arranged on Metal-Containing Conducting Polymer Film," *Cornell University Library,* p. arXiv:1502.02836 [physics.optics], 2015.

Appendix A: Visualizing the Basics of PCA

The following figures are meant to help the reader understand the concept of reducing dimension, which is done during PCA. The aim is to find a plane that provides the most amount of information about the data, while reducing the dimension. For example, in the case of going from a three dimensional image to a two dimensional one, Figure 59 shows a tea pot in four positions; however, only the top position gives information about the handle, the lid, and the spout at the same time. Figure 60 shows the same concept for reducing a graph of two axis to a graph of one axis using a projection based method. Here, projecting onto the *x* and *y* axes results in the loss of information; however, by choosing an axis that follows the trend line of the data, the maximum amount of information can be elicited.

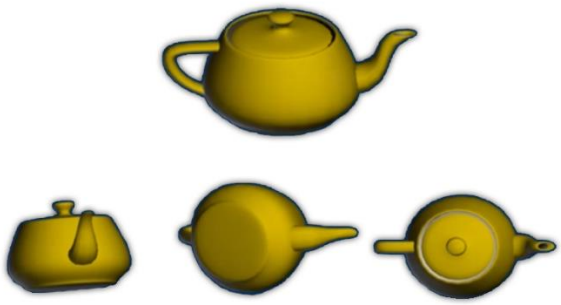

Figure 59: Tea pot in various positions.

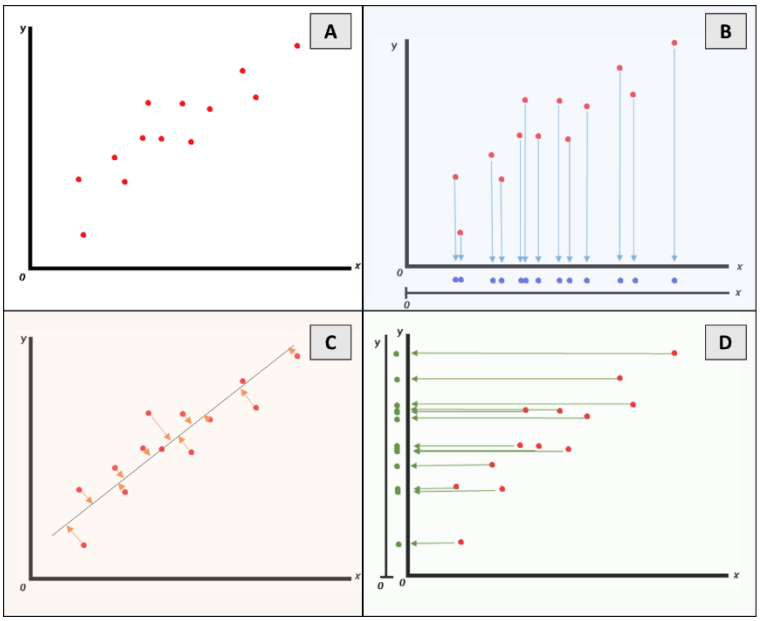

Figure 60: A) A set of data B) and D) Projecting the data onto the x and y axes respective C) Projecting the data onto a new axis along the trendline.

Appendix B: Uptake Results

In order to localize the AgNPs with respect to the cells, two microscopy techniques were explored. Although AgNPs do not have an inherent fluorescence signal, the fluid movement of the stock solution on a glass slide produced a detectable signal when viewed with a fluorescent microscope. The nuclei of the cells were dyed with PI; however, this dye also intercalates with the RNA that exists throughout the cytoplasm. Therefore the entirety of the cells fluoresced under the laser, for both the controls and the samples exposed to 15 µg/mL of AgNPs (Figure 61). This meant that no specific signal could be detected from the NPs. Moreover, the high seeding density resulted in layers of cells that had grown on top of each other; not only does this make it difficult to distinguish each cell, but a higher seeding density also means a lower dose per cell and therefore higher survival rates.

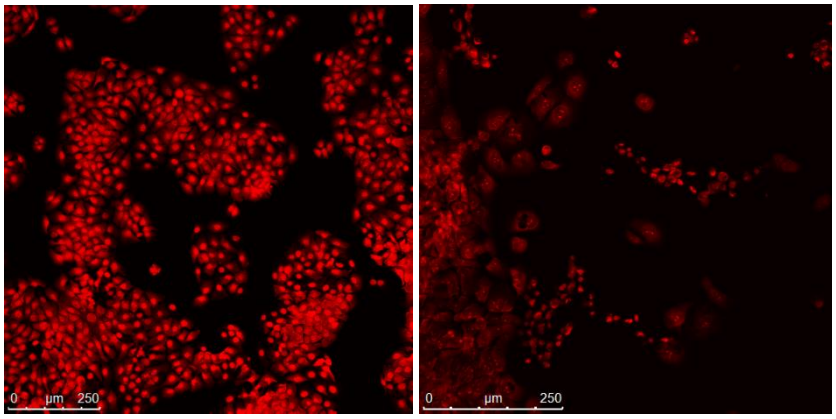

Figure 61: Fluorescence Images of HaCaT cells with 532 nm laser at 10X magnification. Left, Controls; Right, Cells exposed to IC_{50}.

The same samples were also visualized with confocal Raman microscopy. Although the SPR properties of both silver and gold nanoparticles can be used to enhance Raman signals, they are not intrinsically Raman active as metallic bonds are not Raman active in that range. Nevertheless, recent studies have shown various cell components, such as the nucleus, membrane, organelles, etc., to have distinct Raman signatures [296]. The enhancement of these signals in the presence of AgNPs as compared to the control samples, can therefore be used to localize the particles [297].

In these preliminary tests, neither the stock solution nor dried AgNPs on a slide yielded a distinct Raman signal, though the saccharide coating of the particles may have produced the red spectrum in Figure 62A. Furthermore, the presence of PI, the fluorescent dye, created a high background in both the control and exposed samples, preventing the cell component signals from being distinguished. Nevertheless, the same fluorescence signal (3100 to 3600 cm^{-1}) was successfully used for mapping the boundaries of the cells, providing 2D Raman images that were similar to those from the fluorescence microscopy using the 532 nm excitation laser source (Figure 63A).

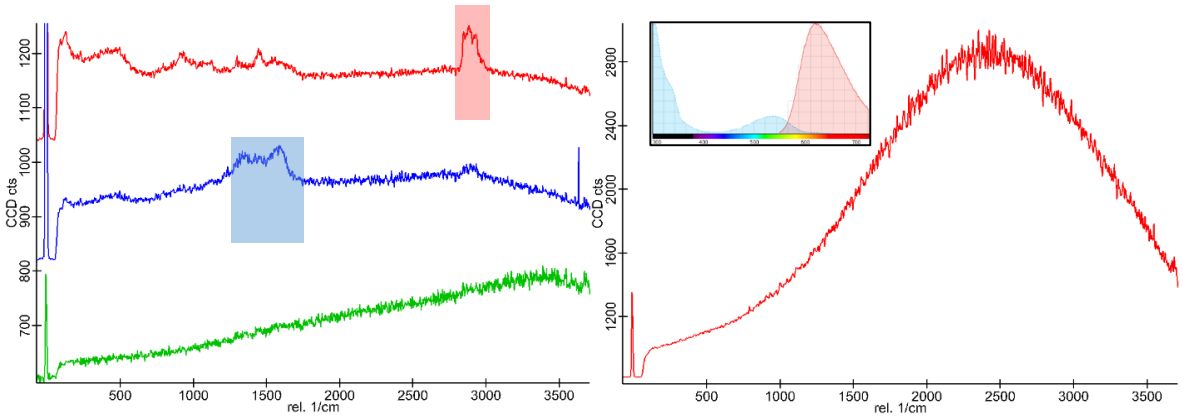

Figure 62: Left, Spectra of stock AgNP solution dried on a glass slide, with the highlighted blue band showing C-C bonds, and the highlighted red band showing C-H bonds; Right, Spectrum of HaCaT cells, showing a high fluorescence background, with the inset showing the absorption/emission spectrum of PI

Changing the laser from 532 to 633 nm, the fluorescent background was eliminated, as the absorption of PI is minimal after 580 nm; however, no signature peaks could be detected. Monitoring the Raman intensity of the band in the range of 100 to 300 cm^{-1}, the 2D Raman images (Figure 63) were obtained with the 532 nm laser (A and B) and the 633 nm laser (C and D).

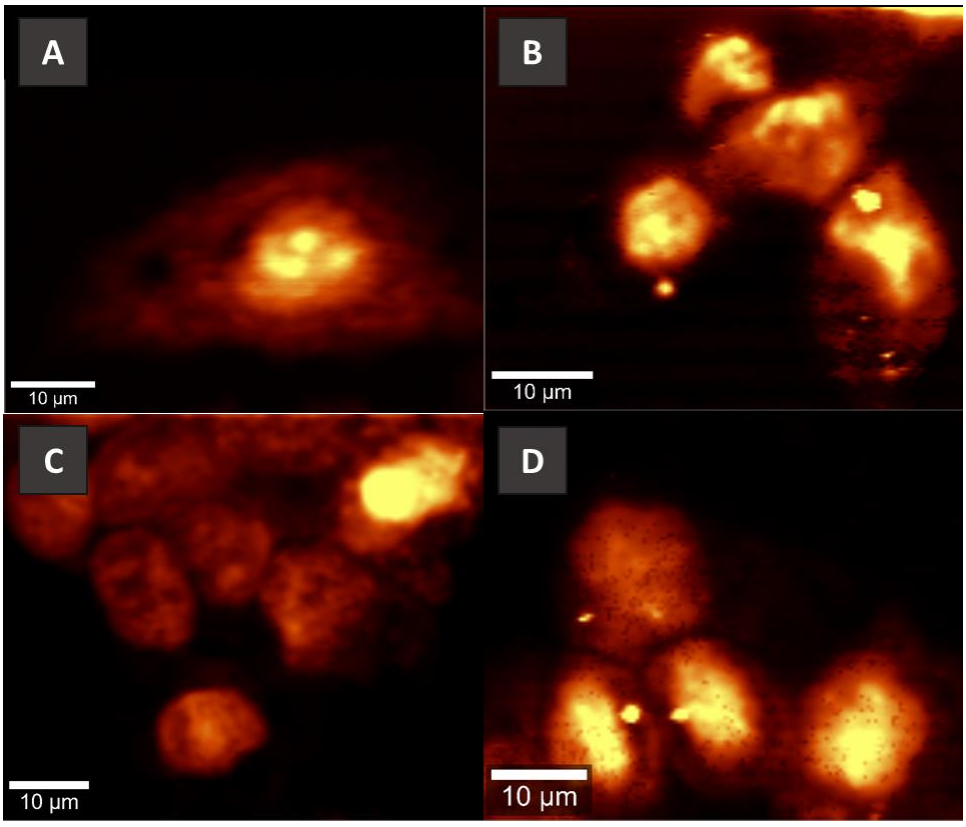

Figure 63: 2D Raman mapping (intensity of the band at 100-300 cm^{-1}) of HaCaT cells; A and B are obtained with 532 nm laser; and C and D with 633 nm laser. A and C are controls, B are cells exposed to 15 µg/mL of AgNPs, and D are cells exposed to 10 µg/ML of AgNPs.

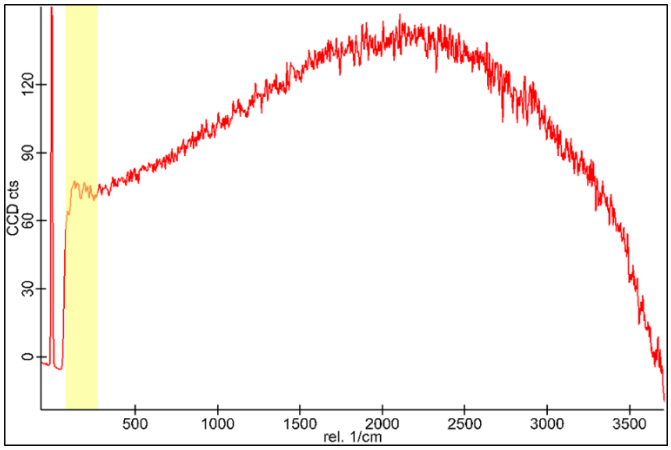

Figure 64: Raman spectrum for 10 µg/mL sample with 633 nm laser; where the highlighted range shows the integrated peak.

A curiuos affect in Figure 63 is the black points that are scattered on top of the cells in D and at their periphery in B, while lacking in A and C, which are the controls. As the peak being integrated is outside the organic range, it cannot be attributed to the cells themselves. The size of the points, as compared to the cells, would suggest something on the nanoscale. That they are in higher quantity and in better arrangement in B than D might corrolate with the higher concentration of AgNPs in B and cell death. On the other hand, as the points are of lower intensity for the integrated peak than their surroundings, it cannot be attributed to scattering or fluorescence of the nanoparticles, nor the bending (100 to 200 cm^{-1}) or stretching (300 to 400 cm^{-1}) of metal-sulfur or metal-nitrogen bonds. A possible, though unlikely hypothesis, would be that the particles are quenching the signal in that range, as elsewhere shown for the quenchign of Raman by CNTs [298] and the quenching of fluorescence by AuNPs [97]. However, this cannot be confirmed without further reproducible experiments and better isolation of variables.

Thus, going forward, it is recommended that the protocol for sample preparation for fluorescence microscopy be modified in the following ways: that fewer cells be seeded on the glass slides; that the cells be treated with RNAse prior to staining with PI; and that the concentration PI and duration of staining be reduced. Similarly for the Raman samples, it is recommended that a lower seeding density be used, and that no fluorescence staining take place. Moreover, it would be worthwhile to determine the signature peaks of the cell components prior to performing uptake and localization studies. If such studies are unsuccessful, the use of a Raman dye with the AgNPs is possible, however, in this case isolation of the toxicity factor may become difficult. Overall, Raman confocal microscopy for the uptake and localization of AgNPs is an intersting technique that can be explored further.